Two-Dimensional Solid State NMR

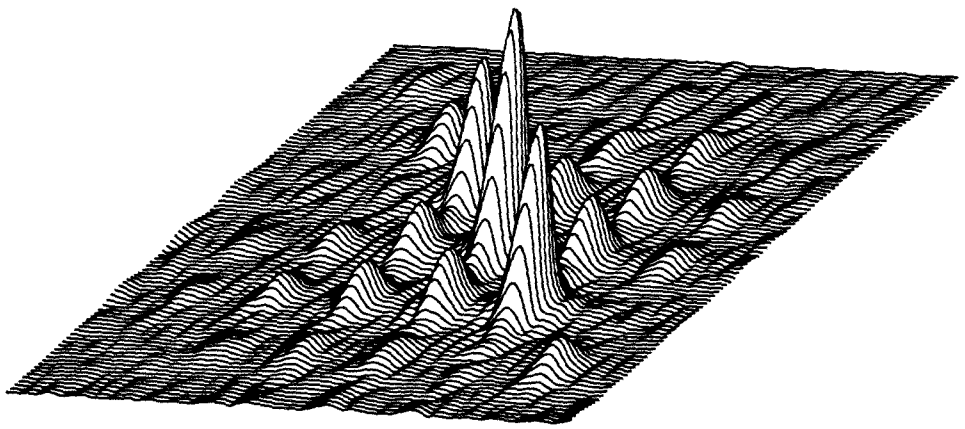

A.P.M. Kentgens

TWO-DIMENSIONAL SOLID STATE NMR

TWO-DIMENSIONAL SOLID STATE NMR

PROEFSCHRIFT

TER VERKRIJGING VAN DE GRAAD VAN DOCTOR
IN DE WISKUNDE EN NATUURWETENSCHAPPEN
AAN DE KATHOLIEKE UNIVERSITEIT TE NIJMEGEN, OP GEZAG VAN
DE RECTOR MAGNIFICUS PROF. DR. B.M.F. VAN IERSEL,
VOLGENS BESLUIT VAN HET COLLEGE VAN DECANEN
IN HET OPENBAAR TE VERDEDIGEN
OP DONDERDAG 4 JUNI 1987
DES NAMIDDAGS TE 1.30 UUR PRECIES

door

ARNOLD PETER MARIA KENTGENS

geboren te Guttecoven

Druk: Quick Service Drukkerij Enschede

PROMOTORES: Prof. Dr. Ir. W.S. Veeman

Prof. Dr. E. de Boer

You can't know everything in the world.
Whatever happens you'll die a fool.

A. Solzhenitsyn

DANKWOORD

Graag wil ik iedereen bedanken die op enigerlei wijze heeft bijgedragen aan het tot stand komen van dit proefschrift.

Alle medewerkers van de afdeling Molecuulspectroscopie dank ik voor de prettige sfeer waarin ik altijd heb kunnen werken. Met name wil ik noemen de hoofd- of bijvak studenten Frank de Jong, Ferdi Geurts, Han Lemmens en Werner Maas die met veel enthousiasme hebben bijgedragen aan het hier beschreven onderzoek. Désirée van der Wey dank ik voor het vele typewerk dat zij voor mij heeft verricht. Onmisbaar was de bijdrage van Jan van Os. Hij zorgde niet alleen voor technische ondersteuning en relativerende woorden; hij heeft ook onze Bruker CXP-300 omgebouwd tot een volwaardige vaste stof spectrometer. De in dit proefschrift beschreven uitbreidingen zoals o.a. de "Synchro Spin Smasher" zijn van zijn hand.

Cees Haasnoot, Pieter van Dael en Jos Joordens dank ik voor hun ondersteuning bij meet- en rekenwerk bij de SON NMR faciliteit. Jos Joordens en Sybren Wijmenga ben ik zeer erkentelijk voor de vriendelijke hulp bij het netjes uitprinten van dit proefschrift.

Van de afdelingen binnen de faculteit Wiskunde en Natuurwetenschappen, waar ik assistentie van heb gehad, wil ik de afdeling Mechaniche Constructie noemen, waar met name Peter van Dijk veel moeite heeft gestoken in het vervaardigen van probes en spinners. Verder dank ik alle medewerkers van de "snelle werkplaats" voor het uitvoeren van diverse haastklussen en de medewerkers van de afdeling Fotografie.

Diverse mensen (o.a. Geert van der Velden en Jan van Bree) dank ik voor het ter beschikking stellen van samples waarop ik mijn meetdrift kon uitleven.

Tenslotte, maar zeker niet op de laatste plaats, dank ik mijn ouders voor de stimulerende werking die steeds van hen is uitgegaan, en Gerda voor het vele geduld en begrip dat zij voor mij heeft gehad. Bij deze verontschuldig ik mij bij haar voor de talloze uren die op heel wat aangenamer wijze doorgebracht hadden kunnen worden.

CONTENTS

		page
	INTRODUCTION	11
	References	13
1	**SOLID STATE NMR**	15
	1.1 Introduction	15
	1.2 Basic interactions of spin systems in solids	16
	1.2.1 Zeeman interaction	16
	1.2.2 Chemical shift	19
	1.2.3 Indirect spin-spin interactions	22
	1.2.4 Direct dipolar interactions	23
	1.2.5 Quadrupole interactions	25
	1.2.6 Irreducuble tensor operators	30
	1.3 Coherent averaging techniques	31
	1.3.1 Heteronuclear decoupling	32
	1.3.2 Homonuclear decoupling	34
	1.3.3 Magic angle spinning	37
	References	43
2	**TWO-DIMENSIONAL NMR**	45
	2.1 Introduction	45
	2.2 General description of two-dimensional NMR	45
	2.2.1 Classical description	46
	2.2.2 Quantum mechanical description	49
	2.3 Different kinds of modulation	51
	2.3.1 Phase modulation	54
	2.3.2 Amplitude modulation	56
	2.3.3 Interconversion of modulation type	57
	2.3.4 Sign discrimination combined with pure absorption line shapes	58
	2.4 Present state of 2D solid state NMR	60
	References	63

3 **HETERONUCLEAR TWO-DIMENSIONAL J-RESOLVED NMR** 67
3.1 Introduction 67
3.2 Experimental realization 68
3.3 Carbon black-filled natural rubber 72
3.3.1 Motions in natural rubber vs adamantane 74
References 78

4 **2D CORRELATION OF CHEMICAL SHIFT AND DIPOLAR INTERACTIONS** 81
4.1 Introduction 81
4.2 Experimental realization 82
4.3 2D correlation of dipolar interactions and chemical shift in POM 83
4.4 Calculation of two-dimensional powder spectra 86
4.5 Orientation of the chemical shift tensor in POM 91
References 92

5 **TWO-DIMENSIONAL EXCHANGE NMR** 93
5.1 Introduction 93
5.2 Simple description of the experiment 94
5.3 Application to natural rubber 96
5.4 2D exchange NMR in slowly rotating solids 98
5.4.1 Theory of 2D exchange under slow MAS conditions 99
5.4.2 Experimental realization 107
5.5 Slow molecular motions in crystalline poly-(oxymethylene) 111
5.5.1 Elucidation of super-slow motions in poly-(oxymethylene) 112
5.5.2 Conclusions 118
References 121

6 TWO-DIMENSIONAL NUTATION NMR OF HALF-INTEGER NUCLEI 123
6.1 Introduction 123
6.2 Calculation of nutation spectra 125
6.3 Experimental aspects of nutation NMR 133
6.3.1 Resonance offset 133
6.3.2 Phasing of the spectra 135
6.3.3 Linebroadening 136
6.3.4 Recycle delay 136
6.3.5 Experimental realization 137
6.4 Application of Nutation NMR 137
6.4.1 Spodumene 137
6.4.2 $Sc_2(SO_4)_3$ 139
6.4.3 Zeolite ZSM-5 139
6.5 Conclusions 142
References 143

APPENDIX I 145

APPENDIX II 149

SUMMARY 167

SAMENVATTING 170

LEVENSLOOP 173

In 1946 the first reports were made of the detection of a nuclear magnetic resonance signal of protons in water by Bloch and coworkers [BL46] and in solid paraffin by the group of Purcell [PU46]. From that point on the development of high resolution NMR of liquids has been a resounding success. It was soon discovered that the detected resonance frequencies depended on a chemical shift and could be used to obtain information about the structure of molecules in solutions. Soon after that spin-spin interactions were found, which give information about the chemical bonding in a molecule [HA52, GU53], and opened the possibility of double resonance experiments. As a result high resolution NMR of solutions rapidly developed into one of the most important tools for structural analysis.

A major step in this evolution was the introduction of Fourier transform techniques. Ernst and Anderson [ER66] demonstrated that it was possible to obtain a NMR spectrum by Fourier transformation of the response of a spin system to pulse excitation. These responses can be added in a computer which means an enormous gain in sensitivity, making it possible to record spectra of rare nuclei like ^{13}C and ^{15}N. The introduction of FT NMR also initiated the development of a lot of ingenious pulsed experiments.

In the course of these developments, Jeener [JE71] proposed in 1971 to perform an experiment as a function of two time variables and Fourier transform the acquired signals with respect to both variables. This idea was picked up by Ernst and coworkers who gave the first thorough theoretical treatment of two-dimensional NMR in 1976 [AU76]. The development of 2D NMR techniques has now led to a stage that it is possible to solve the 3-dimensional structure of proteins in solution.

Meanwhile the initial development of solid state NMR for chemical analysis was less successful. The problems in solid state NMR are the overwhelming dipolar interactions between neighboring spins leading to broad featureless lines. Because of the large line width it is very difficult to extract valuable information from the spectra. In liquids the rapid tumbling of the spins leads to an averaging of all anisotropic interactions such as the dipolar interactions and the resulting spectra consist of very narrow lines determined by the isotropic average of the spin interactions.

The first attempts to overcome the dipolar broadening of solid state spectra were made by Andrew [AR58] and Lowe [LO59]. They demonstrated that

spinning of the sample about an axis inclined 54.7° (the magic angle) with respect to the magnetic field modulates the angular part of the dipolar interaction in such a way that it averages to zero. Unfortunately this approach only works when the spinning speed exceeds the dipolar line width which is often impractical especially when protons, which have a large magnetic moment, are involved.

In 1966 Waugh and coworkers [OS66] and Mansfield [MA66] presented an approach to average homonuclear dipolar interactions by manipulating the spins with cycles of resonant rf pulses. The first successful multiple pulse cycle resulting in high resolution NMR spectra of solids was the WAHUHA cycle of Waugh, Huber and Haeberlen [WA68].

A real breakthrough of solid state NMR as a tool for chemical analysis was achieved when Schaefer and Stejskal [SC76] showed that high resolution spectra of rare spin species (e.g. ^{13}C) in solids could be obtained. This was achieved by irradiating the sample with a strong resonant proton rf field to remove the influence of the carbon-proton dipolar interactions on the spectrum, combined with magic angle spinning to average the ^{13}C chemical shift anisotropy. Furthermore they used cross-polarization [PI73], which is based on the double resonance concept of Hartmann and Hahn [HA62], to improve the sensitivity. The book of Fyfe [FY83] gives an exhaustive survey of applications of solid state NMR in chemistry.

As a result of the enormous capabilities of two-dimensional NMR in solutions, there is now an increased interest in 2D solid state NMR. It is striking, however, that many applications of 2D NMR in solids explicitly exploit the anisotropic character of the spin interactions. The important feature of 2D NMR in this respect is that it can be used to avoid spectral overlap by mapping out interactions in two dimensions. For instance, the possibility exists to use a specific averaging technique in only one time interval of the 2D experiment to suppress a spin interaction in one dimension. This thesis will try to illustrate, by discussing some existing and newly developed 2D solid state experiments, that two-dimensional NMR of solids is a useful and important extension of NMR techniques.

Chapter 1 gives an overview of spin interactions and averaging techniques important in solid state NMR. This overview is probably more suited to give people familiar with NMR an "aha-erlebnis" then that it will give new insights. As 2D NMR is already an established technique in solutions, only the basics of two-dimensional NMR will be presented in chapter 2, with an emphasis on the aspects important for solid spectra. The

following chapters discuss the theoretical background and applications of specific 2D solid state experiments. All these chapters are self-contained if the reader is familiar with NMR or is prepared to take a few facts about NMR for granted. An application of 2D-J resolved NMR, analogous to J-resolved spectroscopy in solutions, to natural rubber is given in chapter 3. In chapter 4 the anisotropic chemical shift is mapped out against the heteronuclear dipolar interaction to obtain information about the orientation of the shielding tensor in poly-(oxymethylene). Chapter 5 concentrates on the study of super-slow molecular motions in polymers using a variant of the 2D exchange experiment developed by us. Finally chapter 6 discusses a new experiment, 2D nutation NMR, which makes it possible to study the quadrupole interaction of half-integer spins.

REFERENCES

AR58 E.R. Andrew, A. Bradbury and R.G. Eades, Nature 182, 1659, 1958.

AU76 W.P. Aue, E. Bartholdi and R.R. Ernst, J. Chem. Phys. 64, 2229, 1976.

BL46 F. Bloch, W.W. Hansen and M. Packard, Phys. Rev. 69, 127, 1946.

ER66 R.R. Ernst and W.A. Anderson, Rev. Sci. Instr. 37, 93, 1966.

FY83 C.A. Fyfe, "Solid State NMR for Chemists", C.F.C. Press, Guelph, 1983.

GU53 H.S. Gutowsky, D.W. McCall and C.P. Slichter, J. Chem. Phys. 21, 279, 1953.

HA52 E.L. Hahn and D.E. Maxwell, Phys. Rev. 88, 1070, 1952.

HA62 S.R. Hartmann and E.L. Hahn, Phys. Rev. 128, 2042, 1962.

JE71 J. Jeener, Ampère International Summer School, Basko Polje, Yugoslavia, 1971.

LO59 I.J. Lowe, Phys. Rev. Lett. 2, 285, 1959.

MA66 P. Mansfield and D. Ware, Phys. Rev. Lett. 22, 133, 1966.

OS66 E.D. Ostroff and J.S. Waugh, Phys. Rev. Lett. 16, 1097, 1966.

PI73 A. Pines, M.G. Gibby and J.S. Waugh, J. Chem. Phys. 59, 569, 1973.

PU46 E.M. Purcell, H.C. Torrey and R.V. Pound, Phys. Rev. 69, 37, 1946.

SC76 J. Schaefer and E.O. Stejskal, J. Am. Chem. Soc. 98, 1031, 1976.

WA68 J.S. Waugh, L.M. Huber and U. Haeberlen, Phys. Rev. Lett. 20, 180, 1968.

CHAPTER 1

SOLID STATE NMR

1.1 Introduction

Nuclear Magnetic Resonance (NMR) has developed to one of the most important tools for structural analysis in liquids. Due to the development of selective averaging techniques, like Magic Angle Spinning (MAS) and multiple pulse techniques, this has also become true for (diamagnetic, non-conducting) solids.

NMR is a spectroscopic method based on the fact that most nuclei of the elements in the periodic system have an intrinsic magnetic moment, the spin, which interacts with an applied magnetic field B. This leads to a situation where the spins can be in energetically different states. Transitions between these states can then be induced by radio frequency radiation. Besides this major interaction with the external magnetic field, the Zeeman interaction, the spins can also interact with each other (dipolar interactions). The electronic charges surrounding a spin are also affected by the external magnetic field and, as a result the spins do not experience the full external field but an effective Zeeman field. The shift due to this "shielding" is called chemical shift. Nuclei which possess an electric quadrupole moment may in addition have an electric interaction with their surrounding charges. In solids most of these interactions are anisotropic and are thus described by tensor interactions. This means that the resulting NMR resonance frequencies will depend on the orientation of the magnetic field with respect to molecular or crystal axes. In randomly distributed poly-crystalline samples all possible orientations of crystallites on a sphere are present, which all give a specific but different contribution to the resulting NMR spectrum. This will lead to very broad NMR line shapes. In liquids this anisotropy is averaged by the rapid, random tumbling of the molecules, and thus an isotropic resonance frequency will be found.

As this thesis is concerned with NMR in solids we will briefly discuss the basic spin interactions present in solids. Furthermore we describe the effect of Magic Angle Spinning (MAS) and multiple pulse techniques on the interactions. This chapter is intended to give a general overview of interactions and techniques. For a more thorough treatment of the principles of magnetic resonance the reader is referred to the monographs of Abragam

[AB61] and Slichter [SL80]. Averaging techniques are extensively discussed in the books of Haeberlen [HA76] and Mehring [ME76]. A very complete discussion of MAS has been given by Maricq and Waugh [MA79].

1.2 Basic interactions of spin systems in solids

Before we explicitly write down the Hamiltonians related to the basic interactions of a spin system we must realize that we treat the spin system as an isolated system. There is, however, a weak interaction of the spin system with all other degrees of freedom of the material (often called the "lattice"). This interaction is very important in relaxation processes. As relaxation processes are not of explicit interest in the present study, they will not be discussed. A detailed account of relaxation can be found in the monographs of Abragam [AB61] and Wolf [WO79].

1.2.1 Zeeman interaction

The main interaction of a nucleus with an angular momentum $I\hbar$ and a magnetic moment $\gamma\hbar I$ (γ is called the gyromagnetic ratio) is the interaction with an external magnetic field B (the Zeeman interaction). In NMR this interaction is usually orders of magnitudes larger than all other interactions. The associated Zeeman Hamiltonian is given by

$$H_Z = -\gamma\hbar\bar{I}\cdot\bar{B} \tag{1.1}$$

For a free spin interacting with a static magnetic field this results in the equation of motion

$$\frac{d\bar{I}}{dt} = \gamma(\bar{I}\times\bar{B}_0) \tag{1.2}$$

In order to solve this equation it is useful to transform to a coordinate system that rotates with frequency ω about the direction of the magnetic field. In NMR jargon this is called the rotating frame. It can be easily established that the equation of motion of the spins in the rotating frame becomes

$$\frac{d\bar{I}}{dt} = \gamma(\bar{I}x(\bar{B}_0+\frac{\bar{\omega}}{\gamma})) \qquad (1.3)$$

This has the same form as equation (1.2) but with the actual magnetic field B_0 replaced with by an effective field $B_{eff} = B_0 + (\omega/\gamma)$. Thus transformation to the rotating frame introduces a fictitious field ω/γ. When choosing a frame rotating with frequency $\omega = -\gamma B_0$, the effective field vanishes, giving $dI/dt = 0$ meaning that the spin vector is static in the rotating frame. Therefore, it precesses with an angular frequency $\omega_0 = -\gamma B_0$ (the Larmor frequency) about the applied field in the laboratory frame (fig. 1.1).

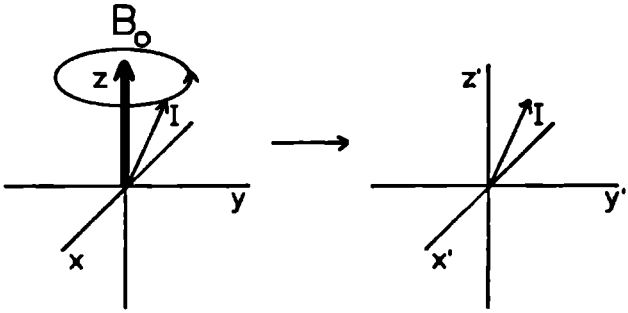

Fig. 1.1 Transformation from the laboratory frame (left) to the rotating frame (right). In the rotating frame there is no effective magnetic field and the nuclear spin vector is static.

When a rotating radiofrequency field perpendicular to the large time-independent field B_0 (// z) is present, the Hamiltonian in the laboratory frame becomes

$$H_Z = -\gamma\hbar B_0 I_z - \gamma\hbar B_1(I_x\cos\{\omega t\} + I_y\sin\{\omega t\}) \qquad (1.4)$$

$$= -\gamma\hbar B_0 I_z - \gamma\hbar B_1 \exp\{-i\omega t I_z\}\cdot I_x \cdot \exp\{+i\omega t I_z\}$$

From this equation it is not easy to visualize the resulting motion of the spins. To find the appropriate expression for the Hamiltonian in the rotating frame we start with the time-dependent Schrödinger equation

$$i\hbar \frac{d\psi}{dt} = H\psi \tag{1.5}$$

To transform to the rotating frame we substitute

$$\psi = R_z(\omega t)\, \psi' \tag{1.6}$$

in equation (1.5). Here ψ' represents the transformed wave function and $R_z(\omega t) = \exp\{-i\omega t I_z\}$ is the transformation operator representing a rotation of the coordinate system over the angle ωt about the z axis. We see that the Schrödinger equation in the rotating frame

$$i\hbar \frac{d\psi'}{dt} = [R_z^{-1}(\omega t) \cdot H \cdot R_z(\omega t) - i\hbar\, R_z^{-1}(\omega t) \cdot \frac{dR_z(\omega t)}{dt}]\psi' \tag{1.7}$$

has the same appearance as in the laboratory frame when we define the Hamiltonian as

$$H_R = R_z^{-1}(\omega t) \cdot H \cdot R_z(\omega t) - i\hbar\, R_z^{-1}(\omega t) \cdot \frac{dR_z(\omega t)}{dt} \tag{1.8}$$

For the Hamiltonian of equation (1.4) this becomes

$$H_R = -\hbar(\omega_0 - \omega) I_z - \hbar\omega_1 I_x \tag{1.9}$$

where $\omega_0 = \gamma B_0$ and $\omega_1 = \gamma B_1$. When the frequency of the rf irradiation ω is equal to the Larmor frequency ω_0, the first term of equation (1.9) vanishes and the spins only experience a static field B_1 along the x axis in the rotating frame. In this frame the magnetization will thus precess with a frequency ω_1 about the x axis as long as the rf field is present. In other words the complex motion of the spins in the presence of a rf field appears to be a superposition of two rotations.

It should be noted that in practice oscillating fields are used in stead of rotating fields. An oscillating field, however, can be written as the sum of two rotating fields, rotating in opposite directions. If $B_1 << B_0$ the effect of a rotating field on a magnetic moment is negligible unless its frequency ω is in the vicinity of the Larmor frequency. Thus an oscillating

field rotating in the opposite direction about the z axis then the magnetic moment can be neglected as it will be off-resonance by 2ω.

The rotating frame concept has proven to be very convenient for the description of magnetic resonance. When we transform to the rotating frame, we get rid of the common Larmor precession of the spins about the magnetic field. It is helpful to view the various internal spin interactions, to be discussed below, in the rotating frame. As the rotating frame moves in line with the free precession of the spins, those terms of an interaction which are static in the rotating frame will affect the spin system, whereas those parts of an interaction with a large time dependence in the rotating frame hardly affect the spins and may thus be neglected. This is called truncation. From equation (1.8) and (1.9) it becomes clear that when the Hamiltonian in the laboratory frame has the form $H_Z + H_{int}$, the Hamiltonian in the rotating frame will have the form $R_z^{-1} \cdot H_{int} \cdot R_z$. Looking at the structure of R_z tells us that those terms of H_{int} which commute with I_z will be static in the rotating frame. The terms of H_{int} that do not commute become oscillating with frequency ω (and 2ω) which means that their time average becomes zero and thus they can be discarded. It is important to realize that the rotating frame is a mathematical concept to describe our spin system and will, of course, not affect the resulting spectra.

1.2.2 Chemical shift

NMR normally concentrates on diamagnetic materials, i.e. samples without electron paramagnetism. As a consequence there exist no direct interactions between the magnetic moments of the electrons and the nuclei. The resonance frequency of a nucleus embedded in bulk matter differs, however, from that of a "bare" nucleus. This frequency shift, named chemical shift, is due to the effect of the static magnetic field B_0 on the electronic charges. In the first place the Lorentz force causes the electronic charges to precess about B_0. The resulting electric current induces an additional magnetic field antiparallel and proportional to B_0. Secondly, the applied field B_0 polarizes the electronic shells thus producing a another small field proportional and parallel to B_0. As a result the nucleus does not experience the applied field B_0, but an effective field $(1-\sigma)B_0$ where σ is a shielding factor independent of the magnitude of B_0

An approach to calculate the chemical shift of a nucleus with a certain electronic surrounding can be found in every advanced textbook on magnetic

resonance [AB61, SL80]. These calculations are, however, very tedious and therefore there are not so many theoretical studies of the chemical shift. Experimentally it was established that the chemical shift is very sensitive to changes in the electronic surrounding of a nucleus. It is because of this sensitivity of the chemical shift that NMR has become such an important tool for structural analysis. The reader will be spared the inevitable proton spectrum of ethyl alcohol which is presented at this point in many textbooks to show the phenomenon of chemical shift by the presence of three lines from the three types of protons in CH_3CH_2OH.

In general the chemical shift is anisotropic and is represented by a symmetric second rank tensor. In the laboratory frame the Hamiltonian is given by

$$H_{CS} = \gamma\hbar\bar{I}\cdot\bar{\bar{\sigma}}\cdot\bar{B}_0 \tag{1.10}$$

As the chemical shift is very small it can be treated by first-order perturbation theory. As a consequence we only take that part of H_{CS} into account that commutes with the Zeeman interaction H_z. This is analogous to truncation of the Hamiltonian in the rotating frame. The secular (or truncated) Hamiltonian now becomes

$$\begin{aligned} H_{CS} &= \gamma\hbar I_z\sigma_{zz}B_0 = \gamma\hbar I_z B_0(\sigma_{XX}\sin^2\theta\cos^2\varphi + \sigma_{YY}\sin^2\theta\sin^2\varphi + \sigma_{ZZ}\cos^2\theta) \\ &= \gamma\hbar I_z B_0(\sigma_{iso} + \tfrac{1}{2}\delta\{(3\cos^2\theta-1) + \eta\sin^2\theta\cos2\varphi\}) \end{aligned} \tag{1.11}$$

where $\delta = \sigma_{ZZ}-\sigma_{iso}$ is called the shift anisotropy and $\eta = (\sigma_{XX}-\sigma_{YY})/\delta$ is the asymmetry parameter. σ_{XX}, σ_{YY} and σ_{ZZ} are the principal values of the chemical shift tensor or, in other words, when we express the chemical shift tensor in its principal axis system, we find the elements σ_{XX}, σ_{YY}, σ_{ZZ} on the diagonal. θ and φ are the polar angles orienting the external magnetic field B_0 in this principal axis system. The trace of the chemical shift tensor is given by $\sigma_{iso} = (\sigma_{XX} + \sigma_{YY} + \sigma_{ZZ})/3$.

In case of isotropic motion as in a fluid, the term of equation (1.11) containing the angular dependence of H_{CS} averages to zero and the NMR frequency is determined by σ_{iso}. When we take the spectrum of a polycrystalline sample of a rigid solid, the result will be a specific powder pattern dispersed around σ_{iso}. This powder spectrum can be written as

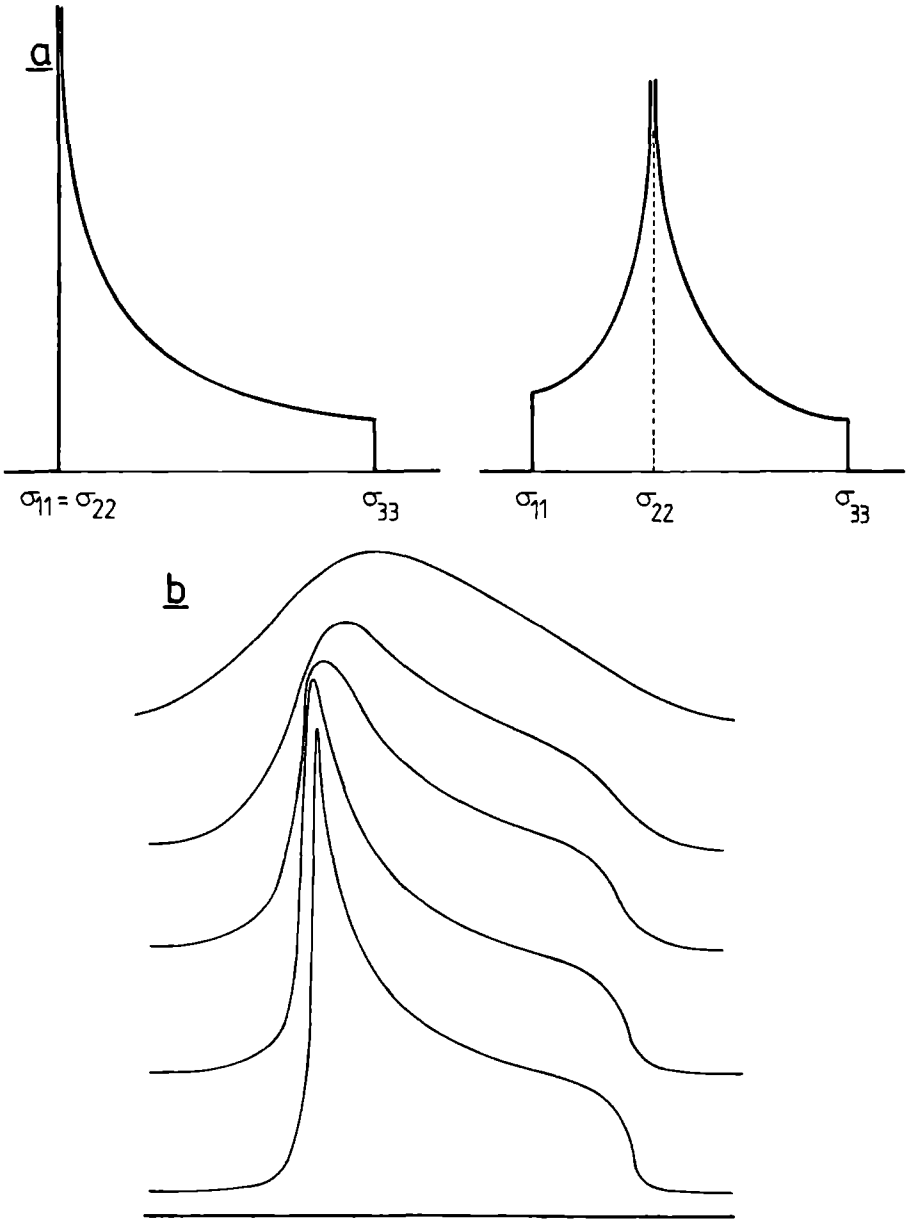

Fig. 1.2 a) Chemical shift powder patterns for an axially symmetric and a general chemical shift tensor. b) The powder line shape of the axially symmetric shift tensor convoluted with Lorentzian broadening functions of different widths.

$$S(\omega) = \int_0^{2\pi}\int_0^{\pi} g[\omega - \omega(\theta,\varphi)]\ \sin\theta d\theta\ d\varphi \qquad (1.12)$$

where $\omega(\theta,\varphi)$ is the resonance frequency of a spin as determined by equation (1.11) and g denotes the line shape function. The powder pattern can thus easily be obtained numerically by sampling θ and φ over a sphere, calculate $\omega(\theta,\varphi)$ in a grid of frequency values and finally convolute the result with the line shape function g. Fig. 1.2 shows the result of such a calculation. An alternative method is to evaluate $\cos\{\omega(\theta,\varphi)t\}$ for every surface element of a sphere, sum all these induction signals, multiply the result by a linebroadening function (e.g. an exponential decay) and then Fourier transform the final result to reveal the powder pattern.

It is also possible to determine the powder pattern analytically. To do so one has to convert the angular distribution function $\sin\theta d\theta d\varphi$ to a distribution function of ω and then calculate the intensity $I(\omega)$. This is not always a straightforward operation. Very characteristic for powder patterns are the peaks and shoulders. Peaks and shoulders are found when singularities and discontinuities occur in $I(\omega)$. This appears to be the case when $d\omega/d\theta = d\omega/d\varphi = 0$. If we work this out in the case of chemical shift anisotropy (equation (1.11)) we find a shoulder for $\omega = \gamma B_0\sigma_{XX}$ and $\omega = \gamma B_0\sigma_{ZZ}$ whereas a peak occurs at $\omega = \gamma B_0\sigma_{YY}$. In other words the principal values of the chemical shift tensor can be directly determined from a powder pattern.

1.2.3 Indirect spin-spin interactions

Another interaction that is brought about by the polarizability of the electron shells is the indirect interaction between nuclear spins. This interaction should not be confused with the direct dipolar interaction between nuclear spins which we discuss later on. The idea is that a nuclear magnetic moment μ_1 produces a field which distorts the electronic shell. This distortion of the electron shell produces a small magnetic field proportional to μ_1 at the site of another nucleus. The interaction is independent of the magnitude of the external field. The Hamiltonian associated with this interaction thus becomes for two spins labeled r and s

$$H_J = \gamma_r\gamma_s\hbar^2\ \bar{I}_r\cdot\bar{\bar{J}}_{rs}\cdot\bar{I}_s \qquad (1.13)$$

where J_{rs} is the spin-spin coupling tensor. Again, as in the case of chemical shift, it is rather difficult to calculate J couplings. But experimentally it has been established that J couplings can give information about the chemical bonds in a molecule and its conformation. Although in theory J is anisotropic, for light atoms this anisotropy is very small. In practice only the isotropic value of J has been studied. In solution only the isotropic value of J can be accessed due to the rapid tumbling of the molecules. In polycrystalline solids, as will be discussed in chapter 3, J can only be measured when averaging techniques are employed which also average the J tensor to its isotropic value. It must be noted, however, that some J tensors have been determined in liquid crystal studies [RO82].

To write down the truncated Hamiltonian we have to distinguish between the heteronuclear (coupling between different isotopes) and the homonuclear (coupling of like spins) case. For heteronuclear spin-spin interactions, the only term surviving truncation is

$$H_J = \hbar J^i_{IS} I_z S_z \tag{1.14}$$

where $J_{IS}{}^i$ is the isotropic value of the J coupling as it is determined directly from the spectrum. The second spin species is now denoted S for convenience. For couplings between like spins the truncated Hamiltonian becomes

$$H_J = \hbar J^i_{rs} \bar{I}_r \cdot \bar{I}_s \tag{1.15}$$

Only when the difference in chemical shift of spin r and spin s is large compared to the J coupling, this reduces to

$$H_J = \hbar J^i_{rs} I_{rz} I_{sz} \tag{1.16}$$

which is identical to the heteronuclear situation.

1.2.4 Direct dipolar interactions

The direct interaction between two nuclear spins depends on the magnitude of their magnetic moments, the internuclear distance and their relative position. The interaction between two magnetic moments is given by

the well-known dipole-dipole coupling

$$H_D = \frac{\gamma_r \gamma_s \hbar^2}{r_{rs}^3} \left(\bar{I}_r \cdot \bar{I}_s - 3\frac{(\bar{I}_r \cdot \bar{r}_{rs})(\bar{I}_s \cdot \bar{r}_{rs})}{r_{rs}^2}\right) \tag{1.17}$$

where r_{rs} is the internuclear distance. Evaluating equation (1.17) in coefficients of I_x, I_y, I_z and then truncating the resulting Hamiltonian (i.e. taking the secular part) gives for the coupling between two like spins

$$H_{II} = \frac{\gamma_I^2 \hbar^2}{2r^3} (1-3\cos^2\theta)[3I_{rz}I_{sz} - \bar{I}_r \cdot \bar{I}_s] \tag{1.18}$$

For the heteronuclear case we get

$$H_{IS} = \frac{\gamma_I \gamma_S \hbar^2}{r^3} (1-3\cos^2\theta) I_z S_z \tag{1.19}$$

θ is the angle of the internuclear vector r with the external field. Note that the interaction is coaxial with the internuclear axis of the two interacting nuclei and that it is independent of the external magnetic field strength. Thus the dipolar interaction can be represented as an axial, symmetric tensor whose principal axis lies along the internuclear axis. The magnitude of the interaction is proportional to r^{-3} and is thus sensitive to changes in internuclear distances. This also means that only nearby spins interact.

The dipolar tensor is traceless, i.e. for rapid isotropic reorientations of the interspin vector the interaction averages to zero. In a solid the dipolar interactions often dominate the spectrum, especially when protons (which have a large γ) are involved. In a polycrystalline sample the angular dependence of equations (1.18) and (1.19) leads to a specific powder pattern. For instance, for a system consisting of isolated spin pairs the well-known Pake pattern will emerge. However, when more spins are involved the dipolar eigenfunctions can no longer be determined and a theoretical description of the powder line shape is no longer feasible. Van Vleck [VL48] developed a method, named the method of moments, which allows the determination of the line shape of a system with several dipole-dipole interactions without

solving the eigenfunctions. This approach has been popular in the early days of NMR of solids.

1.2.5 Quadrupole interactions

The interactions discussed so far are magnetic interactions of the nucleus with its surroundings. In general the nuclear charge distribution is not spherically symmetric. This means that one should, besides magnetic effects, also consider electrical effects on the energy required to reorient the nucleus. As the cylindrically symmetrical nucleus can only be turned end over end for nuclei with I = 1/2 there is no change in the electrostatic energy for such an operation. Consequently these electrical effects play no role for I = 1/2 nuclei. Classically, the interaction energy E of a charge distribution of density ρ with a potential V due to external sources is

$$E = \int \rho(r)V(r)d\tau \tag{1.20}$$

where the integral runs over the whole nuclear volume. Expansion of the potential V(r) in a Taylor series about the centre of gravity of the nucleus allows us to write equation (1.20) as a sum of energy contributions. The first term in this sum represents the electrostatic energy of the nucleus taken as a point charge. This affects every energy level in the same way and thus is of no interest for NMR. The second term involves the electric dipole moment which vanishes because of the symmetry of the nucleus. The third term describes the interaction of the nuclear quadrupole moment with the electric field gradient ($d^2V/dx_i dx_j$). As all higher terms are very small we concentrate on this interaction. The part of this term that depends on the nuclear orientation can be written as

$$E = \sum_{i,j} V_{i,j} Q_{i,j} \tag{1.21}$$

where $V_{i,j}$ represents the electric field gradient tensor and $Q_{i,j}$ the nuclear quadrupole tensor. Equation (1.21) can be converted to its quantum mechanical form using the Wigner-Eckart theorem.

$$H_Q = \frac{eQ}{6I(2I-1)} \sum_{i,j} V_{i,j}[\frac{3}{2}(I_iI_j+I_jI_i) - \delta_{ij}I^2] \qquad (1.22)$$

where the summation runs over all components x,y and z. The magnitude of the nuclear quadrupole moment Q

$$Q = \int (3z^2-r^2)\rho(r)d\tau \qquad (1.23)$$

is a measure of the deviation of the nuclear charge distribution from a spherical distribution. The z direction is here defined by the orientation of the nuclear spin.

In the principal axis system of the (symmetric) field gradient tensor equation (1.22) takes the well-known form

$$H_Q = \frac{e^2qQ}{4I(2I-1)} [3I_Z^2 - I^2 + \eta(I_X^2 - I_Y^2)] \qquad (1.24)$$

with $eq \equiv V_{ZZ}$ and $\eta = (V_{XX}-V_{YY})/V_{ZZ}$. Thus experimental determination of the quadrupole interaction allows us to determine the electric field gradient tensor which is directly determined by the electric charges surrounding the nucleus under study. The closed electron shells in the vicinity of the nucleus are spherically symmetric and thus in first-order do not contribute to the field gradient. So the field gradient is generated by charges outside of the closed shells. These charges will, however, also polarize the closed shells somewhat. Thus the field gradient generated by a charge outside of the closed electron shells will also be determined by the departure of spherical symmetry of the closed shells due to this polarization. This is taken into account with the Sternheimer antishielding factor γ:

$$V_{ZZ} = V_{ZZ}^0(1-\gamma) \qquad (1.25)$$

$$\text{with } V_{ZZ}^0 = e\frac{(3\cos^2\theta-1)}{r^3} \qquad (1.26)$$

where θ is the angle with the principal axis.

In the high field limit we consider H_Q in equation (1.24) to be a perturbation relative to the Zeeman interaction. This situation is thoroughly

treated in the review article by Cohen and Reif [C057]. For a discussion of the low field case were $H_Q >> H_Z$ the reader is referred to the article by Das and Hahn [DA58]. Transformation of equation (1.24) to the laboratory frame followed by a truncation of the result gives the secular Hamiltonian

$$H_{Q,sec} = \frac{e^2qQ}{8I(2I-1)} (3\cos^2\theta - 1 + \eta\sin^2\theta\cos2\varphi)(3I_z^2 - I^2) \qquad (1.27)$$

where θ and φ are the polar angles orienting the external magnetic field (// z) in the principal axis system of the field gradient tensor. Note that equation (1.27) has the same angular dependence as the chemical shift (equation (1.11)). This means that, for a polycrystalline sample, we find a chemical shift-like powder pattern for each transition m,m±1, except for the 1/2,-1/2 transition of a half-integer spin. From equation (1.27) it follows that the m=1/2 and m=-1/2 eigenstates are both shifted by the same amount. Thus the resulting spectrum is a superposition of powder patterns and, for a half-integer spin, a narrow peak of the central 1/2,-1/2 transition.

In many practical cases the quadrupole interaction can become so large that first-order perturbation theory is not sufficient. In practice this often means that the above mentioned powder patterns are too broad to be detected. Then only the central 1/2,-1/2 transition for half-integer spins can be determined. Although narrow in first-order perturbation theory, it becomes a powder pattern due to the second-order shift of the energy levels (fig. 1.3). Second-order perturbation theory gives the expression for the orientational dependence of the resonance frequency of the 1/2,-1/2 transition [NA66]

$$\nu_{\frac{1}{2},-\frac{1}{2}} = -\frac{\nu_Q^2}{6\nu_Z} (I(I+1) - \tfrac{3}{4})(A(\varphi)\cos^4\theta + B(\varphi)\cos^2\theta + C(\varphi)) \qquad (1.28)$$

$$A(\varphi) = -\frac{27}{8} + \frac{9}{4}\eta\cos2\varphi - \frac{3}{8}\eta^2\cos^2 2\varphi$$

$$B(\varphi) = \frac{30}{8} - \frac{1}{2}\eta^2 - 2\eta\cos2\varphi + \frac{3}{4}\eta^2\cos^2 2\varphi$$

$$C(\varphi) = -\frac{3}{8} + \frac{1}{3}\eta^2 - \frac{1}{4}\eta\cos2\varphi - \frac{3}{8}\eta^2\cos^2 2\varphi$$

$$\nu_Q = \frac{e^2qQ/h}{2I(2I-1)}$$

ν_Z is the Zeeman frequency of the central transition. The width of the powder pattern given by equation (1.28) is therefore inversely proportional to the magnetic field strength. Peaks (singularities) and shoulders (discontinuities) of the powder pattern are found when $d\nu/d\theta = d\nu/d\varphi = 0$. These have been determined by Baugher et al. [BA69] and are plotted in fig. 1.4 as a function of η.

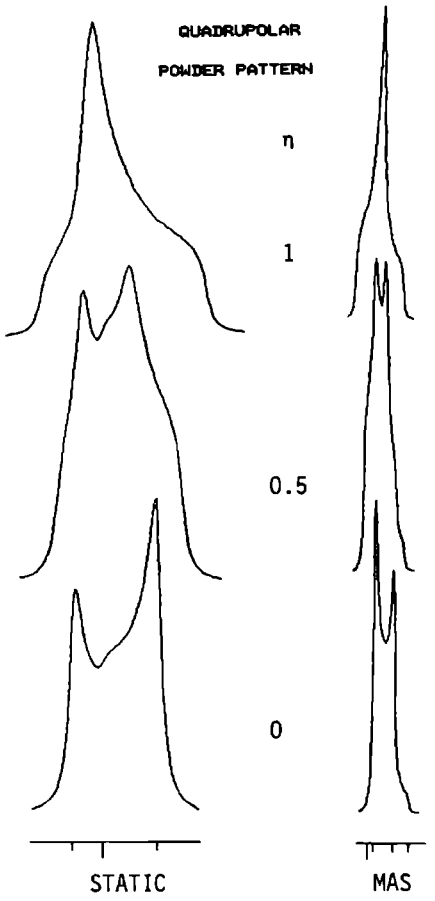

Fig. 1.3 Second-order powder patterns of the 1/2;-1/2 transition of a half-integer quadrupolar nucleus for several values of the asymmetry parameter η. Fast spinning of the sample about the magic angle (MAS) changes the appearance of the pattern and results in a narrowing of a factor ~ 4.

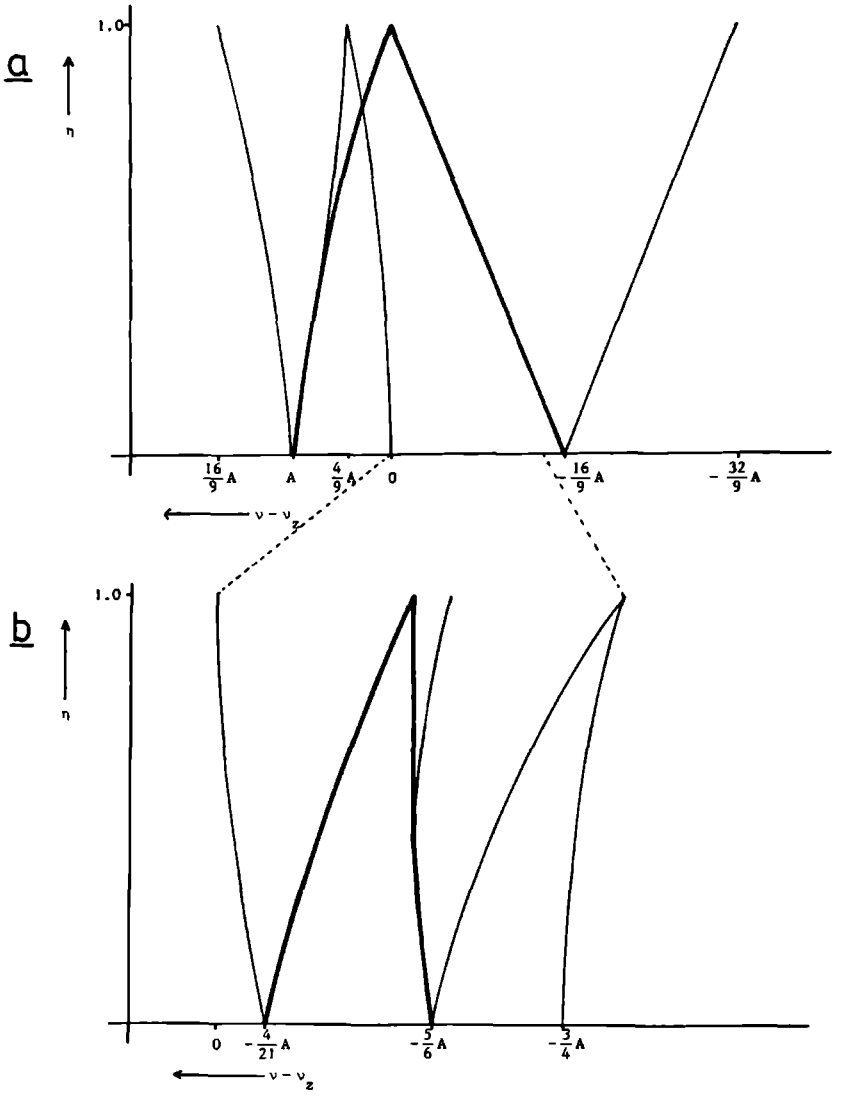

Fig. 1.4 Position of peaks (singularities ▬) and shoulders (discontinuities ——) of the second order 1/2;-1/2 powder pattern as a function of the asymmetry parameter η for a static sample (a) and for a sample spinning about the magic angle (b).

$$A = (\nu_Q^2/16\nu_Z)[I(I+1) - 3/4]$$

1.2.6 Irreducible tensor operators

The internal Hamiltonians H_{CS}, H_J, H_D and H_Q discussed above were all presented in their familiar Cartesian form. Their general appearance can be written as

$$H_X = C^X \sum_{i,j} R^X_{i,j} T^X_{i,j} \tag{1.29}$$

where C contains some fundamental constants and properties of the nucleus under study. The $T_{i,j}$ are the dyadic products of the nuclear spin vector with itself (X=Q), with another nuclear spin vector (X=D,J) or with the magnetic field (X=CS). The $R_{i,j}$ contain the geometrical dependence of the interaction. In view of the averaging techniques in coordinate or spin space, to be discussed in the next paragraphs, it is advantageous to express the Hamiltonians in components of irreducible tensor operators [RO57, BR79]. Under rotations components of irreducible tensors transform among themselves, hence this representation facilitates the study of averaging processes brought about by rotations.

A second-order Cartesian tensor R can easily be decomposed in its irreducible constituents:

$$R_0 = \frac{1}{3} Tr(R), \quad R_1 = \frac{1}{2} (R_{i,j} - R_{j,i}), \quad R_2 = \frac{1}{2} (R_{i,j} + R_{j,i}) - \frac{1}{3} \delta_{ij} Tr(R) \tag{1.30}$$

where R_0 is a scalar which remains invariant under rotations, R_1 is the antisymmetric part of R and R_2 contains the symmetric part of R. The dyadic products $T_{i,j}$ can also be reduced to irreducible bases sets. The result of this operation is given in table 1.1 for every interaction X. The internal Hamiltonians can thus be written as

$$H_X = C^X \sum_{l=0}^{2} \sum_{m=-l}^{l} (-1)^m R^X_{l,-m} T^X_{l,m} \tag{1.31}$$

For symmetric tensor interactions the $R_{l,-m}$ will be zero. When we look at the R tensor in its principal axis system, the irreducible components will be denoted by $\rho_{l,m}$, where only components with m=0, ±2 will be non-zero. The relation between the components of the irreducible tensors and the principal values of the Cartesian tensor are then

$$\rho_{0,0} = \frac{1}{3}\,\mathrm{Tr}(R) = \frac{1}{3}(R_{XX}+R_{YY}+R_{ZZ}) = R_{iso}$$

$$\rho_{2,0} = \sqrt{(3/2)}\,(R_{ZZ}-R_{iso}) = \sqrt{(3/2)}\,\delta \qquad (1.32)$$

$$\rho_{2,\pm2} = \frac{1}{2}\,(R_{XX}-R_{YY}) = \frac{1}{2}\,\eta\delta$$

From these $\rho_{l,m}$ in the principal axis system, the $R_{l,m}$ in the laboratory frame are easily obtained by a transformation

$$R_{l,m} = \sum_{m'} D^{l}_{m',m}(\varphi,\theta,0)\;\rho_{l,m'} \qquad (1.33)$$

where $D^{l}(\alpha,\beta,\gamma)$ represents the Wigner rotation matrix of the order l which is needed to transform a spherical tensor operator $\rho_{l,m}$ over the Euler angles α,β,γ. These angles are here determined by θ and φ which are the polar angles orienting the external magnetic field in the principal axis system of R. The only Wigner matrix we actually need, $D^{2}_{m',m}$, is given in Appendix I.

Table 1.1 Irreducible bases sets $T_{l,m}$ contained in the dyadic vector products of the internal Hamiltonians. $I_{\pm}$ are normalized: $I_{+} = -(I_x+iI_y)/\sqrt{2}$, $I_{-} = (I_x-iI_y)/\sqrt{2}$.

X	C^X	$T_{0,0}$	$T_{2,0}$	$T_{2,\pm1}$	$T_{2,\pm2}$
CS	γ	I_zB_0	$\sqrt{(2/3)}I_zB_0$	$I_{\pm}B_0/\sqrt{2}$	0
J	1	$I_r\cdot I_s$	$(3I_{rz}I_{sz}-I_r\cdot I_s)/\sqrt{6}$	$(I_{r\pm}I_{sz}+I_{rz}I_{s\pm})/\sqrt{2}$	$I_{r\pm}I_{s\pm}$
D	$-2\gamma_r\gamma_s\hbar$	$I_r\cdot I_s$	$(3I_{rz}I_{sz}-I_r\cdot I_s)/\sqrt{6}$	$(I_{r\pm}I_{sz}+I_{rz}I_{s\pm})/\sqrt{2}$	$I_{r\pm}I_{s\pm}$
Q	$eQ/6I(2I-1)\hbar$	I^2	$(3I_z{}^2-I^2)/\sqrt{6}$	$(I_{\pm}I_z+I_zI_{\pm})/\sqrt{2}$	$I_{\pm}{}^2$

1.3 Coherent averaging techniques

As was discussed in the preceding paragraph a spin system experiences, except for the Zeeman interaction, several internal interactions. Knowledge of these interactions can provide, in principle, structural information about

the system under consideration. All these interactions appeared to be anisotropic. As a result each interaction will give a specific powder pattern for a polycrystalline sample. When several spin species are present and/or several interactions act simultaneously on a spin, the resulting spectrum will very often be a featureless line and the spectroscopist will perish in the overabundance of information. In order to avoid this problem one can selectively average certain interactions, while leaving other interactions intact, in that way making it possible for the spectroscopist to extract separate pieces of information from the spin system. In the past years several of these techniques have been developed, which have greatly helped the progress of solid state NMR.

1.3.1 Heteronuclear decoupling

. One of the most used averaging techniques is heteronuclear decoupling which totally removes the influence of a certain spin species on the spectrum of another spin species that is observed. To be more explicit, solid state NMR often studies the ^{13}C resonance of organic molecules and polymers. The informative ^{13}C chemical shifts can, however, not be extracted from the spectrum because of the overwhelming dipolar interactions with the abundant proton nuclei. By irradiating the sample with a strong resonant proton rf field the effect of the protons on the ^{13}C spectrum can be removed. The result is that the ^{13}C (I=1/2) spectrum is exclusively determined by the carbon chemical shift. ^{13}C-^{13}C dipolar interactions are not the present because the natural abundance of ^{13}C is only 1% and thus the average internuclear ^{13}C-^{13}C distance will be very large.

To examine the effect of a rf field on a system consisting of rare spins S coupled to abundant spins I we write down the relevant truncated Hamiltonian in the rotating frame

$$H_R = \hbar(\omega_0-\omega)I_z - \hbar\omega_1 I_x + H_{CS,I} + H_{CS,S} + H_{D,II} + H_{D,IS} + H_{J,IS} \qquad (1.34)$$

where $\omega_0 = \gamma_I B_0$ and $\omega_1 = \gamma_I B_1$. We assumed a rf field along the x axis of the I spin rotating frame (which rotates with a frequency ω with respect to the laboratory frame). The first two terms of equation (1.34) represent an effective magnetic field in the rotating frame of strength $B_e = \sqrt{(B_1^2 + (B_0-\omega/\gamma)^2)}$, which makes an angle $\alpha = \arctan(B_1/(B_0-\omega/\gamma))$ with

the z axis. This effective field causes a common precession of the I spins in the rotating frame, as did the B_0 field in the laboratory frame.

We are now going to use the rotating frame concept again. In the same way we transformed from the laboratory frame to the rotating frame to remove the main Zeeman interaction (except for the small field $B_0-\omega/\gamma$) from our Hamiltonian we are now transforming a second time to a doubly-rotating frame to remove the presence of the effective field from our Hamiltonian. This is done in two steps, first we tilt the rotating frame over angle α to align the z axis with the effective field and then apply a rotation with frequency $\omega_e = \gamma B_e$ about this new z' axis (fig. 1.5). Mathematically this means we have a transformation $U = \exp\{-i\omega_e t I_{z'}\}\exp\{-i\alpha I_y\}$. The internal Hamiltonians H_{int} viewed from this doubly-rotating frame become $U^{-1} \cdot H_{int} \cdot U$. From this transformation we obtain terms that are static in the doubly-rotating frame and terms that oscillate with frequency ω_e (and $2\omega_e$). The time average of these oscillating terms is zero and they are thus of no importance for the system. It must be noted, however, that this is only true when the oscillation is fast enough, in other words the frequency ω_e must be large compared to the spread in frequency due to the internal interactions.

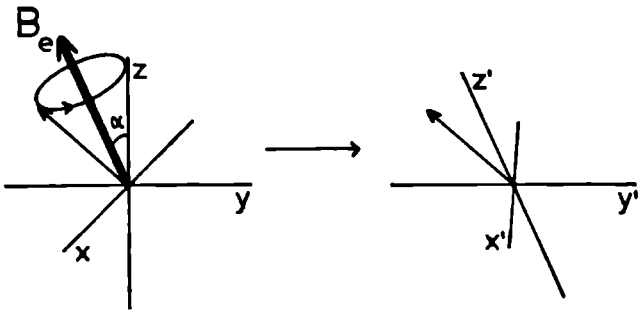

Fig. 1.5 In the rotating frame (left) the spins precess about the effective magnetic field B_e. In the tilted doubly-rotating frame (right) the effect of this effective field is removed and the spins appear to be static.

When we apply these transformations to the internal Hamiltonians of equation (1.34) we see that in the doubly-rotating frame the chemical shift of the S spins remains unchanged. The homonuclear I-I dipolar interaction transforms to [HA68]

$$H_{D,II} = A(3I_{rz},I_{sz},-\bar{I}_r\cdot\bar{I}_s)(3\cos^2\alpha-1) \qquad (1.35)$$

where A contains the geometrical dependence of H_D. The remaining internal Hamiltonians of equation (1.34) contain the I_z operator which transforms to $I_z\cdot\cos\alpha$. Thus for instance the I-S J coupling or the I-S dipolar interaction takes the form

$$H_{IS} = B\cos\alpha\ I_z,S_z \qquad (1.36)$$

This implies that when we make $\alpha = 90°$ the heteronuclear interactions vanish in the doubly-rotating frame and thus when we observe the S spins, only $H_{CS,S}$ will be important. To make $\alpha = 90°$, $B_0-\omega/\gamma$ must be zero which means that the rf radiation has to be resonant for the I spins ($\omega=\omega_0=\gamma B_0$).

1.3.2 Homonuclear decoupling

Equation (1.35) immediately suggests another experiment, namely to make $\alpha = 54.7°$, the magic angle, for which $3\cos^2\alpha-1 = 0$ and the homonuclear I-I dipolar interaction vanishes from the Hamiltonian in the doubly-rotating frame. The interactions dependent on the I_z operator become scaled by a factor $\cos\alpha = 1/\sqrt{3}$ in that case (eq. (1.36)). Consequently, when we irradiate the sample with a rf field that is so far off-resonance that the effective field in the rotating frame makes the magic angle with the z axis, the effect of the homonuclear I-I interactions will vanish from our spectra. This experiment is known as the Lee-Goldburg experiment named after its inventors [LE65]. Suppression of homonuclear I-I interactions is very useful when one wants to study the I-S dipolar interactions from the S spin spectra, as will be shown in chapter 4. Although the I-I dipolar interaction does not directly influence the S spin spectra, it does affect the I-S dipolar interaction because an I spin changes its state constantly in a coupled system due to the so called flip-flop term $I_{r+}I_{s-} + I_{r-}I_{s+}$ contained in the homonuclear dipolar interaction. Hence, to study the pure I-S interaction the I-I dipolar interactions have to be eliminated. In this process, as mentioned above, the I-S interactions are scaled by $1/\sqrt{3}$ in the resulting spectra. In chapter 3 it will be shown how homonuclear decoupling is used in combination with magic angle spinning to reveal the small isotropic J couplings in the solid state.

Homonuclear decoupling of abundant nuclei can also be achieved with cycles of resonant $\pi/2$ pulses. The advantage of the cycles is that there is no need to switch the rf irradiation off-resonance and that the rf radiation is not constantly present so that it becomes possible to monitor the I spin magnetization free of homonuclear interactions, in that way making it possible to study e.g. proton chemical shifts in solids. The first successful cycle was the 4-pulse WAHUHA cycle proposed by Waugh, Huber and Haeberlen [WA68] shown in fig. 1.6

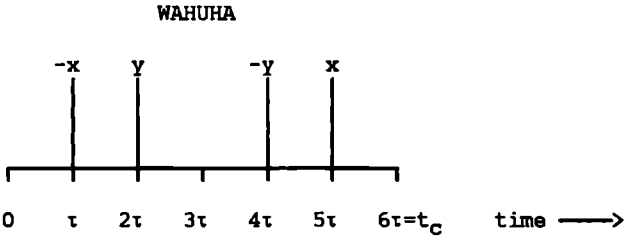

Fig. 1.6 WAHUHA cycle where we assumed the $\pi/2$ pulses to be ideal δ shaped pulses.

To study the effect of this cycle on the homonuclear dipolar interaction we again transform to a sort of "doubly-rotating" frame. However, this frame does not constantly rotate around a fixed axis with respect to the (first) rotating frame. As there is only a rf field present during a pulse, the "doubly-rotating" frame rotates over 90° during this pulse. For each pulse the rotation axis is determined by the phase of the pulse. It must be noted that these pulse phases (fig. 1.6) are defined in the (first) rotating frame. During the so-called windows of the cycle the frame remains static. Accordingly this frame jumps (assuming δ shaped pulses) with respect to the rotating frame in the rhythm imposed by the pulse sequence (fig.1.7). The frame is therefore called the toggling frame. After a full cycle this toggling frame is again aligned with the rotating frame.

When we look at the homonuclear dipolar interactions in the rotating frame we note that it does not become explicitly time-dependent but that it undergoes sudden changes every time a pulse arrives. Assuming the magnetization is sampled at the end of every cycle the system is controlled by the average of the Hamiltonian over one cycle (if $1/t_c$ is large compared to the interaction). When evaluating the homonuclear dipolar interaction and

the terms linear in I_z in the toggling frame one important question arises; how does I_z (in the rotating frame) look as viewed from the toggling frame (fig. 1.7 ,table 1.2). The result is that, as in the case of magic angle irradiation, the average of the homonuclear dipolar interaction vanishes whereas the terms linear in I_z become scaled, because I_z as viewed from the toggling frame lies along the 1,1,1 axis (table 1.2).

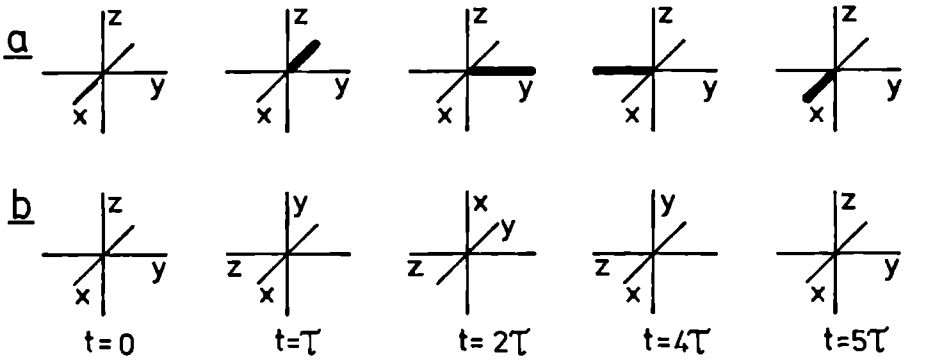

Fig. 1.7 Evolution of the toggling frame (b) during a WAHUHA cycle assuming δ shaped pulses. Every time a pulse arrives in the rotating frame (a), the presence of the magnetic field is removed by an appropriate rotation.

Table 1.2 Appearance of I_z and $3I_{rz}I_{sz}-I_r\cdot I_s$ in the toggling frame during the windows of the multiple pulse cycle shown in fig. 1.6 and their average over one cycle. The vector product $I_r\cdot I_s$ is, of course, invariant under rotations. The pulses are assumed to be δ shaped.

time	$U^{-1}I_zU$	$U^{-1}(3I_{rz}I_{sz}-I_r\cdot I_s)U$
0-τ, 5τ-6τ	I_z	$3I_{rz}I_{sz}-I_r\cdot I_s$
τ-2τ,4τ-5τ	I_y	$3I_{ry}I_{sy}-I_r\cdot I_s$
2τ-4τ	I_x	$3I_{rx}I_{sx}-I_r\cdot I_s$
average	$(I_x+I_y+I_z)/3$	0

In practice $\pi/2$ pulses are never δ shaped pulses, and the success of multiple pulse cycles depends critically on an accurate adjustment of amplitude and phase of the pulses. Problems with the practical exploration of pulse cycles arise from the finite width of the pulses, rf inhomogeneity, variations in the amplitude of the rf field resulting in pulse angle errors, phase errors etc. After the first applications of the WAHUHA cycle several improvements have been proposed, some of which partly compensate pulse errors. From all these cycles MREV-8 [RH73] and BR-24 [BU79] have emerged as the most effective cycles.

1.3.3 Magic angle spinning

In the previous paragraphs it was discussed how interactions can be averaged by manipulating the spins with radiofrequency fields. It was realized very early by the work of Andrew [AN58] and Lowe [LO59] that dipole-dipole interactions could be averaged by mechanically rotating the sample about an axis inclined at the, by now famous, magic angle $\theta_m = 54.7°$ with respect to the external field. As the geometrical part of anisotropic interactions becomes time-dependent due to mechanical rotation, the resulting spectrum will be determined by the time averaged Hamiltonian when the rotation is fast enough. In principle, every interaction which transforms as a second-order spherical harmonic (i.e. every internal interaction except the second-order quadrupole interaction) can be averaged to its isotropic average by magic angle spinning (MAS).

In order to remove dipolar broadening from the spectrum with MAS, the spinning speed must exceed the dipolar line width which is very often not feasible, especially when protons are involved. Due to this restriction the initial interest in MAS soon subsided. MAS regained its popularity after Schaefer and Stejskal [SC76] demonstrated that it could be used to average the ^{13}C chemical shift anisotropy in organic solids when the large dipolar interactions with the surrounding protons were removed simultaneously with heteronuclear decoupling. As these chemical shift anisotropies are generally much smaller than dipolar interactions, the condition that the spinning speed must exceed the line width is much easier fulfilled. It appeared from these studies that the powder patterns of chemical shift anisotropy (contrary to those of homonuclear dipolar interactions) break up into a set of narrow spinning sidebands, when the spinning speed is smaller than the linewidth. An

excellent description of these phenomena has been given by Maricq and Waugh [MA79] and we briefly summarize that description here.

The general appearance of a truncated Hamiltonian in irreducible spherical tensor components is (paragraph 1.2.6)

$$H_X = C^X \, (R^X_{0,0} T^X_{0,0} + R^X_{2,0} T^X_{2,0}) \tag{1.37}$$

$R_{0,0}$ is a scalar which is invariant under rotations. $R_{0,0}$ is only non-zero for the chemical shift in which case it represents the isotropic chemical shift σ_{iso}. The geometrical dependence of the Hamiltonian is contained in the $R_{2,0}$ which becomes time-dependent on sample rotation. We know the appearance of $R_{2,0}$ ($=\rho_{2,0}$) in the principal axis system of R (eq. (1.32)). To obtain $R_{2,0}$ in the laboratory frame we have to transform from the principal axis system (PAS) to a coordinate system fixed in the rotor (RAS), choosing the rotation axis for z axis. We describe this rotation with Euler angles α,β,γ. The next step is to transform from the rotor axis system to the laboratory frame. As the position of the magnetic field in the rotor axis system is given by the polar angles θ_m, $\omega_r t$, the Euler angles for this transformation are $\omega_r t$, θ_m, 0 (fig. 1.8). Summarizing

$$\text{PAS} \xrightarrow{\alpha,\beta,\gamma} \text{RAS} \xrightarrow{\omega_r t,\theta_m,0} \text{LAB} \tag{1.38}$$

$$R_{2,0} = \sum_{m'} D^2_{m',0}(\omega_r t,\theta_m,0) \sum_{m''} D^2_{m'',m'}(\alpha,\beta,\gamma) \, \rho^{PAS}_{2,m''}$$

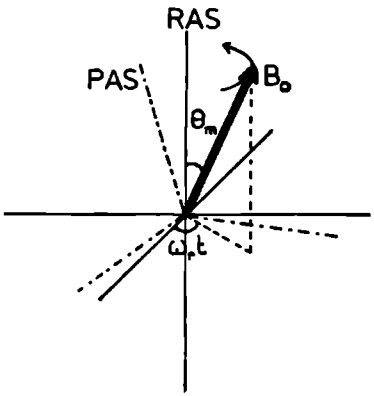

Fig. 1.8 Principal axis system of a spin interaction (PAS) and the external field B_0 as viewed from a coordinate system defined in the rotor (RAS).

Evaluation of eq. (1.38) and substitution in eq. (1.37) gives the resulting time-dependent Hamiltonian

$$H^X = C^X (R_{iso} T_{0,0} + \sqrt{(3/2)} f(t) T_{2,0}) \tag{1.39}$$

with $f(t) = \frac{2}{3}(A\cos(2\omega_r t+2\gamma) + B\sin(2\omega_r t+2\gamma))$

$$+ \frac{2}{3}\sqrt{2} \ (C\cos(\omega_r t+\gamma) + D\sin(\omega_r t+\gamma))$$

$$A = \frac{1}{8}\delta \ (\eta \ (3+\cos 2\beta) \cos 2\alpha + 3(1-\cos 2\beta))$$

$$B = -\frac{1}{2} \delta\eta \cos\beta \sin 2\alpha$$

$$C = \frac{1}{4} \delta \sin 2\beta \ (\eta \cos 2\alpha - 3)$$

$$D = -\frac{1}{2} \delta\eta \sin\beta \sin 2\alpha$$

When the spinning frequency ω_r is large with respect to the frequency spread due to the interaction we are, as in the case of multiple pulse averaging, entitled to take the average Hamiltonian over one cycle. Here the cycle time is simply the rotor period $2\pi/\omega_r$. Consequently, all oscillatory terms vanish from the Hamiltonian leaving only the isotropic term. As was mentioned before it is not always possible to attain spinning speeds larger than the linebroadening. In that case we must realize that the average Hamiltonian we have used so far is in fact the first term in an expansion, the Magnus expansion [HA68, HA76].

$$\bar{H} = H_0 + H_1 + H_2 + \ldots\ldots\ldots \tag{1.40}$$

$$H_0 = \frac{\omega_r}{2\pi} \int_0^{2\pi/\omega_r} H(t')dt', \quad H_1 = \frac{i\omega_r}{4\pi} \int_0^{2\pi/\omega_r} \int_0^{t'} [H(t''),H(t')]dt'dt''$$

The magnitude of the higher-order corrections H_1, H_2, H_n etc. to the average Hamiltonian H_0 are $(t_c/|H|)^n|H|$, where $|H|$ represents the "size" of the Hamiltonian. Thus these higher-order corrections may only be neglected when

$1/t_c >> |H|$. However, all these higher-order terms involve commutators of the time-dependent Hamiltonian with itself at different times. Consequently, for interactions which do commute with itself at different times the average Hamiltonian will give an accurate description of the system (when observations are made at the end of each cycle) even if the condition $1/t_c >> |H|$ is not fulfilled. We call such interactions inhomogeneous. Clearly, the chemical shift anisotropy, heteronuclear dipolar interactions and first-order quadrupole interactions are inhomogeneous. Homonuclear dipolar interactions do not meet this condition because $3I_{rz}I_{sz}-I\cdot I$ does not commute for different spin pairs r,s and r,t. We call such an interaction homogeneous. To summarize if we monitor the time evolution of a spinning system with inhomogeneous interactions synchronously with the rotor revolutions, the result will be determined by the isotropic average of these interactions even if the spinning speed is smaller than the static linewidth.

The next question that arises is how the free induction decay of such a system will look when we do not make our observations synchronous with the rotor. Traditionally the free induction decay of a spin packet with a common resonance frequency is given as $\exp(i\omega t)$. In case of MAS the resonance frequency ω is time-dependent, e.g. for the chemical shift we find

$$\omega(t) = \gamma B_0(\sigma_{iso} + f(t)) \qquad (1.41)$$

It is of course physically incorrect to substitute equation (1.41) in the expression for the FID. We must realize the definition of $\omega = d\varphi(t)/dt$, where $\varphi(t)$ represents the angle over which a certain spin packet has precessed during a time t, and that the FID is given by $\exp(i\varphi(t))$ where $\varphi(t) = \omega t$ only when ω is time independent. Generally the FID becomes

$$\text{FID} \sim \exp\{i \int_0^t \omega(t)\, dt\} \qquad (1.42)$$

Because $\omega(t)$ depends on the orientation of a microcrystallite relative to the field B_0, in a powder every spin packet will follow a specific path determined by $\varphi(t) = \int\omega(t)dt$. The time-dependent part of $\omega(t)$ only contains oscillatory terms of frequency ω_r and $2\omega_r$, therefore the integral of this function will vanish for $t = N2\pi/\omega_r$ (N integer) for every spin packet. This

means that although the magnetization will dephase very quick because every spin packet follows its own path (in the plane perpendicular to B_0), there will be a refocussing of every spin packet at the end of every rotor period. In other words the FID will consist of a train of echoes, generally referred to as rotational echoes (fig. 1.9). Elucidating drawings of the path spin packets follow, are given by Olejniczak et al. [OL84]. Note that the rotor synchronous data acquisition discussed above means sampling at the top of the rotational echoes.

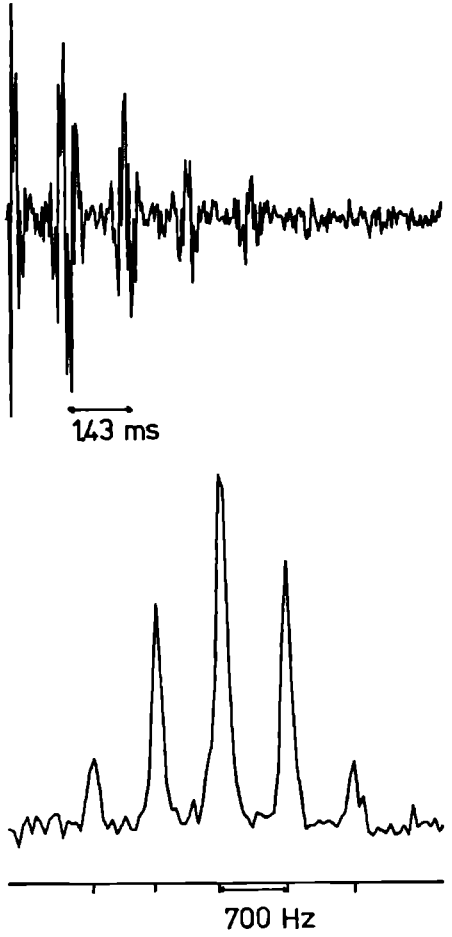

Fig. 1.9 Rotational echo pattern of a sample spinning at the magic angle with a frequency of 700 Hz, which is small compared to the total anisotropy (~ 3300 Hz). The Fourier transform of this signal yields a spectrum consisting of a central line flanked by spinning sidebands.

The Fourier transform of such a train of rotational echoes results in a spectrum that contains the isotropic line flanked by spinning sidebands spaced at the spinning frequency (fig. 1.9). It has been shown by Dixon [DI82] that it is possible to get rid of these sidebands using four properly

spaced π pulses before data acquisition. The sidebands do, however, contain useful information about the total anisotropy. As shown by Maricq and Waugh [MA79] it is possible to recover δ and η by a moment analysis of the sideband spectra. The approach of Herzfeld and Berger [HE80] is to evaluate sideband intensities numerically. They showed that evaluation of equation (1.42) gives, taking all orientations on a sphere in account:

$$\text{FID} = \frac{1}{4\pi}\int_0^{2\pi}\int_0^{\pi} |F|^2 \sin\beta d\beta\, d\alpha\, (\exp\{i(\omega_{iso}t + N\omega_r t)\} \qquad (1.43)$$

$$\text{with } F = \frac{1}{2\pi}\int_0^{2\pi} \exp\{i(-N\theta + \bar{A}\sin 2\theta + \bar{B}\cos 2\theta + \bar{C}\cos\theta + \bar{D}\sin\theta)\}$$

$$\text{where } \bar{A} = -\frac{\gamma B_0}{3\omega_r} A,\ \bar{B} = -\frac{\gamma B_0}{3\omega_r} B,\ \bar{C} = -\frac{\gamma B_0}{3\omega_r} 2\sqrt{2}\ C \text{ and } \bar{D} = -\frac{\gamma B_0}{3\omega_r} 2\sqrt{2}\ D$$

A to D were defined in equation (1.39). Next they calculated sideband intensities for sideband N=-5 to N=5 for a great number of δ and η values and presented the result graphically. These graphs can be used to recover the chemical shift anisotropy of a spinning sample. In chapter 5 of this thesis these calculations are extended to calculate sideband intensities in 2D exchange experiments used to extract information about super-slow motions in solids.

As was mentioned before, the second-order quadrupole interaction does not transform as a second-order spherical harmonic and can therefore not be averaged to zero using MAS. Although there are spinning angles, different from the magic angle, were appreciable narrowing of the second order quadrupole 1/2,-1/2 line shape does occur, no single angle exists where this broadening completely disappears. Spinning about an angle different from the magic angle [BE82, GA82] is only useful in situations where the second order quadrupole interaction is the only linebroadening mechanism, because interactions like the chemical shift anisotropy will no longer be averaged in these so-called Variable Angle Sample-Spinning (VASS) experiments. Nevertheless MAS is advantageous for the central 1/2,-1/2 transition because the resulting powder pattern will be narrowed by a factor ~4. Expressions for the frequency of this central transition under fast MAS have been derived by Behrens and Schnabel [BE82] and by Lippmaa 's group [KU81, SA82] using

second-order perturbation theory. These expressions can be written in the convenient form of equation (1.28) [KE83]

$$\nu_{\frac{1}{2},-\frac{1}{2}} = \frac{\nu_Q^2}{16\nu_Z}\left(I(I+1) - \frac{3}{4}\right)\left(A(\varphi)\cos^4\theta + B(\varphi)\cos^2\theta + C(\varphi)\right) \tag{1.44}$$

$$A(\varphi) = \frac{7}{2} - \frac{7}{3}\eta\cos 2\varphi + \frac{7}{18}\eta^2\cos^2 2\varphi$$

$$B(\varphi) = -3 + \frac{2}{9}\eta^2 + \frac{8}{3}\eta\cos 2\varphi - \frac{7}{9}\eta^2\cos^2 2\varphi$$

$$C(\varphi) = \frac{5}{6} - \frac{1}{3}\eta\cos 2\varphi + \frac{7}{18}\eta^2\cos^2 2\varphi$$

where θ and φ are the polar angles orienting the rotation axis in the principal axis system of the electric field gradient. For polycrystalline samples this leads again to typical powder spectra (fig. 1.3) with peaks and shoulders determined by the condition $d\nu/d\theta = d\nu/d\varphi = 0$ (fig. 1.4).

References

AB61 A. Abragam, "Principles of Nuclear Magnetism", Oxford University Press, London, 1961.

AN58 E.R. Andrew, A. Bradbury and R.G. Eades, Nature 182, 1659, 1958.

BA69 J.F. Baugher, P.C. Taylor, T. Oya and P.J. Bray, J. Chem. Phys. 50, 4914, 1969.

BE82 H.-J. Behrens and B. Schnabel, Physica 114B, 185, 1982.

BR79 D.M. Brink and G.R. Satchler, "Angular Momentum", Oxford University Press, Oxford, 1979.

BU79 D.P. Burum and W.K. Rhim, J. Chem. Phys. 71, 944, 1979.

CO57 M.H. Cohen and F. Reif, "Quadrupole Effects in Nuclear Magnetic Resonance Studies of Solids", in Solid State Physics, vol. 5, F. Seitz and D. Turnbull eds., Academic Press, New York, 1957.

DA58 T.P. Das and E.L. Hahn, "Nuclear Quadrupole Resonance Spectroscopy", in Solid State Physics, supplement 1, F. Seitz and D. Turnbull eds., Academic Press, New York, 1958.

DI82 W.T. Dixon, J. Chem. Phys. 77, 1800, 1982.

GA82 S. Ganapathy, S. Schramm and E. Oldfield, J. Chem. Phys. 77, 4360, 1982.

HA68 U. Haeberlen and J.S. Waugh, Phys. Rev. 175, 453, 1986.

HA76 U. Haeberlen, High Resolution NMR in Solids, in Advances in Magnetic Resonance, Supplement 1, J.S. Waugh Ed., Academic Press, New York, 1976.

HE80 J. Herzfeld and A.E. Berger, J. Chem. Phys., 73, 6021, 1980.

KE83 A.P.M. Kentgens, K.F.M.G.J. Scholle and W.S. Veeman, J. Chem. Phys. 87, 4357, 1983.

KU81 E. Kundla, A. Samoson and E. Lippmaa, Chem. Phys. Lett. 83, 229, 1981.

LE65 M. Lee and W.I. Goldburg, Phys. Rev. A 140, 1261, 1965.

LO59 I.J. Lowe, Phys. Rev. Lett. 2, 258, 1959.

MA79 M.M. Maricq and J.S. Waugh, J. Chem. Phys. 70, 3300, 1979.

ME76 M. Mehring, "High Resolution NMR Spectroscopy in Solids", in "NMR: Basic Principles and Progress", vol. 11, P. Diehl, E. Fluck and P. Kosfeld eds., Springer, New York, 1976.

NA66 K. Narita, J-I. Umeda and H. Kusumoto, J. Chem. Phys. 44, 2719, 1966.

OL84 E.T. Olejniczak, S. Vega and R.G. Griffin, J. Chem. Phys., 81, 4804, 1984.

RH73 W.K. Rhim, D.D. Elleman and R.W. Vaughan, J. Chem. Phys. 59, 3740, 1973.

RO57 M.E. Rose, "Elementary Theory of Angular Momentum", John Wiley and Sons, Inc., New York, 1957.

RO82 J.B. Robert and L. Wiesenfeld, Physics Reports 86, 363, 1982.

SA82 A. Samoson, E.Kundla and E. Lippmaa, J. Magn. Res. 49, 350, 1982.

SC76 J. Schaefer and E.O. Stejskal, J. Am. Chem. Soc. 98, 1031, 1976.

SI80 C.P. Slichter, "Principles of Magnetic Resonance", corrected second printing, Springer, New York, 1980.

VL48 J.H. Van Vleck, Phys. Rev. 74, 468, 1948.

WO79 D. Wolf, "Spin-Temperature and Nuclear Spin Relaxation: Basic Principles and Applications", Oxford University Press, Oxford, 1979.

CHAPTER 2

TWO-DIMENSIONAL NMR

2.1 Introduction

The introduction of Fourier Transform (FT) NMR (in 1966) was a very important step in the development of nuclear magnetic resonance. The great advantage of FT NMR over the traditional Continuous Wave (CW) techniques is the higher sensitivity, arising from the fact that various transitions are excited with one short radiofrequency pulse and that the pulse responses of many experiments can be accumulated. This gain in sensitivity made it possible to record spectra of rare nuclei like ^{13}C. This sensitivity improvement is, however, not the only benefit of FT NMR. With the introduction of pulse techniques a whole new field of experiments was opened, as pulses can be used in various ways to manipulate the spin system.

A major development was the proposition of two-dimensional FT NMR by Jeener in 1971 [JE71]. This concept involves the detection of an NMR signal as a function of two time variables so that it becomes possible to relate the behaviour of the spin system during two time intervals. Subsequent Fourier transformation to both time variables yields a spectrum with two (correlated) frequency domains. It took several years before the first 2D experiments were actually performed and in 1976 the first thorough theoretical treatment appeared in the literature [AU76]. The initial development of 2D NMR was (as was the case with standard NMR) somewhat restrained by computer limitations. But with the booming expansion of computer performance in the early eighties all these restrictions have vanished and a wealth of 2D experiments has emerged. For instance, the elucidation of complex structures like proteins and other large organic compounds in solution has become possible using 2D NMR. At this moment 2D techniques are used on a routine basis in university as well as industrial laboratories for structural analysis of compounds in solution. Two-dimensional solid state NMR has not reached that stage yet but, as we hope to show in this thesis, holds some promises for the future.

2.2 General description of two-dimensional NMR

Aue et al. [AU76] give a thorough quantum mechanical description of 2D NMR. This description is presented in a simplified form in the book of Bax

[BA82]. We see no benefit in repeating such a description here. In this paragraph we first present a less general but more illustrative classical approach using "Bloch-type" magnetization vectors. After that we indicate the quantum mechanical treatment by introducing the density matrix concept.

2.2.1 Classical description

Two-dimensional experiments are divided in four time intervals (fig. 2.1). The preparation period generally consists of a long delay to allow the system to reach thermal equilibrium followed by one or more pulses to bring the system in its initial state (which normally means creation of transverse magnetization). During the subsequent evolution period the system evolves under certain spin interactions chosen by the spectroscopist by eliminating all unwanted interactions. The duration of this evolution period is the first time variable in the 2D experiment.

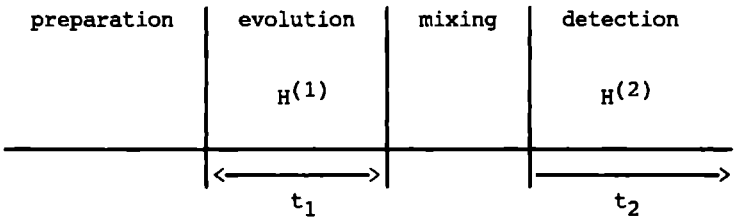

Fig. 2.1 General division of a two-dimensional experiment in four time domains. The mixing time is not always present.

In some experiments there is a mixing period consisting of pulses and fixed delays to relate the evolution to the detection period during which the signal is detected. Thus an experiment is performed for a certain t_1 value. By performing a number of experiments for different t_1 values while leaving all other settings constant a series of time domain signals is obtained. Fourier transformation of these signals with respect to t_2 and t_1 results in a two-dimensional frequency spectrum showing the state of the spin system during evolution and detection period and their possible correlation.

This process is most easily understood when considering a specific experiment and follow the evolution of a few specific spin packets. Consider,

for instance, the so-called proton-flip experiment [BO76] to relate the heteronuclear J_{CH} coupling (in one dimension) to the isotropic ^{13}C chemical shift (in the other dimension). The pulse scheme for this experiment in solution together with the evolution of the magnetization vectors of a ^{13}C nucleus coupled to one proton is given in fig. 2.2. After the system is allowed to reach thermal equilibrium a ^{13}C $\pi/2$ pulse is applied to create transverse magnetization. For a carbon nucleus coupled to one proton we get two magnetization components with a different resonance frequency. The precession of the two magnetization components in the x-y plane of the rotating frame is determined by their resonance frequencies, $\omega_f = \omega_{CS} + 2\pi J/2$ and $\omega_s = \omega_{CS} - 2\pi J/2$, where f and s refer to the fast and slow component. Halfway the evolution time ($t_1/2$) a π pulse is applied to carbon as well as proton spins. The ^{13}C π pulse results in a 180° rotation of the magnetization vectors. Due to the ^1H π pulse every proton changes its state from $|1/2\rangle$ to $|-1/2\rangle$ or vice versa. This means that the resonance frequency of the fast component in the first half of the evolution period now becomes slow: $\omega_{CS} - 2\pi J/2$, and that the slow component now becomes fast: $\omega_{CS} + 2\pi J/2$. At time t_1 one of the magnetization components will thus have precessed through the angle $(2\pi J/2)t_1$ and the other component through the angle $-(2\pi J/2)t_1$, independent of the chemical shift. At this point the ^{13}C signal will be acquired under heteronuclear decoupling, which means that the resonance frequency of both magnetization components will be ω_{CS} during the detection period t_2. Thus the signal acquired during t_2 will be modulated in phase by the heteronuclear J coupling in t_1

$$S(t_1,t_2) = M_0 \exp\{i(\omega_{CS}t_2 \pm (2\pi J/2)t_1)\} \exp\{-\frac{t_1}{T_2^{(1)}}\} \exp\{-\frac{t_2}{T_2^{(2)}}\} \qquad (2.1)$$

where $T_2^{(1)}$ and $T_2^{(2)}$ are the decay rates expressing the decay of magnetization during the evolution and detection period. Fourier transformation of this signal gives a 2D spectrum with two peaks whose position are given by ν_{CS} in the F_2 dimension and by $\pm J/2$ in the F_1 dimension. In chapter 3 it will be shown how this experiment can be performed in solids using magic angle spinning and multiple pulse decoupling.

In the case of 2D-J spectroscopy discussed above the signal detected during t_2 was modulated in phase by the J coupling present during the evolution period. Another possibility is that the magnitude of the magnetization vectors, whose precession is detected during t_2, depends on the

interaction present during the evolution period. In that case one speaks of amplitude modulation. The general expression for the detected signal is then given by

$$S(t_1,t_2) = M_0 \cos(\omega_1 t_1) \exp(i\omega_2 t_2) \exp\{-\frac{t_1}{T_2^{(1)}}\} \exp\{-\frac{t_2}{T_2^{(2)}}\} \qquad (2.2)$$

where ω_1 and ω_2 represent the resonance frequency in respectively the evolution and detection period. An example of amplitude modulation is the 2D exchange experiment discussed in chapter 5. The effect of phase- and amplitude modulation on the resulting line shapes will be discussed in paragraph 2.3.

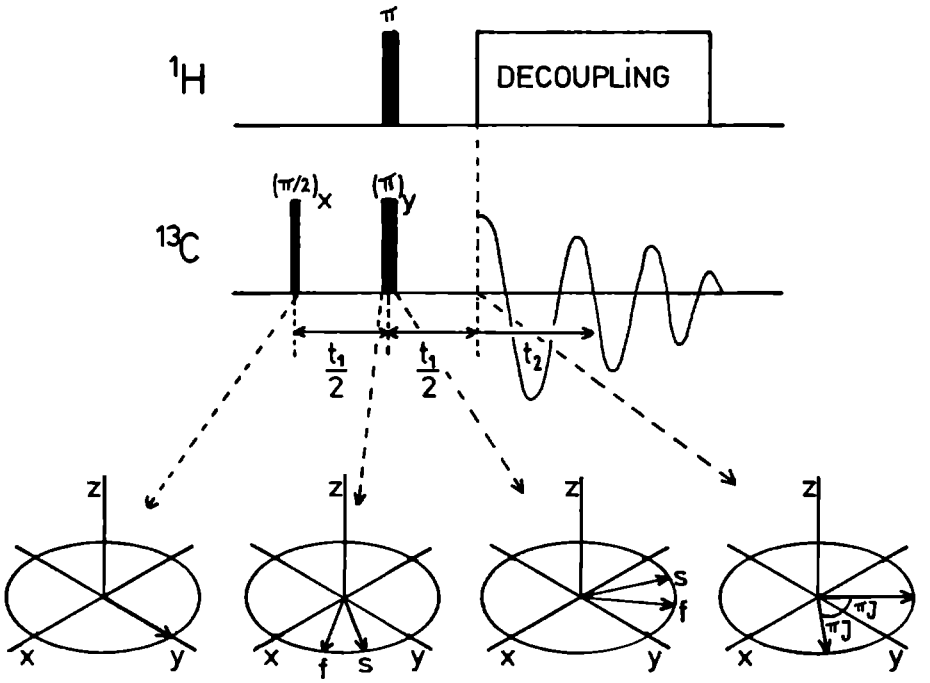

Fig. 2.2 Pulse sequence for the proton flip experiment in solutions, and the evolution of the magnetization components of carbon spins coupled to one proton. f and s refer to the fast and slow magnetization component, $\omega_f = \omega_{CS} + 2\pi J/2$ and $\omega_s = \omega_{CS} - 2\pi J/2$.

2.2.2 Quantum mechanical description

It is not always possible to describe an experiment by a simple picture using classical magnetization vectors as was done for the 2D-J experiment in the previous section. Especially when multiple quantum transitions play a role in the evolution period such a classical description is no longer possible. This is because multiple quantum transitions do not lead to observable magnetization, still in certain experiments they can modulate the signal acquired during the detection period t_2. In such a case we have to resort to a density matrix calculation.

The density matrix concept is used to give a statistical description of an ensemble of spins. Consider an isolated spin system which can be described with a complete set of eigenstates $|n\rangle$. It is possible to expand a general state ψ in a linear combination of these eigenstates

$$\psi = \sum_n c_n |n\rangle \tag{2.3}$$

Consequently, the expectation value $\langle A \rangle$ of an operator A becomes

$$\langle A \rangle = \langle \psi | A | \psi \rangle = \sum_{m,n} c_m^* c_n \langle m | A | n \rangle \tag{2.4}$$

For an ensemble of identical spin systems, which individually can of course be in different states, we have to take the average over the whole ensemble:

$$\overline{\langle A \rangle} = \sum_{m,n} \overline{c_m^* c_n} \langle m | A | n \rangle \tag{2.5}$$

The average of the products of the complex coefficients c are considered to be elements of a matrix, the (Hermitian) density matrix σ

$$\sigma_{nm} = \overline{c_m^* c_n} = \overline{|c_n||c_m| \exp\{i(\alpha_n - \alpha_m)\}} \tag{2.6}$$

where $|c_n|$ represents the absolute value of coefficient c_n and α_n the corresponding phase angle. Using the density matrix the expectation value in equation (2.5) is given by the trace $Tr\{\sigma \cdot A\}$.

The diagonal elements σ_{nn} of a normalized ($\Sigma\ \sigma_{nn} = 1$) density matrix give the probability to find an arbitrary spin system in state $|n\rangle$. Accordingly, if one multiplies this number with the total number of spin system one finds the population of state $|n\rangle$. The off-diagonal elements of σ can only be non-zero when there is a coherence between the phase angles α_m and α_n. In thermal equilibrium these elements are always zero (random phase approximation).

The time dependence of a state ψ in a system described by the time-independent Hamiltonian H follows from the Schrödinger equation

$$i\hbar \frac{d\psi}{dt} = H\psi \tag{2.7}$$

Substitution of the expansion of eq. (2.3) in equation (2.7), considering only the coefficients c_n to be time dependent, is used to obtain the time evolution of the density matrix

$$\frac{d\sigma}{dt} = -\frac{i}{\hbar}[H,\sigma] \tag{2.8}$$

This equation is generally known as the Liouville - von Neumann equation, whose solution gives

$$\sigma(t) = \exp\{-iHt/\hbar\}\cdot\sigma(0)\cdot\exp\{iHt/\hbar\} \tag{2.9}$$

In a basis of eigenfunctions of H this becomes

$$\sigma_{nm}(t) = \exp\{i(E_m-E_n)t/\hbar\}\ \sigma_{nm}(0) \tag{2.10}$$

Thus when a coherence between two different states $|m\rangle$ and $|n\rangle$ exists, the corresponding density matrix element is oscillatory with frequency $\omega_{nm} = E_m-E_n/\hbar$. Usually we work in the rotating frame and the time evolution of σ in the rotating frame is found by taking the truncated Hamiltonian in the rotating frame for H in equation (2.9).

The description of a 2D experiment now simply means the calculation of the evolution of the density matrix during the pulse sequence, starting with the density matrix in thermal equilibrium. The effect of a ideal $\pi/2$ pulse along x axis in the rotating frame, for instance, can be calculated as

$$\sigma(t_+) = \exp\{i\frac{\pi}{2} I_x\}\cdot\sigma(t_-)\cdot\exp\{-i\frac{\pi}{2} I_x\} \qquad (2.11)$$

where t_- and t_+ refer to the time directly before and after the pulse. According to the time scale of fig. 2.1 we have to calculate the density matrix in four steps [BA82]:

σ_{eq} thermal equilibrium
$\sigma(0)$ at the end of the preparation period
$\sigma(t_1)$ at the end of the evolution period
$\sigma(t_1,0)$ at the end of the mixing period
$\sigma(t_1,t_2)$ at time t_2 during the detection period.

When $\sigma(t_1,t_2)$ has been calculated the detected signal during the detection period is given by

$$S(t_1,t_2) = Tr\ \{\sigma(t_1,t_2)\cdot(I_x+iI_y)\} \qquad (2.12)$$

Here we assumed quadrature detection, which means that the magnetization is monitored along the x axis and y axis of the rotating frame. It is clear that only those elements of $\sigma(t_1,t_2)$ which correspond to single quantum coherences give a contribution to the detected signal. These elements can, however, contain contributions of multiple and/or zero quantum coherences of the density matrix $\sigma(t_1)$ during the evolution period. So these multiple quantum transitions can be made visible by observing how they modulate the normal single quantum transitions during the detection period. In chapter 6 we discuss nutation NMR of half-integer quadrupole nuclei using the density matrix concept. In that case there are several transition in an $I > 1/2$ system that play a role during the evolution period whereas only the central 1/2,-1/2 transition is detected during t_2.

2.3 Different kinds of modulation.

As was mentioned above we distinguish two kinds of modulation in 2D experiments. Although the information a phase or amplitude modulated spectrum gives is in principle the same, they give different line shapes in the frequency domain. To understand this we first have to consider a normal 1D signal, obtained using quadrature detection. Assume we have a spectrum consisting of a single line at frequency F. The signal can be written as

$$S(t) = M_0 \exp\{iFt\} \exp\{-\frac{t}{T_2}\} \qquad (2.13)$$

A complex Fourier transformation of this signal gives

$$S(\omega) = \int_0^\infty S(t) \exp\{i\omega t\}\, dt = A(\omega) + iD(\omega) \qquad (2.14)$$

with $A(\omega) = \dfrac{T_2}{1 + T_2^{\,2}(\omega-F)^2}$ and $D(\omega) = \dfrac{T_2^{\,2}(\omega-F)}{1 + T_2^{\,2}(\omega-F)^2}$

Actually the computer system stores the real (along x axis) and imaginary (along y axis) signal in separate buffers. The complex Fourier transformation is performed by separately transforming the contents of these buffers with a sine and a cosine function. Therefore it is useful to know the result of a cosine transformation on a cosine signal etc.:

Signal	Fourier Transform	Result
cos(Ft)	cos(ωt)	A(ω)+A(-ω)
cos(Ft)	sin(ωt)	D(ω)-D(-ω)
sin(Ft)	cos(ωt)	D(ω)+D(-ω)
sin(Ft)	sin(ωt)	-A(ω)+A(-ω)

The exponential decay function has been omitted and should be thought to be implicitly present. By combining these expressions properly the result of equation (2.14) is obtained. It is obvious from these expressions that quadrature detection is needed to discriminate between positive and negative resonance frequencies. The process of Fourier transformation and the resulting line shape is given in fig. 2.3. The real part resulting from the Fourier transformation, which is the spectrum normally displayed, consists of an absorptive Lorentzian line shape. The imaginary term consists of a dispersive line shape. The disadvantage of the dispersive signals is that they are very broad because of their wide tails, and thus result in a lower spectral resolution.

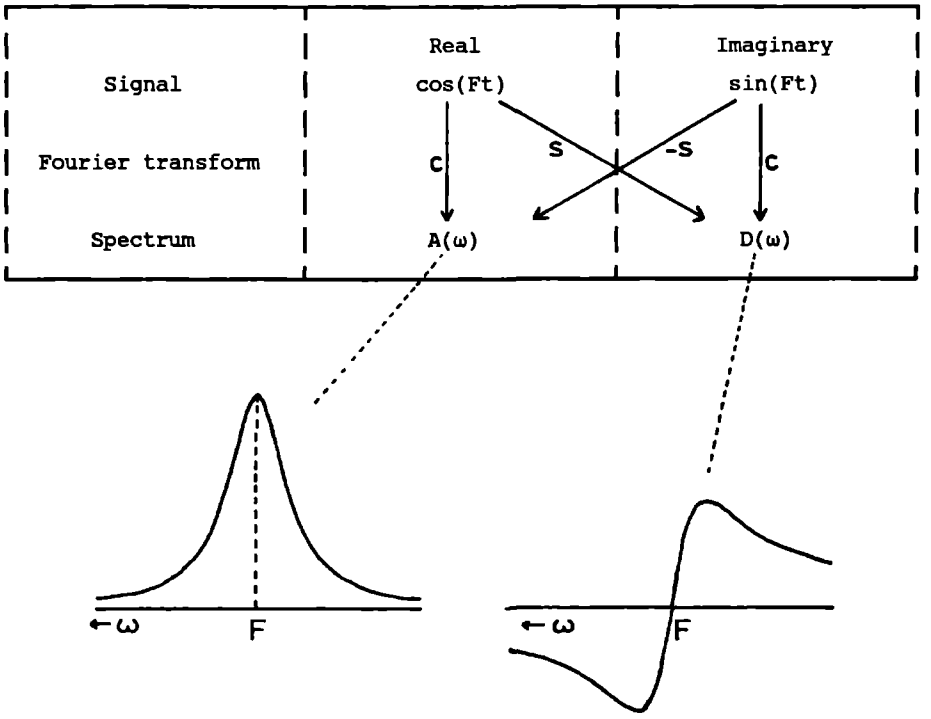

Fig. 2.3 Schematic presentation of a NMR signal obtained with quadrature detection and the resulting spectrum after Fourier transformation. The letters c and s refer to cosine and sine transform.

In a 2D experiment a series of (complex) FID's are collected as a function of t_1. These FID's are then transformed in the way described above. This gives a series of spectra which are modulated in phase or amplitude (fig. 2.4). The next step is to take the n^{th} point of the real and imaginary buffer of each spectrum and combine these points to form the n^{th} (complex) interferogram, in other words we take a slice along t_1 out of the spectra shown in fig. 2.4. These interferograms are damped oscillating functions of t_1 like a FID. These interferograms are then Fourier transformed to obtain the 2D spectrum.

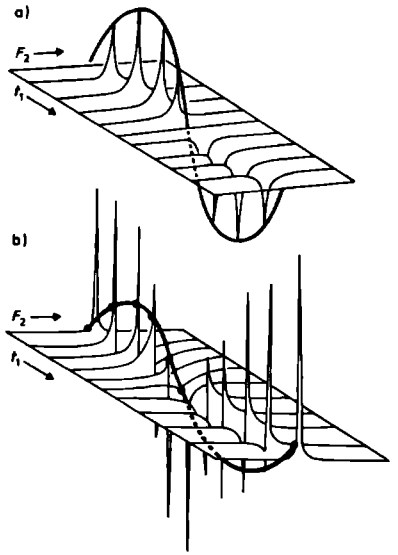

Fig. 2.4 Amplitude (a) and phase (b) modulation in a 2D spectrum. The picture shows the situation after the first Fourier transformation to t_2. Slices in t_1 direction displaying the modulation as function of t_1 are called interferograms. (reproduced from [BE83]).

2.3.1 Phase modulation

It appears that the result of this operation depends on the type of modulation. Consider one line in a 2D spectrum with frequency F_1 during the evolution period t_1 and frequency F_2 during t_2. In case of phase modulation we get

$$S(t_1,t_2) = C \exp\{i(F_1t_1+F_2t_2)\} \qquad (2.15)$$

For clarity the exponential decay functions are omitted. The Fourier transformations and the resulting line shape are given in fig. 2.5. As can be seen the real part of the resulting spectrum is a superposition of a 2D absorptive and dispersive line shape. In fact we have obtained the notorious "phase-twisted" line shape [BO77] which has broad flanks. If we divide this line in four quadrants, two flanks are positive whereas the two other flanks are negative. These phase-twisted line shapes are not very popular in 2D spectroscopy of solutions where high resolution is very important. In 2D solid state NMR, however, the phase-twisted line shape can lead to disastrous results. Here not the lower resolution is a problem, but the negative flanks. 2D powder patterns consist of broad ridges because the spins have different resonance frequencies due to the anisotropy of the spin interactions [LI80].

When the negative flanks of neighboring lines in a ridge point to each other this leads to an extinction of the ridge (fig. 2.6). Even when this extinction does not (completely) occur the phase-twisted line shape generally distorts the resulting spectrum so much that it is no longer possible to interpret the spectra "intuitively" using ones common knowledge of the appearance of powder patterns. We will show in chapter 4, however, that it is possible to interpret the spectrum by convoluting calculated spectra with the appropriate line shape.

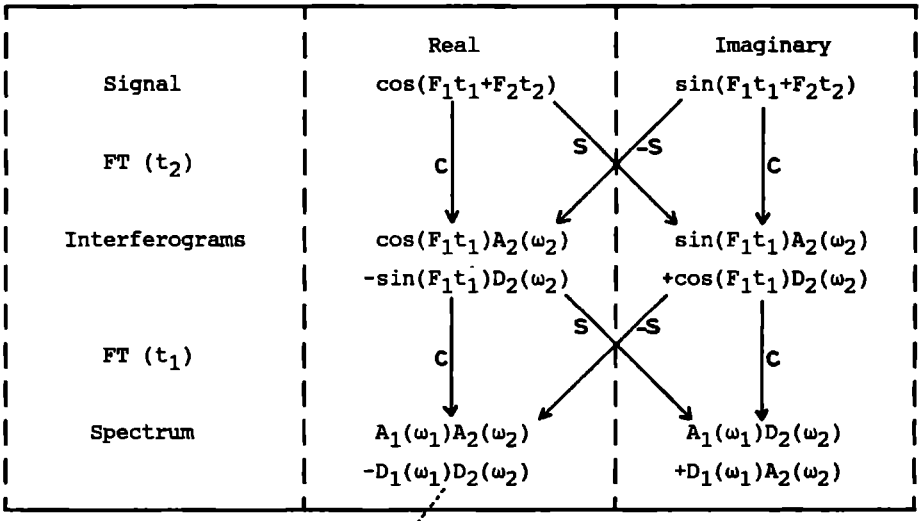

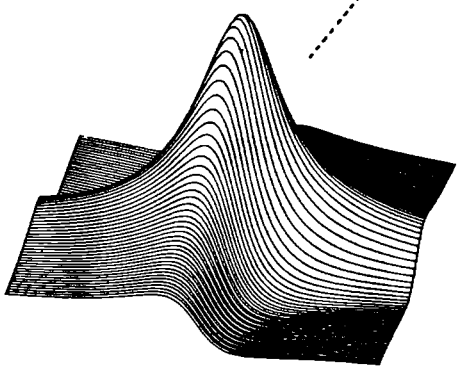

Fig. 2.5 Schematic presentation of the processing of a phase modulated signal and the resulting phase twisted line shape. In practice not these phase twisted line shapes are displayed but a magnitude calculation ($\sqrt{(R^2 + I^2)}$ where R is the real and I is the imaginary signal) is performed before displaying the spectrum. This to avoid phasing problems.

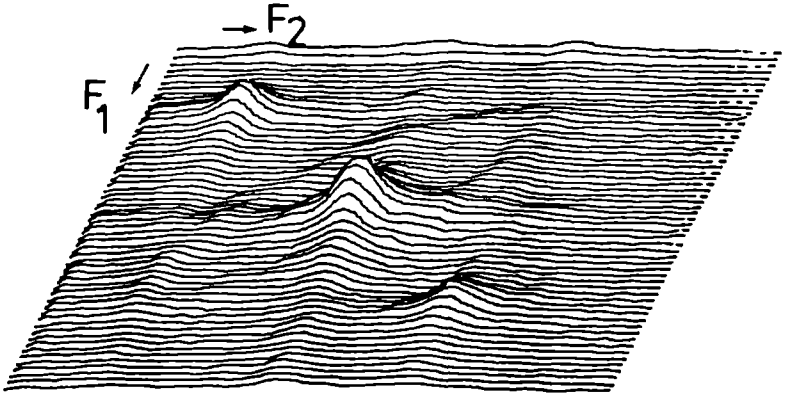

Fig. 2.6 Stacked plot of a chemical shift powder pattern with phase twisted line shapes. As a result of destructive interference we do not observe the expected chemical shift powder pattern along the diagonal. Only some intensity at the positions of peaks and shoulders of the pattern is left.

2.3.2 Amplitude modulation

In case of amplitude modulation, omitting the exponential decay, the signal becomes

$$S(t_1,t_2) = C \cos\{F_1 t_1\} \exp\{iF_2 t_2\} \qquad (2.16)$$

When we transform this signal in the same way as mentioned above, again phase-twisted line shapes will be obtained. However if we apply only a real transform to the interferograms, the result will be a pure 2D absorptive line shape. This effect can be reached by blanking the imaginary buffer before the second Fourier Transform is applied (fig. 2.7). Although amplitude modulation is favorable in view of line shape it has also a disadvantage. As can be seen from the expressions in fig. 2.7 it is no longer possible to determine the sign of F_1. Without sign discrimination the spectrum will be mirrored with respect to the transmitter reference frequency, thus making it impossible to know which resonance frequencies are larger and which are smaller than the reference frequency. This problem can be avoided by placing the transmitter reference frequency at one side of the spectral region. Doing so requires a

doubling of the sampling frequency to avoid aliasing of resonance lines about the Nyquist frequency. The Nyquist frequency is half the sampling frequency, it is the highest frequency that can be sampled properly. In other words when dealing with amplitude modulation, one has to obtain twice as many FID's as a function of t_1 as compared to phase modulation.

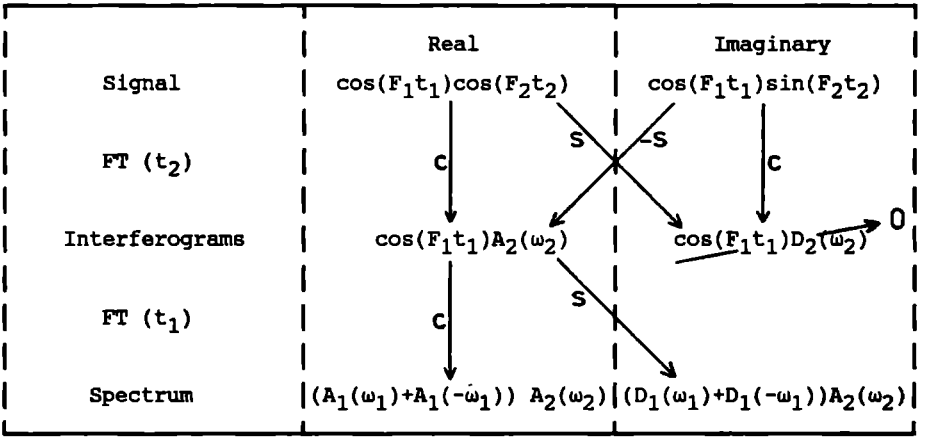

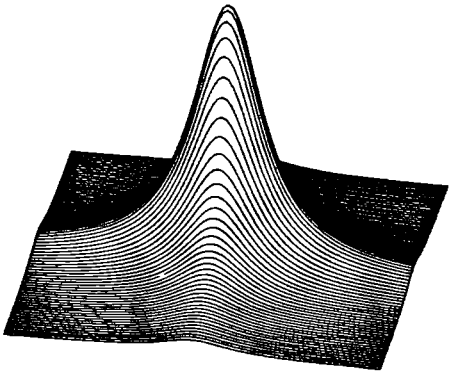

Fig. 2.7 Schematic presentation of the processing of an amplitude modulated signal. When the imaginary buffer is blanked prior to the second Fourier transformation, a pure absorption line shape can be obtained.

2.3.3 Interconversion of modulation type

As we have seen both types of modulation have their shortcoming, and it depends on the specific conditions which type of modulation is preferred. It is possible to convert amplitude modulation into phase modulation using proper phase cycling of the pulses. This is achieved by carrying out the experiment which gives the cosine modulation (eq. (2.16)) first. Then the phases of the pulses preceding the evolution period are shifted by $\pi/2$

radians (for single quantum transitions) to give a $\sin(F_1t_1)$ modulated signal. Simultaneously the receiver phase is shifted $\pi/2$ radians, causing a $\pi/2$ shift of the detected signal. The signal then becomes

$$S(t_1,t_2) = C \sin\{F_1t_1\} \exp\{i(F_2t_2 + \pi/2)\} \tag{2.17}$$

Adding of this signal to that of equation (2.16) obviously results in a phase modulation

$$\begin{aligned} S(t_1,t_2) &= C [\cos\{F_1t_1\}+\sin\{F_1t_1\} \exp\{i\pi/2\}] \exp\{iF_2t_2\} \\ &= C \exp\{iF_1t_1\} \exp\{iF_2t_2\} \end{aligned} \tag{2.18}$$

This means that in an amplitude modulation experiment sign discrimination of F_1 can be obtained, however, with the introduction of phase-twisted line shapes.

The conversion from phase modulation into amplitude modulation is only possible when a so-called reversed precession signal can be obtained [BA77]. This is achieved by inserting a π pulse at the end of the evolution period. This π pulse changes the angle $\varphi = F_1t_1$ a spin packet has precessed through during t_1, to $-\varphi$. Thus the sum of the normal and the reversed precession signal results in an amplitude modulated signal ($\exp\{-iF_1t_1\} + \exp\{iF_1t_1\} = \cos\{F_1t_1\}$). When the π pulse mixes the spin states (as is the case when homonuclear couplings are present) this approach is not applicable [BA77].

2.3.4 Sign discrimination combined with pure absorption line shapes

Two methods have been proposed to obtain spectra which consist of pure absorption line shapes and allow discrimination of the sign of F_1 as well. In the method due to States et al. [ST82] a cosine and a sine modulated signal are recorded separately. These two signals are then transformed with respect to t_2

$$\begin{aligned} C \cos\{F_1t_1\}\exp\{iF_2t_2\} &\xrightarrow{FT} C \cos\{F_1t_1\}(A_2(\omega_2) + iD_2(\omega_2)) \\ C \sin\{F_1t_1\}\exp\{iF_2t_2\} &\xrightarrow{FT} C \sin\{F_1t_1\}(A_2(\omega_2) + iD_2(\omega_2)) \end{aligned} \tag{2.19}$$

The imaginary parts of these two sets of interferograms are (after proper phasing of the F_2 spectra) eliminated and the real parts of the files are merged to form one set of complex interferograms

$$S(t_1,\omega_2) = C\ (\cos\{F_1 t_1\} + i\sin\{F_1 t_1\})\ A_2(\omega_2) \qquad (2.20)$$

A Fourier transformation with respect to t_1 now gives a spectrum whose real part has a pure absorption line shape $S(\omega_1,\omega_2) = A_1(\omega_1)A_2(\omega_2)$, which means that the intended result has been achieved.

The method proposed by Marion and Wühtrich [MA83] is based on the time-proportional phase incrementation (TPPI) technique [RE75] used to obtain quadrature detection with only one ADC (Bruker spectrometers work with this principle). In the TPPI method the phase of the receiver is shifted $\pi/2$ radians after every sample point. This series of sample points is stored in one buffer. With a sampling time τ the signal can be written as

$$\begin{aligned}
&\text{first point:} && S(t) = C\cos(F\tau) && = C\sin\{(F+(\pi/2\tau))\tau\}\\
&\text{second point:} && S(t) = -C\sin(F2\tau) && = C\sin\{(F+(\pi/2\tau))2\tau\}\\
&\text{third point:} && S(t) = -C\cos(F3\tau) && = C\sin\{(F+(\pi/2\tau))3\tau\}\\
&\text{fourth point:} && S(t) = C\sin(F4\tau) && = C\sin\{(F+(\pi/2\tau))4\tau\}\\
&\text{generally:} && S(t) = C\sin\{(F+(\pi/2\tau))t\}
\end{aligned} \qquad (2.21)$$

As $\pi/2\tau$ is equal to half of the spectral width, the spectrum resulting after transformation will be shifted by half the spectral width, thus making it possible to put the transmitter in the centre of the spectral region and discriminate between negative and positive frequencies even though we only collected one series of data instead of a separate real and imaginary signal as is common in quadrature detection. The 2D generalization of this method means that the phase of the pulse preceding the evolution period is increased $\pi/2$ radians for every t_1 value to achieve a TPPI for the t_1 amplitude modulation. After Fourier transformation and elimination of the complex signal, the interferograms look like

$$S(t_1,\omega_2) = C\sin\{(F+(\pi/2\tau))t_1\}\ A_2(\omega_2) \qquad (2.21)$$

which obviously can be transformed with a sine to yield pure absorption line

shapes combined with sign discrimination because of the $\pi/2\tau$ frequency offset.

As was mentioned before it is advantageous to obtain pure absorption line shapes for optimal resolution and minimal file sizes. Therefore it is obvious that one would also like to use the techniques of States et al. [ST82] and Marion and Wüthrich [MA83]. The programs to process the acquired data in the appropriate way have recently come available on commercial spectrometers. If it is not possible to use these techniques, then for 2D solid state powder spectra, amplitude modulation is preferred.

2.4 Present state of 2D solid state NMR

The main aim in the development of solid state NMR has been toward high resolution to obtain spectra that could be compared to spectra obtained in solution. Especially for ^{13}C NMR the combined use of magic angle spinning and heteronuclear decoupling has been very successful in this respect. This technique is, however, not restricted to ^{13}C. For instance, ^{29}Si which is important in silicates attracts a lot of attention these days. Recently also some progress is made in high resolution proton NMR of solids, combining magic angle spinning with homonuclear dipolar decoupling techniques (generally known as CRAMPS [PE77, SC76]).

Some attempts have been made to obtain two-dimensional solid state spectra which are analogous to spectra obtained in solution. Caravatti et al. have succeeded in obtaining heteronuclear carbon-proton chemical shift correlated spectra of single crystals [CA82]. A variation of this experiment was applied to powders by Caravatti et al. [CA83] and Roberts et al. [RO84]. Heteronuclear 2D-J resolved NMR of solids [TE82, MA84, MI86, KE87], discussed in chapter 3 of this thesis, is also based on experiments in solution. To perform these experiments multiple pulse techniques are needed which demand an accurate setting of the spectrometer. For 2D experiments these settings must be stable over longer periods of time. Although commercial high power spectrometers suitable for executing multiple pulse cycles are available, most multiple pulse experiments were carried out by only a few groups which have a long experience with these techniques.

Bax et al. [BA83] and Takegoshi and McDowell [TA86] showed that methods relying on the same idea as used for liquid state coherent off-resonance decoupling can be applied in solids to determine proton chemical shifts. Menger et al. [ME84] demonstrated that it is possible to observe carbon-

carbon couplings in solids analogous to the multiple quantum experiments used to determine these couplings in solutions. It must be noted, however, that none of the above mentioned "liquid like" 2D solid state experiments have found many applications of physically or chemically interesting systems.

It appears that there are more 2D experiments that explicitly exploit the anisotropic character of the spin interactions in solids. The advantage of 2D NMR in studies of anisotropic interactions is the possibility to map out different interactions in two dimensions, thus preventing spectral overlap and creating the possibility to study the geometrical interdependence of the spin interactions. For instance, as will be discussed in chapter 4, it is possible to separate heteronuclear dipolar interactions from the chemical shift anisotropy. Waugh and coworkers [HE76, RY77, OP77] used this technique to obtain information on the orientation of C-H bonds in several single crystals and oriented polymers. Stoll et al. [ST76] and Linder et al. [LI80] applied the technique to powdered samples, demonstrating the potential of the technique to obtain geometrical, orientational and motional information. In chapter 4 we show how the orientation of the chemical shift tensor in poly-(oxymethylene) could be determined using this technique [MA87]. Munowitz et al. [MU81, MU82, MN82, MU84] developed a slow spinning variant of this experiment, which has been used by Schaefer et al. [SC83, SC84, SH84, SA84, SC85] to study motions in the kHz regime in polymers. These spinning experiments were extended by Terao, Miura and Saika [TE86, MU86] who switch the spinning axis on and off the magic angle between the evolution and detection period in order to obtain scaled-down powder patterns of the dipolar interactions to facilitate the interpretation of the spectra. Schuff and Haeberlen [SU83] described a 2D experiment to obtain homonuclear dipolar-coupled spectra.

The above mentioned switching of the spinning axis from off the magic angle (during the evolution time) to on the magic angle (during the detection time) was originally proposed by Bax, Szeverenyi and Maciel [BX83] to determine the chemical shift anisotropy in molecules with several chemically different sites. In the evolution period when the sample is spinning off the magic angle the chemical shift anisotropy is not fully averaged whereas in the detection period with MAS an isotropic spectrum is obtained. Thus for every chemically different site in the F_2 direction, a scaled powder pattern is found in the F_1 dimension and the problem of spectral overlap is circumvented. Two other approaches to obtain this same results have been proposed by the same group. One involves the use of a series of rotor

synchronized π or 2π pulses [BS83]. In the other very fancy technique the sample is not spun about the magic angle but rotated over 120° in discrete steps [BZ83]. Due to the low sensitivity of this magic angle hopping experiment it was never used in real applications. The most straightforward method to relate isotropic and anisotropic chemical shifts in a 2D experiment is to acquire data synchronously with the rotor during the evolution time (giving an isotropic spectrum) and asynchronously during the detection period (which leads to a specific spinning sideband pattern dependent on the anisotropy) [AU81, AU84]. Harbison and Spiess [HA86] proposed a 2D experiment for the study of partially ordered solids, in which the evolution period is started at a fixed orientation of the rotor. This experiment which gives information about the chemical shift tensor and the degree of order in the sample looks very promising for the study of fibers like the new "super-strong" fibers. Correlation of chemical shifts in single crystals have been studied by Carter et al. [CA85].

In two-dimensional exchange experiments of solids, discussed in chapter 5, the chemical shift is present in the evolution and detection period. The object of this experiment is to detect some kind of spin exchange between spins with a different chemical shift during a mixing time that separates the evolution and detection period [SZ82]. This has been used in an analogous way as in experiments in solutions, to study chemical exchange [SZ83, HA85] or spin diffusion [SU82, BR83, CO85, TK86] between chemically different sites. The anisotropy of the chemical shift is explicitly used to study spin diffusion between orientationally different, but chemically identical spins [ED84, HE84]. The discussion in chapter 5 is focussed on the detection of super-slow molecular motions in static [KE87] and slowly rotating samples [JO84, KE85, KE86, KN87] via natural abundance ^{13}C NMR. 2D deuteron NMR of D-enriched samples has been used by Spiess and coworkers to detect such super-slow molecular motions [SC86].

The recent interest in zeolites, clays and ceramics has focused the attention on obtaining structural information from NMR spectra of quadrupolar spins. It appears that it is generally very difficult to determine quadrupole parameters from high field NMR spectra. In 2D nutation NMR [SA83, SM83] the evolution of the spin system is followed in the rotating frame where the first-order quadrupole interaction plays a prominent role. In the detection period the normal high-field spectrum is acquired, modulated by the first-order quadrupolar interactions in t_1. This experiment is evaluated in chapter 6 [KT87]. The first preliminary applications of this method show promising

results [GE85, TR85, MA85, MA86, LI86, KT87]. With the knowledge that the majority of nuclei in the periodic table possess a quadrupole moment this experiment is likely to find many applications.

Multiple quantum NMR is also developing very rapidly, and it seems a very promising technique. For a review about these experiments the reader is referred to Munowitz and Pines [MN86].

References

AU76 W.P. Aue, E. Bartholdi and R.R. Ernst, J. Chem. Phys. 64, 2229, 1976.

AU81 W.P. Aue, D.J. Ruben and R.G. Griffin, J. Magn. Res. 43, 472, 1981.

AU84 W.P. Aue, D.J. Ruben and R.G. Griffin, J. Chem. Phys. 80, 1729, 1984.

BA77 P. Bachmann, W.P. Aue, L. Müller and R.R. Ernst, J. Magn. Res. 28, 29, 1977.

BA82 A. Bax, "Two-Dimensional Nuclear Magnetic Resonance in Liquids", D. Reidel Publishing Co., Dordrecht, 1982.

BA83 A. Bax, T.A. Early and G.E. Maciel, J. Magn. Res. 52, 35, 1983.

BS83 A. Bax, N.M. Szeverenyi and G.E. Maciel, J. Magn. Res. 51, 400, 1983.

BX83 A. Bax, N.M. Szeverenyi and G.E. Maciel, J. Magn. Res. 55, 494, 1983.

BZ83 A. Bax, N.M. Szeverenyi and G.E. Maciel, J. Magn. Res. 52, 147, 1983.

BE83 R. Benn and H. Günter, Angew. Chem. 95, 381, 1983.

BO76 G. Bodenhausen, R. Freeman, R. Niedermeyer and D.L. Turner, J. Magn. Res. 24, 291, 1976.

BO77 G. Bodenhausen, R. Freeman, R. Niedermeyer and D.L. Turner, J. Magn. Res. 26, 133, 1977.

BR83 C.E. Bronniman, N.M. Szeverenyi and G.E. Maciel, J. Chem. Phys. 79, 3694, 1983.

CA82 P. Caravatti, G. Bodenhausen and R.R. Ernst, Chem. Phys. Lett. 89, 363, 1982.

CA83 P. Caravatti, G. Bodenhausen and R.R. Ernst, Chem. Phys. Lett. 100, 305, 1983.

CA85 C.M. Carter, D.W. Alderman and D.M. Grant, J. Magn. Res. 65, 183, 1985.

CO85 C. Connor, A. Naito, K. Takegoshi and C.A. McDowell, Chem. Phys. Lett. 113, 123, 1985.

ED84 H.T. Edzes and J.P.C. Bernards, J. Am. Chem. Soc. 106, 1515, 1984.

GE85 F.M.M. Geurts, A.P.M. Kentgens and W.S. Veeman, Chem. Phys. Lett. 120, 2, 1985.

HA85 G.S. Harbison, D.P. Raleigh, J. Herzfeld and R.G. Griffin, J. Magn. Res. 64, 284, 1985.

HA86 G.S. Harbison and H.W. Spiess, Chem. Phys. Lett. 124, 128, 1986.

HE76 R.K. Hester, J.L. Ackerman, B.L. Neff anf J.S. Waugh, Phys. Rev. Lett. 36, 1081, 1976.

HE84 P.M. Henrichs and M. Linder, J. Magn. Res. 58, 458, 1984.

JE71 J. Jeener, Ampère International Summer School, Basko Polje, Yugoslavia 1971.

JO84 A.F. de Jong, A.P.M. Kentgens and W.S. Veeman, Chem. Phys. Lett. 109, 337, 1984.

KE85 A.P.M. Kentgens, A.F. de Jong, E. de Boer and W.S. Veeman, Macromolecules 18, 1045, 1985.

KE86 A.P.M. Kentgens, A.F. de Jong, E. de Boer and W.S. Veeman in "Integration of Fundamental Polymer Science and Technology", L.A. Kleintjes and P.J. Lemstra eds., Elsevier Applied Science Publishers, London, 1986.

KE87 A.P.M. Kentgens, W.S. Veeman and J. van Bree, to appear in Macromolecules.

KN87 A.P.M. Kentgens, E. de Boer and W.S. Veeman, to be published.

KT87 A.P.M. Kentgens, J.J.M. Lemmens, F.M.M. Geurts and W.S. Veeman J. Magn. Res. 71, 62, 1987.

LI80 M. Linder, A. Höhener and R.R Ernst, J. Chem. Phys. 73, 4959, 1980.

LI86 E. Lippmaa, A. Samoson and M. Mägi, J. Am. Chem. Soc. 108, 1730, 1986.

MA83 D. Marion and K. Wüthrich, Biochem. Biophys. Res. Commun. 113, 967, 1983.

MA84 C.L. Mayne, R.J. Pugmire and D.M. Grant, J. Magn. Res. 56, 151, 1984.

MA85 P.P. Man, H. Theveneau and P. Papon, J. Magn. Res. 64, 271, 1985.

MA86 P.P. Man, J. Magn. Res. 67, 78, 1986.

MA87 W.E.J.R. Maas, A.P.M. Kentgens and W.S. Veeman, to be published.

ME84 E.M. Menger, S. Vega and R.G. Griffin, J. Magn. Res. 56, 338, 1984.

MI86 H. Miura, T. Terao and A. Saika, J. Magn. Res. 68, 593, 1986.

MN82 M.G. Munowitz, W.P. Aue and R.G. Griffin, J. Chem. Phys. 77, 1686, 1982.

MN86 M.G. Munowitz and A. Pines, Adv. Chem. Phys. 66, 1, 1986.

MU81 M.G. Munowitz, R.G. Griffin, G. Bodenhausen and T.H. Huang, J. Am. Chem. Soc. 103, 2529, 1981.

MU82 M.G. Munowitz and R.G. Griffin, J. Chem. Phys. 76, 2848, 1982.

MU84 M.G. Munowitz, T.H. Huang, C.M. Dobson and R.G. Griffin, J. Magn. Res. 57, 56, 1984.

MU86 H. Miura, T. Terao and A. Saika, J. Chem. Phys. 85, 2458, 1986.

OP77 S.J. Opella and J.S. Waugh, J. Chem. Phys. 66, 4919, 1977.

PE77 R.G. Pembleton, L.M. Ryan, R.C. Wilson and B.C. Gerstein, J. Chem. Phys. 66, 36, 1977.

RE75 A.G. Redfield and S.D. Kunz, J. Magn. Res. 19, 250, 1975.

RO84 J.E. Roberts, S. Vega and R.G. Griffin, J. Am. Chem. Soc. 106, 2506, 1984.

RY77 E.F. Rybaczewski, B.L. Neff, J.S. Waugh and J.S. Sherfinski, J. Chem. Phys. 67, 1231, 1977.

SA83 A. Samoson and E. Lippmaa, Chem. Phys. Lett. 100, 205, 1983.

SA84 J. Schaefer, M.D. Sefcik, E.O. Stejskal, R.A. McKay, W.T. Dixon and R.E. Cais, Macromolecules 17, 1107, 1984.

SC76 B. Schnabel, U. Haubenreisser, G. Scheler and R. MÜller, Proceedings of the 19th Colloque Ampère, p. 441, 1976.

SC83 J. Schaefer, R.A. McKay, E.O. Stejskal and W.T. Dixon, J. Magn. Res. 52, 123, 1983.

SC84 J. Schaefer, E.O. Stejskal, R.A. McKay and W.T. Dixon, J. Magn. Res. 57, 85, 1984.

SC85 J. Schaefer, E.O. Stejskal, D. Perchak, J. Skolnick and R. Yaris, Macromolecules 18, 368, 1985.

SC86 C. Schmidt, S. Wefing, B. Blümich and H.W. Spiess, Chem. Phys. Lett. 130, 84, 1986.

SH84 J. Schaefer, E.O. Stejskal, R.A. McKay and W.T. Dixon, Macromolecules 17, 1479, 1984.

SM83 A. Samoson and E. Lippmaa, Phys. Rev. B 28, 6567, 1983.

ST76 M.E. Stoll, A.J. Vega and R.W. Vaughan, J. Chem. Phys. 65, 4093, 1976.

ST82 D.J. States, R.A. Haberkorn and D.J. Ruben, J. Magn Res. 48, 286, 1982.

SU82 D. Suter and R.R. Ernst, Phys. Rev. B, 25, 6038, 1982.

SU83 N. Schuff and U. Haeberlen, J. Magn. Res. 52, 267, 1983.

SZ82 N.M. Szeverenyi, M.J. Sullivan and G.E. Maciel, J. Magn. Res. 47, 462, 1982.

SZ83 N.M. Szeverenyi, A. Bax and G.E. Maciel, J. Am. Chem. Soc. 105, 2579, 1983.

TE82 T. Terao, H. Miura and A. Saika, J. Am. Chem. Soc. 104, 5228, 1982.

TE86 T. Terao, H. Miura and A. Saika, J. Chem. Phys. 85, 3816, 1986.

TA86 K. Takegoshi and C.A. McDowell, J. Magn. Res. 66, 14, 1986.

TK84 K. Takegoshi and C.A. McDowell, J. Chem. Phys. 84, 2084, 1984.

TR85 A. Troniker, P.P. Man, H. Theveneau and P. Papon, Solid State Comm. 55, 929, 1985.

WA75 J.S. Waugh, Second Specialized Colloque Ampère, Budapest, 1975.

CHAPTER 3

HETERONUCLEAR TWO-DIMENSIONAL J-RESOLVED NMR

3.1 Introduction

Isotropic J coupling constants can give information about the electronic environment and chemical bonds in a molecule and various one- and two-dimensional experiments exist to extract this information. In liquids ^{13}C-^{1}H coupling constants have proven to be very useful for spectral assignment and conformational analysis. If available, they could also play an important role in high-resolution solid state NMR. In liquids, all anisotropic interactions are averaged by rapid molecular reorientations and thus J-resolved ^{13}C spectra are easily obtained by collecting data without proton decoupling. Usually, high resolution ^{13}C spectra of solids are obtained with the CP-MAS technique, where magic angle spinning is used to average the anisotropy in the chemical shift and linebroadening due to heteronuclear dipolar interactions is removed by high-power proton decoupling. Evidently proton decoupling also removes the scalar ^{13}C-^{1}H J coupling from the spectrum.

In principle, dipolar interactions can be averaged by fast MAS, because of their angular dependence of $(3\cos^2\theta - 1)$. The isotropic J term in the Hamiltonian has no angular dependence and is not affected by MAS, and thus the intended result, a J-coupled ^{13}C spectrum, would be achieved. In case of averaging with MAS, however, we have to distinguish between homogeneous and inhomogeneous interactions [MA79]. In case of a homogeneous interaction the resonance frequency of the spins is not static, in which case MAS is only successful when the spinning rate exceeds the line width of the spectrum of a static sample. For an inhomogeneous interaction, however, magic angle spinning can narrow the resonance line even if the spinning speed is smaller than the total width of the spectrum. In that case spinning sidebands arise. The relevant term in the heteronuclear dipolar ^{13}C-^{1}H interaction looks like $H = C(3\cos^2\theta - 1)I_zS_z$, which at first site clearly qualifies as an inhomogeneous interaction. However, the homonuclear dipolar ^{1}H-^{1}H interaction contains a term $C(I_{r+}I_{s-} + I_{r-}I_{s+})$, the so-called flip-flop term. Due to this term the resonance frequency of each proton spin is modulated, and thus the ^{1}H-^{1}H interaction becomes homogeneous. The presence of this homonuclear proton dipolar interaction then makes the heteronuclear proton carbon interaction also homogeneous [MA79]. As dipolar interactions are homogeneous

and of the order of tens of kHz it becomes clear that averaging of these interactions by MAS is not yet feasible.

The solution to this problem is to selectively average the homonuclear proton dipolar interaction. This can be done with magic angle irradiation [LE65], where the sample is irradiated with a steady proton rf field, shifted off-resonance so that in the rotating frame the spins experience an effective field oriented at the magic angle with respect to the z axis, in which case the spin part of the homonuclear dipolar interaction averages to zero. The same effect can be achieved with a sequence of strong rf pulses. These multiple pulse cycles, which have exotic names like WAHUHA and MREV-8, produce spin rotations which cause the homonuclear dipolar interaction to average to zero [HA76, HA85]. This selective averaging of the homogeneous ^{1}H-^{1}H dipolar interaction renders the heteronuclear dipolar interactions inhomogeneous, which can then be averaged with MAS even at low spinning speeds. As a result only the isotropic J couplings remain present in the spectrum, although they will be scaled by the multiple pulse decoupling. Terao et al. [TE81] were the first to perform this experiment on adamantane.

Until now most applications of this technique were on spherical organic molecules, like camphor and adamantane [TE81, TE82, TR82, ZI82, MA84], which, at room temperature, are in a "plastic" crystalline state where the molecules reorient rapidly around their symmetry axes and even diffuse through the lattice. This results in considerable averaging of the dipolar interactions. The remaining part of the homonuclear dipolar interaction can then relatively easy be averaged by proton multiple pulse decoupling. For rigid systems this technique is usually less successful due to the fact that the rf circuitry in standard CP-MAS probes of commercial solid state spectrometers does not yet allow to get short multiple pulse cycles necessary to average large dipolar interactions existing in rigid solids, although progress is made in this direction. Most of this work has been done by Terao, Miura and Saika and it must be noted that they recently succeeded in resolving J multiplets in rigid solids using a double bearing probe with accurate setting of the rotation axis and a short multiple pulse cycle (i.e. short $\pi/2$ pulses) [MI86].

3.2 Experimental realization

The experiment to obtain 2D-J resolved spectra is depicted in fig. 3.1, it is essentially the solid state analogue of what is referred to as the proton flip experiment [BA82]. First, transverse ^{13}C magnetization is created

by cross polarization or a $\pi/2$ pulse, followed by multiple pulse decoupling in the t_1 interval. At time $t_1/2$ a π-pulse is applied to both proton and carbon spins in order to refocus the chemical shift at time t_1 while leaving the scalar coupling intact. A further advantage of the π-pulse is that it also refocuses linebroadening effects arising from chemical shift distributions and/or susceptibility effects. In case of rigid solids it will be necessary to synchronize the evolution period t_1 with the spinner in order to get refocussing from the π-pulse and to avoid the occurrence of spinning sidebands in the F_1 dimension. In the detection period t_2 a FID will be acquired, with high-power proton decoupling, that is modulated exclusively by the scaled isotropic ^{13}C-^{1}H J coupling.

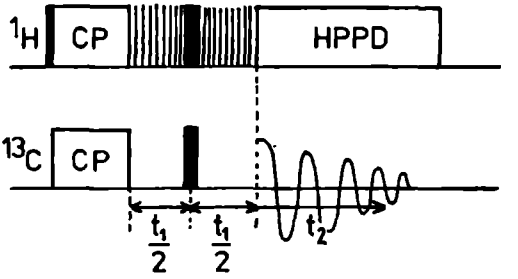

Fig. 3.1 Pulse scheme of the solid state analogon of the proton flip experiment. Transverse ^{13}C magnetization is created via cross-polarization (CP). During the evolution period homonuclear proton dipolar interactions are removed using multiple pulse techniques. In the detection period high power proton decoupling (HPPD) is used to remove the influence of the protons on the ^{13}C spectrum.

The experimentally most difficult part of this experiment is the multiple pulse decoupling during the evolution period t_1. It is now generally accepted that the most effective schemes for homonuclear decoupling are the MREV-8 [RH73] and the BR-24 [BU79] cycle. As no proton NMR signal has to be observed during the multiple pulse decoupling, the pulse widths can be increased to the semiwindowless limit [BU81], in which the small spaces between the pulses disappear and the cycle becomes a sequence of joined pulse pairs. This makes experimental realization more easy, particulary within the restrictions of a double resonance probe. An important point when employing multiple pulse decoupling is that the phases of the four pulses have to be exactly in quadrature and their amplitudes have to be equal. For accurate

adjustments of the pulses several "tune up" cycles exist [HA79, BR81]. As amplitudes and phases of the rf pulses in the decoupler channel of our Bruker CXP-300 are not easily accessed, the rf signal was fed through a specially built "four-phase modulator", which allowed full control of phases and amplitudes, in that way circumventing the built in high-power decoupler. At the time these experiments were carried out, our spectrometer was equipped with an Aspect 2000 computer and Z70 pulse programmer. This means that the length of pulse programs is restricted to 16 lines. It is impossible to program the pulse scheme of fig. 3.1 using only 16 lines, especially when a long multiple pulse cycle is used. Therefore the multipulse decoupling is carried out by a separate pulse programmer, the "Spin Smasher", which has several multiple pulse schemes preprogrammed. This Spin Smasher can be activated with a single gate from the pulse programmer within the spectrometer, and thus multiple pulse decoupling (even BR-52) will only take one line in a pulse program. A further advantage of this setup is that one can switch from one multiple pulse scheme to the other simply by setting a switch on the Spin Smasher.

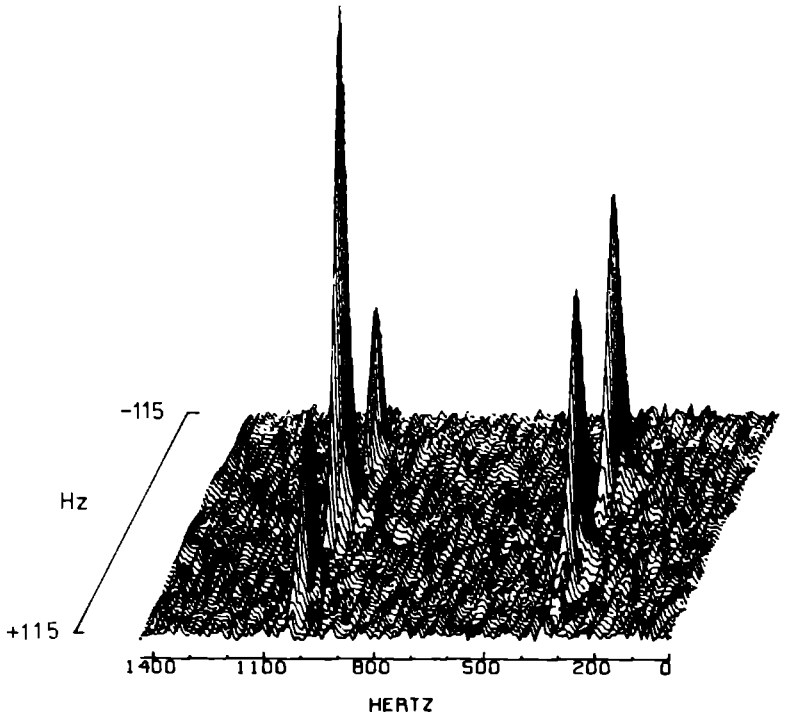

Fig. 3.2 Heteronuclear 2D-J resolved spectrum of adamantane.

Fig. 3.2 shows the heteronuclear 2D-J resolved spectrum of adamantane obtained with this setup, where semiwindowless MREV-8 was used for homonuclear decoupling. It can be seen that the scaled J multiplets are well-resolved in the F_1 direction.

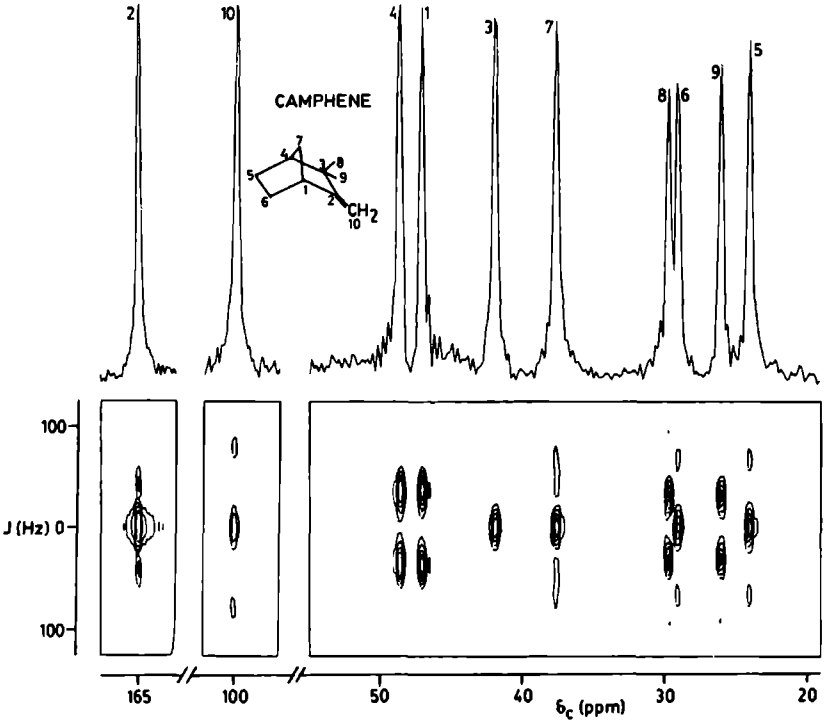

Fig. 3.3 Contour plot of the 2D-J resolved spectrum of camphene together with its F_2 projection, which gives the normal proton decoupled ^{13}C spectrum of camphene. The J couplings in the F_1 direction are scaled by a factor 0.48 due to the multiple pulse decoupling.

Another example of a spherical molecule is camphene, here the J multiplets would severely overlap in a 1D spectrum and the advantage of the 2D spectrum becomes clear in fig. 3.3. Again, the J multiplets appear to be well-resolved but scaled due to the decoupling by a factor 0.48. The F_2 projection shows the normal proton decoupled ^{13}C spectrum of camphene. The chemical shifts found are, within the experimental error of 1 ppm, identical with the values found in liquid [WE72]. If we look at the assignment of the

resonances by Werstiuk et al.[WE72], however, we see that in the solid state spectrum carbons C-8 and C-6 have changed position, as well as C-9 and C-5. This is probably due to a misassignment, or it is due to some effect in the solid but that seems, considering the resemblances of the total spectrum, unlikely. Because of the line widths in the solid, the C-H couplings can only be determined with an accuracy of several Hertz. For the C-10 carbon we find, taking the scaling factor into account, 159 Hz which is a normal value for sp^2-hybrids. For the carbons C-1, C-4 and C-7 we find approximately 140 Hz. These values are in agreement with those in solution [WE73] and show that these carbons are the most strained. For carbons C-5, C-6, C-8 and C-9 a value of ~130 Hz is found. These results show that the information obtained from solid state spectra is identical with that obtained from spectra of liquids. This makes this experiment interesting for conformation studies in insoluble systems, or in systems were special effects are to be expected in the solid state i.e. more strain of certain bonds in the crystal.

3.3 Carbon black-filled natural rubber

Early proton NMR studies of rubber samples by Gutowsky et al. [GU53, GU57] show very narrow lines at room temperature indicating that dipolar interactions are averaged by CH_3 rotation and segmental motions. Duch and Grant [DU70] succeeded in getting direct ^{13}C spectra of natural rubber using conventional high resolution techniques. Thus natural rubber seems a good candidate for J-resolved spectroscopy in the solid state. It appears that even for cured, carbon black-filled, rubber, MAS alone is sufficient to obtain heteronuclear J-resolved spectra, showing that there are extensive molecular motions present. The nature of these motions are discussed by comparing a series of spectra, obtained with and without MAS and dipolar decoupling, to those of the well studied plastic crystal adamantane.

The studied rubber samples were prepared from Standard Malaysian Rubber and contained 50 phr HAF carbon black. The samples were cured with 2.5 phr Sulfur. The average molecular weight between cross-links is of the order of ten thousand. Spectra were recorded on a Bruker CXP 300 (carbon frequency 75.4 MHz) and on a homebuilt 180 MHz spectrometer (carbon frequency 45.3 MHz). On the CXP 300 spectra were obtained in a double-bearing CP-MAS probe operating with 4.5 μsec 90° pulses. The MAS experiments were carried out with spinning speeds between 2 and 3 kHz.

Fig. 3.4 shows the heteronuclear 2D-J spectrum of cured, carbon black-filled, natural rubber at room temperature, again obtained with the proton-flip experiment [BA82], but now no multiple pulse decoupling was applied during the evolution period. Thus unlike the "plastic" crystals it is not necessary to apply multiple pulse decoupling, meaning that dipolar interactions are averaged to an even greater extent in the rubber sample than in e.g. adamantane. In the F1 dimension we now find the full unscaled scalar ^{13}C-^{1}H couplings, being 150 Hz for the C-2 carbon and 127 Hz for the carbons C-3, C-4 and C-5. These values are identical with those found in a chloroform solution of depolymerized natural rubber. The chemical shift values are, within the experimental error of 1 ppm, identical with those found by Duch and Grant [DU70].

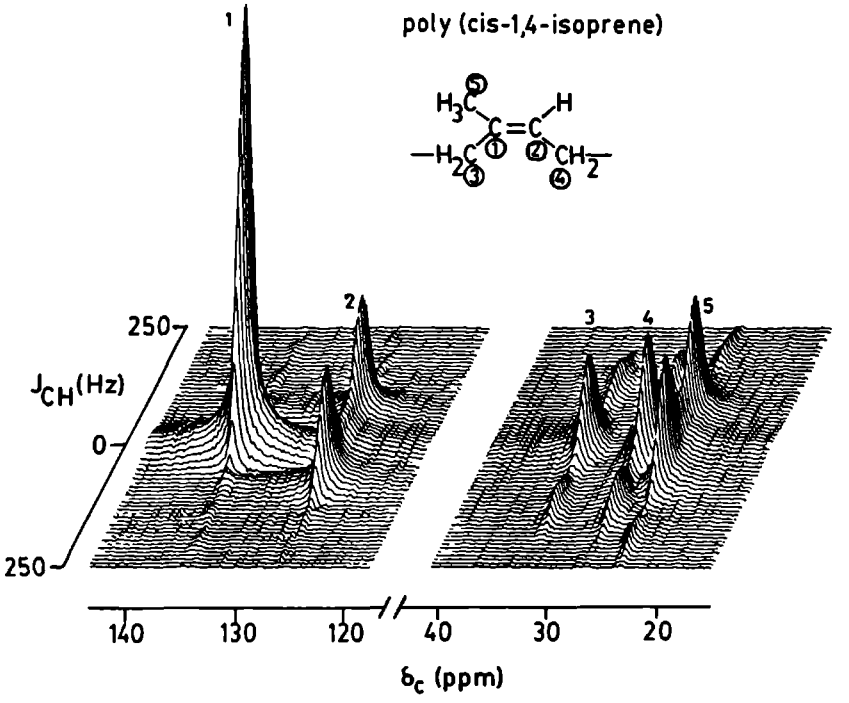

Fig. 3.4 Stacked plot of the heteronuclear 2D-J spectrum of cured, carbon black-filled natural rubber. The proton flip experiment was used with high power proton decoupling during the detection time (but without multiple pulse decoupling during t_1). The experiment was performed with the sample spinning at the magic angle.

3.3.1 Motions in natural rubber vs adamantane

In order to get more insight in the motional processes causing this averaging of dipolar interactions in rubber we took spectra under various conditions and compared them to adamantane spectra (fig. 3.5). Adamantane molecules are globular molecules that are cubic close packed (fcc). The barrier to molecular reorientation at a site is low. As a result adamantane rotates fast about its molecular axes in the crystal (τ = 1.7 10^{-11} sec at room temperature) [RE69]. Proton second moment studies [MC60, SM61] show that this rotation averages intramolecular dipolar interaction to zero; at room temperature the proton second moment is determined by intermolecular dipolar interactions whose magnitude depends on the distance between the molecular centers (lattice parameter 9.45 Å) and amounts to 9 kHz. Diffusion is not very prominent at room temperature, only at temperatures above 475 K diffusion influences the proton T_2.

Gutowsky and Meyer [GU53] performed proton second moment studies of poly-(cis 1,4-isoprene) (natural rubber) as a function of temperature and cure time. With rising temperature the line width shows two regions of change. The lines start to narrow at temperatures of 140 - 170 K, this is assigned to the onset of CH_3 group rotation. A second larger decrease (per K) in line width was observed at ~ 225 K, assigned to the onset of segmental motion. The lines do not narrow further at temperatures above 263 K. The line width is relatively narrow for a solid indicating that the chain segments are undergoing a considerable amount of random reorientational motions at frequencies of the order of 50 kHz or faster [GU57]. ^{13}C free-induction decays of poly-isoprenes have been obtained by Schaefer [SC72] and also indicate that there is considerable motional narrowing. In a carbon black-filled rubber the lines appear to be 5-10 times broader which is interpreted as inhibition of certain motions of the polymer chains by the filler. This line broadening can be partly removed by MAS [SH72]. Multiple pulse narrowing of the proton resonance of both filled poly-isoprene and the pure gum has been carried out by Dybowski and Vaughan [DY75], showing that in both samples a linebroadening is introduced by anisotropic reorientational motions. Such spatial anisotropy of molecular motions has also been found in poly-(cis-1,4-butadiene) by English and Dybowski [EN84, EN85]. They found that the ^1H and ^{13}C NMR lines could be narrowed by coherent averaging techniques i.e. MAS and multiple pulse NMR. This anisotropy in the motion, even without the presence of cross-links and filler material, is attributed to the presence of

chain entanglements whose lifetime seems to be long on the time scale of an NMR experiment. Extensive theoretical and experimental work on the effect of chain entanglements has been done by Cohen-Addad and coworkers [CO74, CH74, CO82, CO85] using high-resolution NMR on, among others, molten polybutadiene and poly-(dimethylsiloxane).

Fig. 3.5A shows adamantane and filled rubber ^{13}C spectra obtained without MAS and without high-power proton decoupling. For adamantane we see one broad resonance ~ 1500 Hz wide, whereas the rubber lines are much narrower (~ 400 Hz). With high-power proton decoupling, while leaving the sample static (fig. 3.5B), the rubber lines are narrowed to 300 Hz. For adamantane the change is more drastic, now we can see the two separate carbon resonances each ~ 180 Hz wide. In the adamantane spectrum of fig. 3.5A the line width is determined by intermolecular dipolar interactions, these are removed by the proton decoupling in fig. 3.5B. The adamantane lines in fig. 3.5B are inhomogeneously broadened either by chemical shift anisotropy or by susceptibility effects. Broadening by chemical shift anisotropy, however, is very unlikely because the rapid reorientations of the molecule which average intramolecular dipolar interactions will also average the chemical shift anisotropy due to intramolecular interactions. It has been reported that compressing adamantane into a sphere reduces the line widths [GA81]. It is thought that the compression removes most of the voids in the sample and thus reduces the susceptibility distribution through the sample. The result of the rubber spectra can be explained along the same lines. It has to be noted, however, that the broadening by dipolar interaction of the rubber lines in fig. 3.5A is one order of magnitude smaller than for adamantane (100 Hz vs 1000 Hz).

The broadening of the rubber spectrum in fig. 3.5B is quite substantial (300 Hz), and is proportional to the field (a line width of 180 Hz is found on a 180 MHz spectrometer). As the contribution of dipolar interaction to the line width in fig. 3.5A amounts to only 100 Hz, it is evident that there are fast, nearly isotropic, motions present which average the dipolar interaction and, of course, the chemical shift anisotropy is averaged along with it. Thus the rubber line width found in fig. 3.5B is probably due to microscopic inhomogeneities generated by the carbon black filler particles. This is in contradiction with the result of Schaefer et al. [SH72] who state that the ^{13}C NMR line in a non-spinning, filled, vulcanized sample is purely homogeneous.

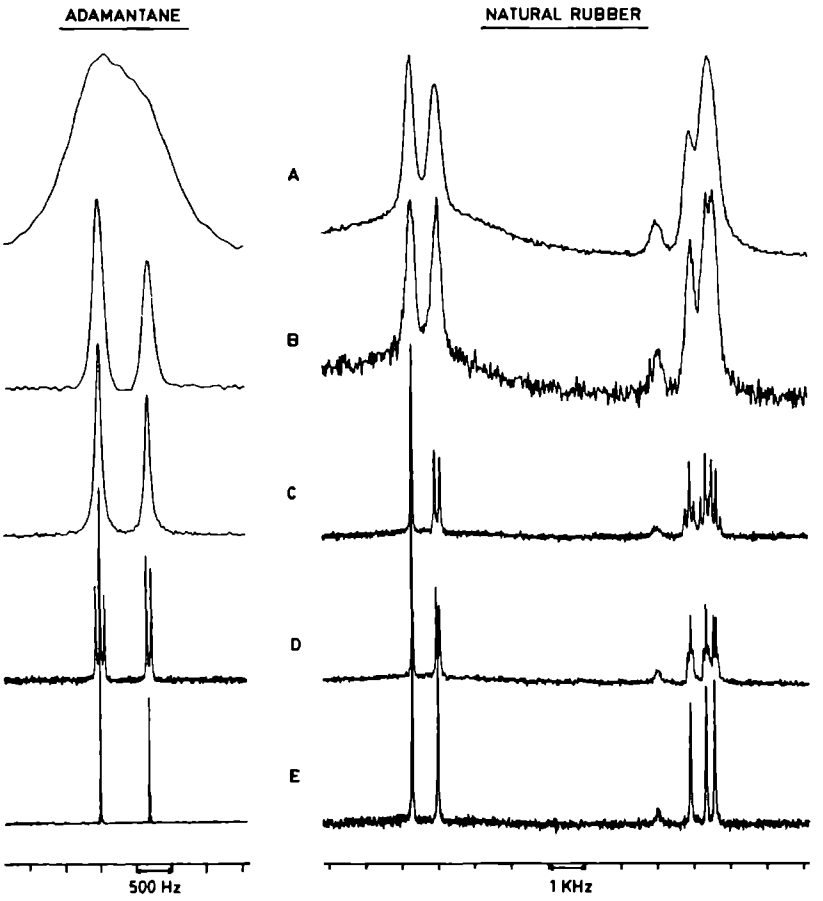

Fig. 3.5 Spectra of adamantane and natural rubber obtained under various conditions. In the rubber spectra there is an extra line present at 43 ppm from an antidegradant which was no subject of the present study. A. No decoupling and no magic angle spinning. The line width for adamantane (ADA) is 1500 Hz and 380 Hz for natural rubber (NR). B. High power proton decoupling but no magic angle spinning. ADA 180 Hz; NR 300 Hz. C. Magic angle spinning but no decoupling. ADA 90 Hz; NR 35 Hz. D. Magic angle spinning combined with multiple pulse decouplong (semi-windowless MREV-8 [BU81]). ADA 11 Hz; NR 35 Hz. E. MAS and high power proton decoupling. ADA 3 Hz; NR 35 Hz.

If we now turn the proton decoupling off but spin the sample at the magic angle we observe well resolved J-multiplets in rubber. This means that all interactions except for the isotropic chemical shift and the scalar J coupling are averaged to zero by MAS. In adamantane line widths of 90 Hz are observed but although the scalar coupling is approximately 130 Hz no sign of a splitting of the lines into J-multiplets is observed. Here MAS is not capable of averaging the homonuclear proton dipolar coupling which is of the order of 9 kHz. So there are residual proton dipolar fluctuations which modulate the coupling Hamiltonian J I•S (I = proton, S = carbon) i.e. make it time dependent. As a result $J\langle I_z S_z \rangle$ is too small to be observed. In adamantane a combination of MAS and multiple pulse decoupling (fig. 3.5D) is necessary to observe scalar couplings. However, we believe that MAS alone will be sufficient at spinning speeds above 10 kHz. In the rubber sample the residual dipolar couplings are small enough to be completely averaged by 2 kHz spinning. Here the only effect of multiple pulse decoupling is to scale the J-couplings which results in a reduction of the resolution (fig. 3.5D). Fig. 3.5E shows the adamantane and rubber spectrum obtained with a combination of MAS and proton decoupling resulting in 3 Hz wide lines for adamantane and 30 Hz line width for the rubber. This residual line width in rubber is probably caused by susceptibility effects not averaged by MAS and/or a macroscopic distribution of chemical environments. In conclusion these experiments show us that the heteronuclear carbon-proton as well as the homonuclear proton-proton dipolar interaction is much smaller in cured, filled, natural rubber than in adamantane. This is supported by the fact that it is very difficult to establish cross-polarization for the spinning rubber sample whereas for adamantane polarization transfer is still possible although magic angle spinning already has his effect on the transfer as has been studied by Stejskal et al. [ST77].

Of course it is not possible to simply translate adamantane results to the natural rubber because the systems are very different. Still we can draw some conclusions. The fact that intra chain dipolar interactions are averaged (which is of the order of tens of kHz) shows that there must be fast motions using different degrees of freedom of the chain segments. A simple rotation of the chains for instance would scale the dipolar interaction but cannot make it vanishingly small. However, the motion must still be restricted i.e. cannot use all the degrees of freedom of a chain segment otherwise magic angle spinning at the moderate speed of 2 kHz would not be capable to narrow the lines further as we observed in fig. 3.5 [AN81]. Several authors have

pointed out before that the motions of elastomers above the glass temperature are anisotropic. This anisotropy already exists in uncured rubbers without filler material due to chain entanglements [DY75, EN84, EN85] and the effects can even be observed by high-resolution NMR [CO74, CH74, CO82, CO85]. So these entanglements have a lifetime longer than the time scale of the NMR experiment. The only effect of cross-links and filler material is to magnify the spatial restrictions on the polymer chain. The fact that (inter) dipolar interactions between different chain segments are also very small is surprising. As mentioned before inter molecular proton dipolar interactions in adamantane are rather big ($\tilde{}$ 9 kHz). In the rubber sample discussed here and elsewhere [SC72, SH72, DY75] the average ^{1}H-^{1}H dipolar interaction for protons located on neighboring chains or chain segments is at least 50 times smaller than in adamantane. This in spite of the fact that there are filler particles, cross-links and entanglements holding different chains together. It means that either the inter-chain distance is very large or that there is enough diffusion in the natural rubber to average this interaction. With diffusion large scale lateral movements of chains with respect to each other are meant. It would implicate that large parts of the polymer network have to reorient. If this is the case will be investigated further using 2D-exchange NMR, as will be described in chapter 5.

References

AN81 E.R. Andrew, Philos. Trans. R. Soc. London. A 299, 505, 1981.

BA82 A. Bax, Two-Dimensional Nuclear Magnetic Resonance in Liquids, D. Reidel Publishing Company, Dordrecht, 1982.

BR81 D.P. Burum, M. Linder and R.R. Ernst, J. Magn. Res. 43, 463, 1981.

BU79 D.P. Burum and W.K. Rhim, J. Chem. Phys. 71, 944, 1979.

BU81 D.P. Burum, M. Linder and R.R. Ernst, J. Magn. Res. 44, 173, 1981.

CH74 J.P. Cohen-Addad and J.P. Faure, J. Chem. Phys. 61, 1571, 1974.

CO74 J.P. Cohen-Addad, J. Chem. Phys. 60, 2440, 1974.

CO82 J.P. Cohen-Addad, J. Physique 43, 1509, 1982.

CO85 J.P. Cohen-Addad and R. Dupeyre, Macromolecules 18, 1612, 1985.

DU70 M.W. Duch and D.M. Grant, Macromolecules 3, 165, 1970.

DY75 C.R. Dybowski and R.W. Vaughan, Macromolecules 8, 50, 1975.

EN84 A.D. English and C.R. Dybowski, Macromolecules 17, 446, 1984.

EN85 A.D. English, Macromolecules 18, 178, 1985.

GA81 A.N. Garroway, D.L. VanderHart and W.L. Earl, Philos. Trans. R. Soc. London. A 299, 609, 1981.

GU53 H.S. Gutowsky and L.H. Meyer, J. Chem. Phys. 21, 2122, 1953.

GU57 H.S. Gutowsky, A. Saika, M. Takeda and D.E. Woessner, J. Chem. Phys. 27, 534, 1957.

HA76 U. Haeberlen, High Resolution NMR in Solids, in Advances in Magnetic Resonance, Supplement 1, J.S. Waugh Ed., Academic Press, New York, 1976.

HA79 U. Haubenreisser and B. Schnabel, J. Magn. Res. 35, 175, 1979.

HA85 U. Haeberlen, Magn. Res. Rev. 10, 81, 1985.

LE65 M. Lee and W.I. Goldburg, Phys. Rev. A 140, 1261, 1965.

MA79 M.M. Maricq and J.S. Waugh, J. Chem. Phys. 70, 3300, 1979.

MA84 C.L. Mayne, R.J. Pugmire and D.M. Grant, J. Magn. Res. 56, 151, 1984.

MC60 D.W. McCall and D.C. Douglass, J. Chem. Phys. 33, 777, 1960.

MI86 H. Miura, T. Terao and A. Saika, J. Magn. Res. 68, 593, 1986.

RE69 H.A. Resing, Mol. Cryst. Liquid Cryst. 9, 101, 1969.

RH73 W.K. Rhim, D.D. Elleman and R.W. Vaughan, J. Chem. Phys. 59, 3740, 1973.

SC72 J. Schaefer, Macromolecules 5, 427, 1972.

SH72 J. Schaefer, S.H. Chin and S.I. Weissman, Macromolecules 5, 798, 1972.

SM62 G.W. Smith, J. Chem. Phys. 35, 1134, 1962.

ST77 E.O. Stejskal, J. Schaefer and J.S. Waugh, J. Magn. Res. 28, 105, 1977.

TE81 T. Terao, H. Miura and A. Saika, J. Chem. Phys. 75, 1573, 1981.

TE82 T. Terao, H. Miura and A. Saika, J. Magn. Res. 49, 365, 1982.

TR82 T. Terao, H. Miura and A. Saika, J. Am. Chem. Soc. 104, 5228, 1982.

WE72 N.H. Werstiuk, R. Taillefer, R.A. Bell and B. Sayer, Can. J. Chem. 50, 2146, 1972.

WE73 N.H. Werstiuk, R. Taillefer, R.A. Bell and B. Sayer, Can. J. Chem. 51, 3010, 1973.

ZI82 K.W. Zilm and D.M. Grant, J. Magn. Res. 48, 524, 1982.

2D CORRELATION OF CHEMICAL SHIFT AND DIPOLAR INTERACTIONS

4.1 Introduction

Many spin interactions in a solid are described by a tensor. As tensor interactions are related to molecular and crystal axes, the information contained in such a tensor interaction can be used to obtain geometrical information about the molecule or crystal being studied. It is well-known, for example, that the magnetic dipole interaction between two spins is coaxial with the internuclear axis of the two interacting nuclei. Knowledge of the complete tensor of the dipolar interaction between a ^{13}C and a ^{1}H, for instance, yields quantitative information about the C-H distance and the orientation of the C-H axis with respect to the molecule.

The first technique to record dipolar modulated ^{13}C spectra of solids, the 2D separated local field (SLF) experiment, was proposed by Waugh [WA75] and applied to single crystals and oriented polymers by his coworkers [HE76, RY77, OP77]. Here dipolar modulation refers to the fact that ^{13}C FIDs are collected during the detection period of the 2D experiment, which are phase-modulated by the dipolar interaction of the ^{13}C spin with surrounding protons. Stoll et al. [ST76] were the first to use the technique in powders. They analyzed the spectra after a single Fourier transform, leaving the dipolar modulation in the time-space. Linder et al. [LI80] showed that it is advantageous to apply a complete two-dimensional Fourier transform of the acquired signals, thus obtaining very characteristic 2D powder patterns.

Munowitz et al. [MU81, MU82, MN82, MU84] applied this technique, that separates the chemical shift and heteronuclear dipolar interactions, to samples spinning at the magic angle. As both interaction are inhomogeneous (see chapter 1), the resulting two-dimensional spectrum consists of a set of spinning sidebands. The analysis of these 2D spinning sideband spectra can also give the geometrical information one wants to obtain. Schaefer et al. [SC83] used the experiment of Munowitz to detect the averaging of dipolar interactions, in that way obtaining information about molecular motions in the kHz regime. This has been applied to various polymers.

Another example of the use of a tensor interaction will be extensively treated in the next chapter. There the chemical shift tensor of ^{13}C spins is used to detect and analyze slow molecular rotations. Via a novel two-

dimensional solid state NMR experiment it can be determined for such a case about what axis the rotations take place and about what angle. One piece of information, however, is needed before the motion can be analyzed: the orientation of the chemical shift tensor of the particular ^{13}C spin, relative to the molecular axes. Most conveniently, this can be determined from single crystal studies, at least when single crystals are available. For the system described in the next chapter, poly-(oxymethylene), single crystals of sufficient dimensions can not be obtained. Fortunately, the two-dimensional SLF solid state NMR technique allows the determination of a complete ^{13}C chemical shift tensor, including the orientation relative to molecular axes, even for non-crystalline material [LI80]. With this technique the orientation of the ^{13}C chemical shift tensor is determined relative to the dipolar ^{13}C-^{1}H tensor interaction. Since the orientation of the latter is known, the ^{13}C chemical shift tensor can be determined relative to molecular axes. In this chapter we apply this technique to poly-(oxymethylene), in order to be able to analyze slow molecular motions in this polymer, as described in the next chapter.

4.2 Experimental realization

The pulse scheme (fig. 4.1) used to obtain spectra which correlate heteronuclear dipolar interactions and chemical shielding anisotropy is very similar to the 2D J-resolved experiment discussed in chapter 3. The main difference is that the sample is now static and thus, as multiple pulse decoupling is used during t_1, the (scaled) heteronuclear dipolar ^{13}C-^{1}H interaction is the major interaction modulating the signal detected during the period t_2. When no π pulse is applied in the middle of the evolution period, the chemical shift anisotropy will not be refocussed at the end of t_1 and has to be taken in account as well. In the detection period normal high-power proton decoupling is used which means that the carbon resonance frequencies are determined exclusively by the chemical shift anisotropy. The description of this experiment in a vector picture is very straightforward. A certain spin packet precesses through an angle $\omega^{(1)}t_1$ during the evolution period, at that point the detection is started. Consequently the detected signal is modulated in phase by the interactions present in the evolution period.

As in the case of J-resolved spectroscopy, the multiple pulse decoupling is the experimental bottleneck in this experiment. Basically the same setup

as described in chapter 3 is used. Here we want to average homonuclear dipolar interactions in rigid solids, however, meaning that we need short multiple pulse cycles (i.e. short π/2 pulses). For this purpose a standard double resonance probe was equipped with a horizontal coil (Ø = 6 mm) of flat copper wire, allowing π/2 pulses as short as 1.5 μsec. The sample used in this experiment was a cylindrical (5 x 11 mm) piece of poly-(oxymethylene) (commercially available Hostaform-C from Hoechst).

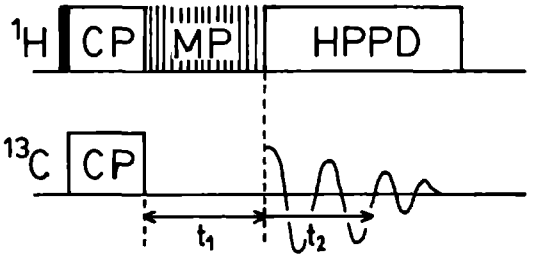

Fig. 4.1 Pulse scheme for dipolar correlated chemical shift spectra. Transverse ^{13}C magnetization is created via cross-polarization (CP). Multiple pulse decoupling (MP) is used in t_1 to remove homonuclear proton dipolar interactions. In the detection period protons are decoupled from the carbons using high power proton decoupling (HPPD).

4.3 Correlation of dipolar interactions and chemical shift in POM

Poly-(oxymethylene), with chain structure $(-CH_2-O-)_n$, is the polymerization product of formaldehyde. It is rather difficult to grow large crystals of the polymer, but some x-ray studies of small single crystals have been made. The stable form of POM has trigonal symmetry, with the chains arranged in a helical conformation. Within a single crystal only helices with the same handedness are found, with right or left handedness equally probable. Huggins [HU45] proposed the 9/5 model, meaning that the unit cell consists of chains with 9 CH_2-O monomer units in 5 turns of the helix. Uchida and Tadokoro [UC67] refined this to a 29/16 model. Both helices are so similar, however, that it is difficult to decide which model is the most reasonable [WU73]. The local tetrahedral symmetry of the CH_2O_2 unit appears to be hardly distorted by the helix formation (O-C-O bond angle ~ 111°). The H-C-H angle is 109° and the C-H bond length is 1.09 Å. The H-C-H plane makes an angle of 55° with the helix axis [UC67]. This information of the proton

positions allows us to find the orientation of the chemical shift tensor within the molecule.

Bulk-crystallized POM has a spherulitic structure, consisting of crystalline lamellae connected to each other by amorphous material. The lamellae, in which the molecular chains are folded, are approximately 100 Å thick [MC67]. The crystallinity is approximately 60 %. A detailed description of a spherulitic structure in crystalline polymers is given by Sharples [SH72].

Proton-decoupled ^{13}C spectra of a static sample of bulk-crystallized POM at room temperature show separate signals of the crystalline and the amorphous phase [VE79] (fig. 4.2b). Because the glass temperature of the amorphous phase is below room temperature, a lot of motion exists in this part of the polymer. In fact there is so much motion in the amorphous material that the chemical shift anisotropy is largely averaged, which results in a fairly narrow line in the NMR spectrum. For the rigid crystalline regions in the sample we observe a structured line determined by the chemical shielding anisotropy.

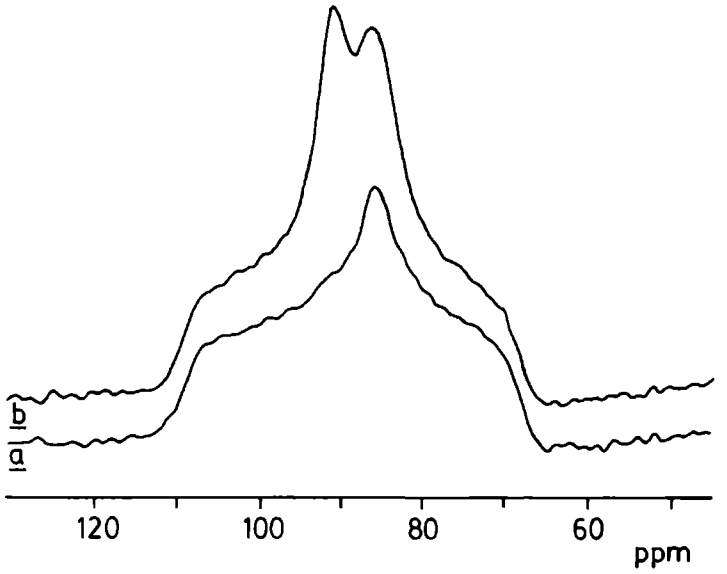

Fig. 4.2 ^{13}C chemical shift spectra of bulk-crystallized poly-(oxymethylene). spectrum b) gives the direct signal showing, besides the powder pattern of the crystalline parts of the polymer, the motionally narrowed line of the amorphous part. In spectrum a) the amorphous signal is removed by a selection on T_1 (fig. 4.3a).

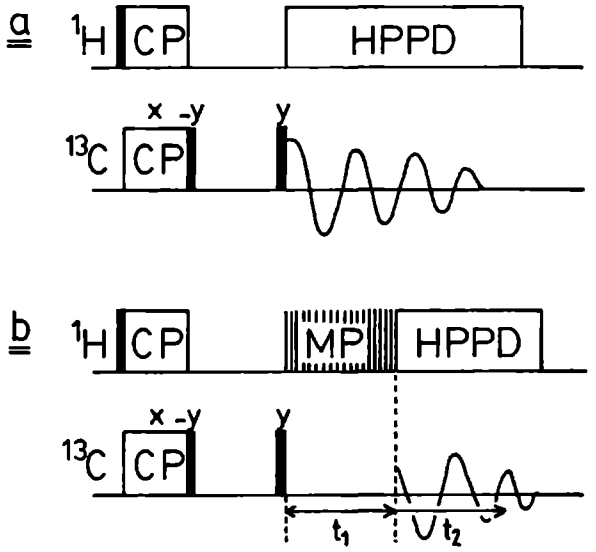

Fig. 4.3 a) Pulse scheme to obtain a chemical shift powder pattern of the crystalline part of POM without the amorphous signal via a T_1 selection (see text). Scheme b) is used to obtain a 2D dipolar correlated spectrum free of the signal of the amorphous POM.

The presence of the signal of the amorphous part obstructs the recovery of the principal values of the chemical shielding tensor from a 1D spectrum, as well as the determination of the orientation of the tensor from a 2D dipolar correlation spectrum. Therefore we want to eliminate the signal of the spins in the amorphous regions from our spectra. This is easy because the spin-lattice relaxation time T_1 is vastly different for the amorphous and the crystalline phase. At 75 MHz we find a ^{13}C T_1 = 90 msec for the amorphous region and T_1 = 18 sec for the crystalline region, in accordance with observations of Menger et al. [ME82] at 45 MHz. Fig. 4.3 displays the pulse scheme to eliminate the signal of the amorphous phase. First, transverse ^{13}C magnetization, from amorphous as well as crystalline spins, is created using cross-polarization. This magnetization is rotated immediately to the negative z axis with a $\pi/2$ pulse. Now the spins are affected by spin-lattice relaxation only, and thus relaxation to the positive z axis will start. At the point where the magnetization of the amorphous spins passes through zero, another $\pi/2$ pulse is applied, bringing the magnetization of the crystalline regions, which (because of its long T_1) is hardly influenced by the short

delay, back in the x-y plane of the rotating frame. At this point we can start collecting data for a 1D powder pattern or start the evolution period of the 2D dipolar correlation experiment (fig. 4.3). Fig. 4.2a shows the spectrum of the crystalline regions obtained in this way, giving the principal values σ_{XX} = 67 ppm, σ_{YY} = 86 ppm and σ_{ZZ} = 111 ppm. The 2D spectrum separating heteronuclear dipolar interactions from the chemical shielding anisotropy, obtained with the pulse scheme of fig. 4.3b, is shown in fig. 4.4a. MREV-8 ($\pi/2$ pulse length 1.6 μsec) was used for homonuclear decoupling during t_1. We observe a well resolved 2D powder pattern which should enable us to find the orientation of the shielding tensor in the molecule by simulation of the spectrum for different relative orientations of the ^{13}C-^{1}H dipolar tensor and the ^{13}C shift tensor.

4.4 Calculation of two-dimensional powder spectra

A general description of the calculation of powder spectra resulting from experiments correlating tensorial interactions is given by Linder et al. [LI80]. Here we describe the specific case of the correlation of the heteronuclear dipolar interaction to the chemical shielding anisotropy in a CH_2 group of poly-(oxymethylene). During the evolution period t_1, the strong homonuclear ^{1}H-^{1}H is suppressed by multiple pulse decoupling. Thus the relevant Hamiltonian for the ^{13}C spins is determined by the chemical shift H_{CS} and the heteronuclear dipolar interaction H_D. During the detection period normal high-power proton decoupling is applied so that only the ^{13}C Zeeman interaction remains.

$$H^{(1)} = H_{CS} + C\,H_D \qquad H^{(2)} = H_{CS} \tag{4.1}$$

where C represents the scaling factor due to the homonuclear decoupling. Of course it is possible to remove the influence of H_{CS} during t_1 by applying a π pulse in the middle of the evolution period, as has been described by Stoll et al. [ST76]. But the effect of H_{CS} during t_1 can also be calculated, therewith avoiding the need of an accurately adjusted π pulse in the experiment.

Evaluation of the Hamiltonians $H^{(1)}$ and $H^{(2)}$ gives us the resonance frequencies during evolution and detection period, thus allowing the calculation of the total 2D powder pattern. Summing over all transitions (i and j), with resonance frequencies $\omega_i^{(1)}(\theta,\varphi)$ and $\omega_j^{(2)}(\theta,\varphi)$, we get

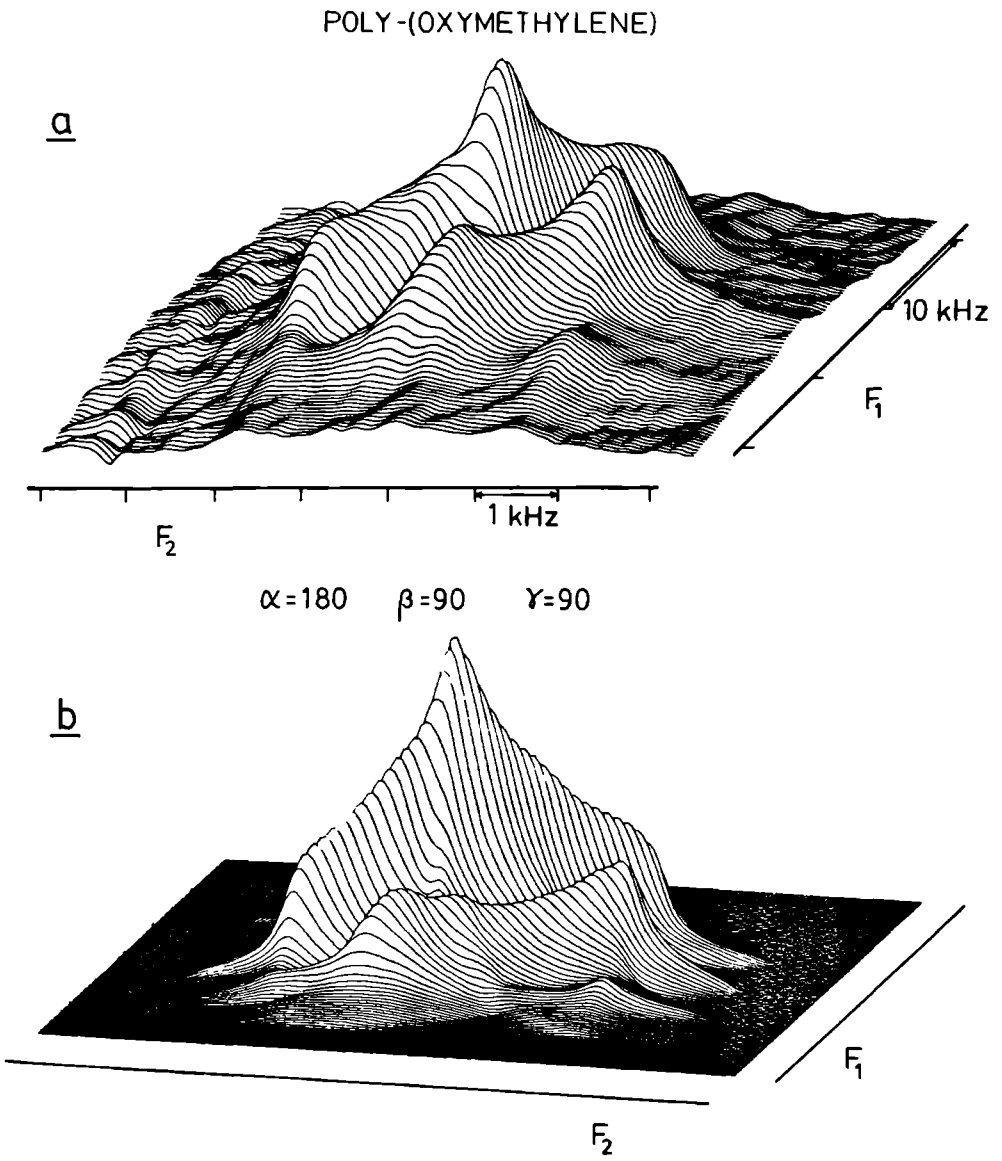

Fig. 4.4 a) 2D dipolar correlated ^{13}C spectrum of crystalline poly-(oxymethylene) obtained with the pulse scheme of fig. 4.3b. MREV-8 ($\pi/2$ pulse length 1.6 μs, cycle time 28.8 μs) was used during t_1. 400 scans were accumulated for 34 t_1 values. In t_1 a cosine filter was applied prior to Fourier transformation. b) Simulation of spectrum a) giving the orientation of the chemical shift tensor in POM (see text).

$$S(\omega_1,\omega_2) = \sum_i \sum_j \int_0^{2\pi} \int_0^{\pi} g_i^{(1)}[\omega_1-\omega_i^{(1)}(\theta,\varphi)]\; g_j^{(2)}[\omega_2-\omega_j^{(2)}(\theta,\varphi)]\; \sin\theta d\theta\, d\varphi \quad (4.2)$$

where θ and φ are the polar angles that describe the orientation of randomly distributed microcrystals with respect to the external magnetic field. The line shapes are denoted by the functions g.

The resonance frequency of a certain ^{13}C spin during the evolution period depends on the eigenstate of the connected protons and on the orientations of the chemical shielding and dipolar tensors with respect to the external field.

$$\begin{aligned}
\omega_1^{(1)} &= \omega_{CS}(\theta,\varphi) + C\,(\omega_{D1}(\theta,\varphi,\alpha,\beta,\gamma) + \omega_{D2}(\theta,\varphi,\alpha,\beta,\gamma)) \\
\omega_2^{(1)} &= \omega_{CS}(\theta,\varphi) + C\,(\omega_{D1}(\theta,\varphi,\alpha,\beta,\gamma) - \omega_{D2}(\theta,\varphi,\alpha,\beta,\gamma)) \\
\omega_3^{(1)} &= \omega_{CS}(\theta,\varphi) - C\,(\omega_{D1}(\theta,\varphi,\alpha,\beta,\gamma) - \omega_{D2}(\theta,\varphi,\alpha,\beta,\gamma)) \\
\omega_4^{(1)} &= \omega_{CS}(\theta,\varphi) - C\,(\omega_{D1}(\theta,\varphi,\alpha,\beta,\gamma) + \omega_{D2}(\theta,\varphi,\alpha,\beta,\gamma))
\end{aligned} \quad (4.3)$$

During the detection period we simply find

$$\omega^{(2)} = \omega_{CS}(\theta,\varphi) \quad (4.4)$$

Here θ and φ are the polar angles which orient the external magnetic field in the principal axis system of the chemical shielding tensor. α,β and γ are the Euler angles relating the dipolar interaction to the principal axis system of the CS tensor. The expression for ω_{CS} is easily obtained by transforming the Hamiltonian H_{CS} from the principal axis system to the laboratory frame over the Euler angles $\varphi,\theta,0$:

$$\omega_{CS}(\theta,\varphi) = \omega_{XX}\sin^2\theta\cos^2\varphi + \omega_{YY}\sin^2\theta\sin^2\varphi + \omega_{ZZ}\cos^2\theta \quad (4.5)$$

with $\omega_{XX} = \gamma B_0 \sigma_{XX}$ etc. In order to obtain expressions for ω_{D1} and ω_{D2} for the two protons, we have to evaluate the dipolar Hamiltonian H_D in the laboratory frame. To get similar expressions for both protons we define a local axis

system (LOC) in the CH_2O_2 unit whose z axis is the bisector of the H-C-H angle and the y axis perpendicular to the H-C-H plane (fig. 4.5). To come from the principal axis system of the dipolar interaction (D-PAS) to this axis system, one has to rotate over an angle $\frac{1}{2}\delta$ about the y axis for proton 1 and $-\frac{1}{2}\delta$ for proton 2 (δ = H-C-H angle = 109°). As we like to determine the orientation of the chemical shielding tensor within the molecule, we transform from this local axis system to the principal axis system of the chemical shielding tensor (CS-PAS) over the Euler angles α,β,γ. These angles α,β,γ are thus the unknown parameters which we want to recover from the simulated spectra. The last step is then to transform from the CS-PAS to the laboratory frame (LAB) over angles $\varphi,\theta,0$.

$$\text{D-PAS} \xrightarrow{0,\pm\frac{1}{2}\delta,0} \text{LOC} \xrightarrow{\alpha,\beta,\gamma} \text{CS-PAS} \xrightarrow{\varphi,\theta,0} \text{LAB} \qquad (4.6)$$

$$H_D = \sum_m D^2_{m,0}(\varphi,\theta,0) \sum_{m'} D^2_{m',m}(\alpha,\beta,\gamma) \; D^2_{0,m'}(0,\pm\tfrac{1}{2}\delta,0) \; \gamma_C\gamma_H\hbar^2 r_{CH}^{-3} \; I_z S_z$$

Some algebra eventually yields the contributions of the dipolar interactions to the resonance frequencies during t_1

$$\omega_{D1,2} = -\tfrac{1}{2}\gamma_C\gamma_H\hbar \; r_{CH}^{-3} \; [1 - 3 \; (A \sin\{\pm\tfrac{1}{2}\delta\} + B \cos\{\pm\tfrac{1}{2}\delta\})^2] \qquad (4.7)$$

with $A = \sin\theta \; (\cos\alpha \cos\beta \cos\{\varphi+\gamma\} - \sin\alpha \sin\{\varphi+\gamma\}) + \cos\theta \cos\alpha \sin\beta$

and $B = -\sin\theta \sin\beta \cos\{\varphi+\gamma\} + \cos\theta \cos\beta$

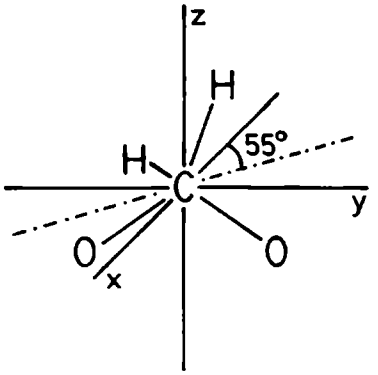

Fig. 4.5 Local axis system (LOC) in the CH_2O_2 unit. The O-C-O plane is chosen as the yz plane, and the H-C-H plane as the xz plane. The helix axis (-•-) makes an angle of 55° with the H-C-H plane.

Before we can calculate the 2D powder pattern from these resonance frequencies using eq. (4.2), there is still one point to consider, namely the line shape for each resonance. As was discussed in chapter 2 this depends on the type of modulation and how the data are Fourier transformed. In this case we have to do with phase modulation, i.e. the phase of the signal detected during t_2 is a linear function of length of the evolution period t_1. Successive complex Fourier transforms with respect to t_2 and t_1 gives the following line shape of mixed absorption and dispersion signals.

$$S(\omega_1,\omega_2) \sim [A_1(\omega_1)A_2(\omega_2) - D_1(\omega_1)D_2(\omega_2) + i\{A_1(\omega_1)D_2(\omega_2) + D_1(\omega_1)A_2(\omega_2)\}] \qquad (4.8)$$

with $A_i(\omega_i) = \dfrac{T_2}{1 + T_2^2(\omega_i-\omega)^2}$ and $D_i(\omega_i) = \dfrac{T_2^2(\omega_i-\omega)}{1 + T_2^2(\omega_i-\omega)^2}$

Generally an absolute value calculation is performed on such a signal, i.e. the square root of the sum of the squares of the real and the imaginary signal is calculated.

The presence of dispersion mode signals lowers the resolution of a spectrum, and can even lead to the disappearance of certain ridges in a 2D powder pattern. Pure absorption mode spectra can be achieved by performing a second experiment for each t_1 value with an additional ^{13}C π pulse at the end of the evolution period and coaddition the thus obtained FID with the FID of the original experiment [BA77]. The limited numbers of lines in a pulse program on a Bruker CXP-300 with Z70 pulse programmer, however, does not allow this in a straightforward way. Thus we have to calculate the effect of dispersion mode signals in our spectrum. This is legitimate because the experimental spectrum in fig. 4.4a shows, despite of dispersive signals, characteristic features which should allow the recovery of the orientation of the chemical shift tensor.

The 2D spectra were calculated in a rectangular grid of 100 x 100 frequency values (ω_1,ω_2). Generally 90000 sampling points were evaluated over a whole sphere. The spectrum thus calculated is subsequently convoluted with the line shape function described in eq. 4.8, followed by an absolute value calculation, resulting in a spectrum that can be compared to the experimental one.

4.5 Orientation of the chemical shift tensor in POM

Looking at the structure of poly-(oxymethylene), one expects the orientation of the chemical shielding tensor to be determined either by the local tetrahedral symmetry of the CH_2O_2 unit or by the overall symmetry of the helix (or even by both). Simulation of these possibilities gives very different 2D powder patterns, and the right solution is easily determined. Fig. 4.4b shows the calculated spectrum for $\alpha = 180°$, $\beta = 90°$, $\gamma = 90°$ which agrees very well with the experimental spectrum of fig. 4.4a. This means that the orientation of the chemical shielding tensor is determined by the local tetrahedral symmetry of the CH_2O_2 unit, which seems very reasonable, as the helix formation has hardly affected the local tetrahedron. The Z axis is oriented perpendicular to the O-C-O plane, the Y axis is located within the O-C-O plane and bisects the O-C-O angle. The X axis is of course perpendicular to the Y and Z axis (fig. 4.6).

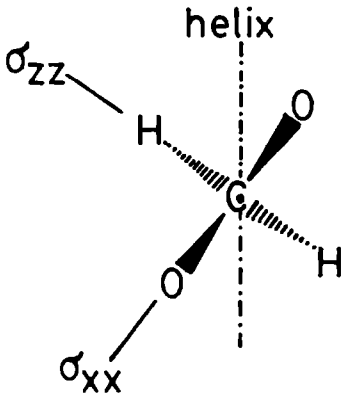

Fig. 4.6 Projection of the local CH_2O_2 unit in POM showing the orientation of the chemical shift tensor in the molecule, obtained by transforming the axis system in fig. 4.5 over the Euler angles 180, 90, 90. The Y axis points perpendicular to the plane of the drawing.

By varying the angles α,β,γ in little steps we were able to determine the accuracy of this experiment. If one of the angles is changed by more than 5° the resulting spectrum diverts clearly from the experimental spectrum. This means, taking eventual experimental variations into account, that the accuracy must be at least 10°.

References

BA77 P. Bachmann, W.P. Aue, L. Müller and R.R. Ernst, J. Magn. Res. 28, 29, 1977.

HE76 R.K. Hester, J.L. Ackerman, B.L. Neff anf J.S. Waugh, Phys. Rev. Lett. 36, 1081, 1976.

HU45 M.L. Huggins, J. Chem. Phys. 13, 37, 1945.

LI80 M. Linder, A. Höhener and R.R Ernst, J. Chem. Phys. 73, 4959, 1980.

MC67 N.G. McCrum, B.E. Read anf G. Williams, "Anelastic and Dielectric Effects in Polymeric Solids", J. Wiley and Sons, Inc., London, 1967.

ME82 E.M. Menger, W.S. Veeman and E. de Boer, Macromolecules 15, 1406, 1982.

MN82 M.G. Munowitz, W.P. Aue and R.G. Griffin, J. Chem. Phys. 77, 1686, 1982.

MU81 M.G. Munowitz, R.G. Griffin, G. Bodenhausen and T.H. Huang, J. Am. Chem. Soc. 103, 2529, 1981.

MU82 M.G. Munowitz and R.G. Griffin, J. Chem. Phys. 76, 2848, 1982.

MU84 M.G. Munowitz, T.H. Huang, C.M. Dobson and R.G. Griffin, J. Magn. Res. 57, 56, 1984.

OP77 S.J. Opella and J.S. Waugh, J. Chem. Phys. 66, 4919, 1977.

RY77 E.F. Rybaczewski, B.L. Neff, J.S. Waugh and J.S. Sherfinski, J. Chem. Phys. 67, 1231, 1977.

SC83 J. Schaefer, R.A. McKay, E.O. Stejskal and W.T. Dixon, J. Magn. Res. 52, 123, 1983.

SH72 A. Sharples in "Polymer Science", vol.1, chpt 4, A.D. Jenkins ed., North Holland Publishing Co., Amsterdam, 1972.

ST76 M.E. Stoll, A.J. Vega and R.W. Vaughan, J. Chem. Phys. 65, 4093, 1976.

UC67 T. Uchida and H. Tadokoro, J. Polym. Sci. A2 5, 63, 1967.

VE79 W.S. Veeman, E.M. Menger, W. Ritchey and E. de Boer, Macromolecules 12, 924, 1979.

WA75 J.S. Waugh, Second Specialized Colloque Ampère, Budapest, 1975.

CHAPTER 5

TWO-DIMENSIONAL EXCHANGE NMR

5.1 Introduction

In 1979, Jeener et al.[JE79] proposed a three-pulse sequence to study rate processes like spin relaxation, spin diffusion and chemical exchange. In high resolution NMR the NOESY variant of this experiment has proven to be a powerful tool for elucidating the 3-dimensional structure of large biochemical molecules in solution. In solid state NMR the 2D exchange experiment can also play an important role in the determination of very slow molecular motions, chemical exchange and spin diffusion.

Szeverenyi et al.[SZ82] were the first to transfer the Jeener experiment to the solid state. They showed that the experiment could be used in solids, under fast MAS conditions, in the same way as in liquids to study chemical exchange and spin diffusion between nuclei in different chemical environments. Furthermore, they demonstrated the effect of ^{14}N relaxation on the coupled ^{13}C spin and determined the ^{13}C NMR line shape for different linebroadening mechanisms. In a subsequent paper [SZ83] proton exchange rates in solid tropolone were thoroughly studied. Harbison et al.[HA85] combined the 2D exchange experiment with chemical shift scaling to investigate exchange between chemically different sites in the slow spinning regime.

^{14}N spectral spin diffusion among the four non-equivalent NH_4^+ ions in a single crystal of ammonium sulfate has been studied extensively by Suter and Ernst [SU82]. Edzes and Bernards [ED84] proposed to apply the 2D exchange NMR experiment to static powdered solids, where the full chemical shielding anisotropy is preserved. This experiment can detect changes in the orientation of the chemical shielding tensor of a particular spin due to molecular motion and/or spin diffusion. However, it cannot discriminate between the two processes and has the further disadvantage that the signal is distributed over a broad 2D powder pattern which implies time consuming experiments and limits its application to systems with one or at most a few non-overlapping NMR powder lines. In this way Edzes and Bernards detected spin diffusion between differently oriented chains in polyethylene. Henrichs and Linder [HE84] did so for ^{13}C-enriched zinc acetate dihydrate. Bronniman et al.[BR83] used the experiment to measure spin diffusion in adamantane.

This work was extended by Takegoshi and McDowell [TA86] who investigated spin diffusion within the J-multiplets.

The fact that a three-pulse sequence can be used to study slow molecular motions with correlation times even longer than T_2^*, the effective transverse relaxation time (which is the limit for relaxation measurements), has been exploited by Spiess [SP85 and references therein]. Spiess applied the Jeener-Broekaert sequence [JE67] to deuterons, using the (anisotropic) interaction of the electric quadrupole moment with the electric field gradient as a mechanism to detect motions. This method is very elucidating when a full 2D powder pattern is recorded [SC86]. The disadvantage is of course that samples have to be deuterated.

In this chapter it will be shown how the 2D exchange experiment is used to demonstrate (the absence of) molecular diffusion in carbon black-filled natural rubber, after the linebroadening mechanism is established [KE87]. Furthermore, a detailed theoretical and experimental description of how this technique can be used to investigate slow molecular motions via natural abundance ^{13}C NMR, using slow magic angle spinning to combine the advantages of a MAS experiment with the information one can get from static powder spectra [JO84, KE85].

5.2 Simple description of the experiment

The pulse sequence for the ^{13}C CP-MAS analogue of the Jeener experiment is depicted in fig. 5.1. The preparation period of the experiment involves the creation of transverse magnetization. This can be done either by a $\pi/2$ pulse or, as is shown in fig. 5.1, by cross polarization. In the latter case transverse ^{13}C magnetization will build up along the ^{13}C rf field. In the subsequent evolution period the ^{13}C spins undergo a particular interaction, generally the Zeeman interaction. This is achieved by eliminating ^{1}H-^{13}C dipolar interactions through high-power proton decoupling. Thus during the evolution period the ^{13}C spins are allowed to precess freely, only subject to the Zeeman interaction. At time t_1 a $\pi/2$ pulse is applied to the system, therewith creating for each spin isochromat a magnetization vector along the z axis whose magnitude depends on the angle Θ the spin isochromat has passed through, in the rotating frame, during evolution. (In case of a static sample or a fast spinning sample this angle is equal to ωt_1, where ω is the resonance frequency of the particular spin. In case of slow MAS a difficulty arises, because then the resonance frequency is no longer constant during the

evolution period. This special case will be treated separately in paragraph 5.4.) The remaining transverse magnetization dephases quickly because proton decoupling is turned off during the mixing time τ_m. So during the mixing period the magnetization vector of each spin isochromat is aligned along the z axis, with an amplitude determined by the resonance frequency during the evolution period. It is in this time interval (which can be as long as the spin-lattice relaxation time T_1) that the exchange process can take place. The simplest process to envisage is chemical exchange were certain spins move to a chemically different environment and thus change their resonance frequency during the mixing period. At the end of the mixing period a $\pi/2$ is applied to reestablish observable ^{13}C magnetization. During the detection period, the system undergoes the same interaction as in the evolution period, and the resonance frequency of each spin isochromat is monitored (by collecting a FID).

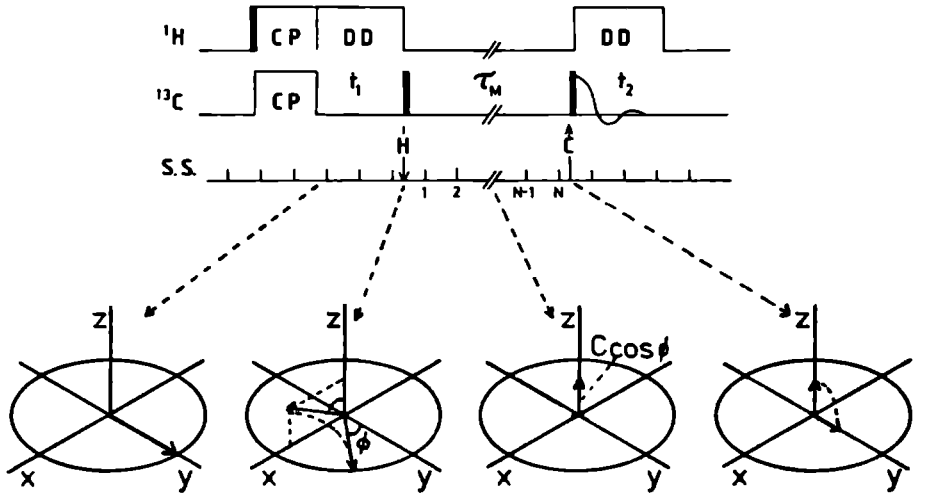

Fig. 5.1 Pulse sequence for the 2D exchange experiment in solids, with cross polarization (CP) and high-power dipolar decoupling (DD). 90° pulses are black. In the case of slow magic angle spinning a synchronous mixing time is obtained with the Synchro-Spin (SS). With an optical signal from the spinner, the Synchro-Spin holds the pulse programmer at point H and lets it continue after N spinner rotations at point C. The evolution of a spin packet during the experiment is shown below.

If there is no exchange mechanism present during the mixing period, each spin will have the same resonance frequency during the evolution and the detection period, meaning that the signal of each isochromat collected during t_2 will be amplitude-modulated by a sine or cosine (depending on the phase of the $\pi/2$ pulses) function with that very same resonance frequency. The resulting two-dimensional spectrum will only have signals on the diagonal. This spectrum on the diagonal will be identical to the ordinary one-dimensional CP-MAS spectrum, when we assume that no intensity has been lost through spin-lattice relaxation. If, however, some spins have (ex)changed their frequency during mixing this will show up by the presence of off-diagonal peaks, whose positions are determined by the resonance frequencies during t_1 and t_2. The intensity of these cross peaks will be determined by the rate of the exchange process. A more detailed theoretical account is given by Jeener et al.[JE79], whereas the special case of slow magic angle spinning will be treated in paragraph 5.4.

5.3 Application to natural rubber

In chapter 3 it was seen that there are extensive molecular motions in carbon black-filled natural rubber. Taking ^{13}C NMR spectra of the rubber under various conditions, and comparing them to adamantane spectra, led us to the conclusion that the heteronuclear carbon-proton as well as the homonuclear proton-proton dipolar interactions are averaged to a great extent. The fact that intra-chain dipolar interactions (which are of the order of tens of kHz) are averaged shows that there must be fast motions using different degrees of freedom of the chain segments.

The fact that dipolar interactions between different chain segments are also very small is surprising. As mentioned in chapter 3, inter-molecular dipolar interactions in adamantane are rather big (≈ 9 KHz). In the rubber sample discussed here and elsewhere [SC72, SH72, DY75] the average ^1H-^1H dipolar interaction for protons located on neighboring chains or chain segments is at least 50 times smaller than in adamantane. This in spite of the fact that there are filler particles, cross-links and entanglements holding different chains together. It means that either the inter-chain distance is very large or that there is, in addition to chain rotations, enough diffusion in the natural rubber to average this interaction. With diffusion large scale lateral movements of chains with respect to each other

are meant. It would implicate that large parts of the polymer network have to reorient.

To investigate if such a molecular diffusion exists we make use of the fact that the rubber ^{13}C lines in the absence of MAS but with proton decoupling are inhomogeneously broadened, presumably by susceptibility effects due to the presence of the filler. In this picture it is believed that different sites relative to a filler particle have different susceptibility and therefore different resonance frequencies. We performed a Jeener-type 2D exchange experiment with high-power proton decoupling during the detection and evolution period on a non-spinning rubber sample. As T_1 values are of the order of 80 msec (except for the quaternary carbon which has a much longer T_1) a mixing time of 40 msec was chosen. The result of this experiment is shown in fig. 5.2. The fact that the lines are extended along the diagonal shows that they are inhomogeneously broadened [SZ82], because in an inhomogeneously broadened line each spin isochromat has a fixed resonance frequency, and thus it will resonate exactly along the diagonal in a 2D exchange spectrum. In a homogeneously broadened line, however, the resonance frequency of a certain spin is modulated constantly and will, generally, not have exactly the same resonance frequency during evolution and detection period. This results in a line shape that is broadened in both dimensions of the 2D spectrum.

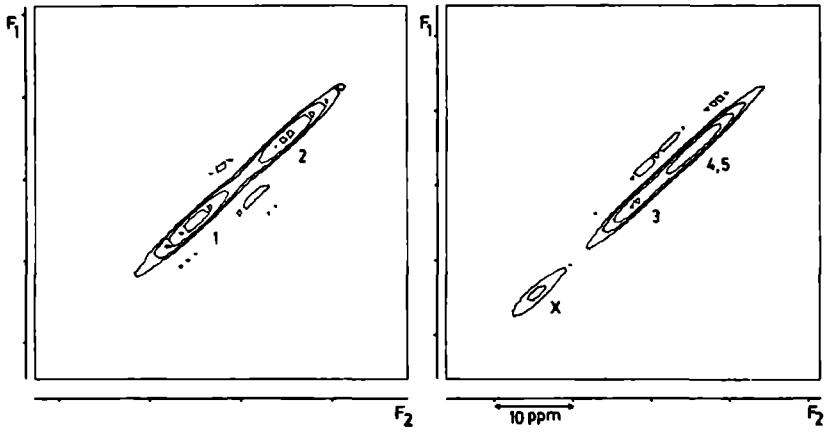

Fig. 5.2 Contour plot of a 2D exchange spectrum (τ_m = 40 ms) of a non-spinning rubber sample with high power proton decoupling during evolution and detection period. For the assignment of the lines see chapter 3. The line denoted X is from an antidegradant.

From these line shapes it can further be concluded that the polymer chains do not diffuse through great volumes in the sample and thereby allowing each ^{13}C spin to sample different values of the inhomogeneous magnetic field on a time scale of 40 msec. If this were so than the lines would, as in the case of a homogeneously broadened line, spread out in the direction perpendicular to the diagonal. A spin which has diffused to another location in the sample experiencing a different field during the detection period than it did during the evolution period will not resonate on the diagonal. Thus with this 2D experiment no molecular diffusion can be detected. The negative result may point to the absence of diffusion on a time scale of 40 msec in which case the relatively small inter-chain dipolar interactions must be due to a large distance between different segments. An alternative explanation can be, however, that reorientations are limited to small regions, i.e. in voids between filler particles, where the magnetic field is rather constant.

5.4 2D exchange NMR in slowly rotating solids

As we have seen the 2D exchange experiment relies on the fact that, in the absence of exchange, the resonance frequency of a certain spin is the same in evolution and detection period, and in the resulting 2D spectrum NMR intensity is found at the diagonal only. In the presence of exchange NMR lines occur outside the diagonal. If we apply this principle to a solid state NMR experiment the resulting 2D spectrum depends on the experimental situation. If we exclude for a moment the possibility of (chemical or spin) exchange then for a static sample each spin has a fixed resonance frequency, depending on the orientation of the chemical shift tensor with respect to the external magnetic field B_0. The 2D spectrum has diagonal lines only, unless in the case of molecular motion which changes the orientation of the chemical shift tensor. For a sample where fast magic angle spinning averages the chemical shift tensor, the 2D spectrum is diagonal again in the absence of exchange. In this case molecular reorientations, between chemically identical sites, cannot give any off-diagonal intensity in the 2D spectrum.

In the case of slow magic angle spinning, slow relative to the chemical shift anisotropy, the situation is different. Now the resonance frequency of a certain spin is no longer constant, but modulated by the spinning. In a 1D experiment this manifests itself as the presence of a pattern of spinning sidebands [MA79, HE80]. In a 2D exchange experiment this results in a 2D

spinning sideband pattern with diagonal as well as off-diagonal peaks, whether there is exchange (which includes motions) or not. This is not a desirable situation when one wants to detect any kind of exchange. The question of course arises why it could be of interest to work under slow MAS conditions. Fast MAS (i.e. total averaging of the chemical shift anisotropy) is preferred if we like to determine the rate of exchange between chemically different sites. However, if we would like to determine the relative orientations of the chemical shift tensors related by the exchange process or if we want to study exchange (including molecular motions) between chemically equivalent but orientationally different sites, then we need information about the chemical shielding tensors involved. Of course, a static sample will yield this information but this has the disadvantage that we "smear out" the intensity over a whole 2D powder pattern, moreover with several overlapping lines present the problem may easily become insoluble. With slow MAS these sensitivity and resolution problems are circumvented, overlapping powder patterns are resolved and the total intensity is confined to a restricted number of sidebands. These sidebands, however, do contain all the information about the chemical shielding tensor [MA79, HE80]. In the next section we will show that it is possible to derive a condition for the mixing period τ_m for which the off-diagonal spinning sidebands disappear when there is no exchange.

5.4.1 Theory of 2D exchange under slow MAS conditions

In order to derive a formula to describe the intensity of each sideband in a 2D spectrum, we follow the classical approach of Herzfeld and Berger [HE80], who calculated sideband intensities as a function of CSA tensor values and spinning speed in a 1D spectrum (see also chapter 1). First we have to evaluate the Hamiltonian during the evolution period, expressed in spherical tensor operators this is [HA76, MA79]:

$$H_{CS} = \sum_{l=0,2} \sum_{m=-l}^{l} (-1)^m R_{l,-m} T_{l,m} \qquad (5.1)$$

After truncation we have two terms left :

$$H_{CS} = \gamma\hbar (R_{0,0}T_{0,0} + R_{2,0}T_{2,0}) \qquad (5.2)$$

with the spin dependent terms $T_{0,0} = I_z B_0$ and $T_{2,0} = \sqrt{(2/3)}\, I_z B_0$. $R_{0,0}$ is a scalar equal to the isotropic chemical shift σ, which is the same in every axis system. So we have to evaluate the term $R_{2,0}$ which expresses the spatial dependence of the Hamiltonian. To do so we start in the principal axis system (PAS) of the shielding tensor were R is known ($R=\rho$ with $\rho_{0,0}=\sigma$, $\rho_{2,0}=\sqrt{(3/2)}\delta$ and $\rho_{2,\pm2}=\delta\eta/2$, where $\delta = \sigma_{ZZ} - \sigma$ and $\delta\eta = \sigma_{XX} - \sigma_{YY}$), followed by a transformation to a coordinate system fixed in the rotor (RAS, the rotation axis is chosen as the z-axis). In this (rotating) coordinate system, the static magnetic field vector B_0 appears to be precessing around the z-axis at the magic angle θ_m (see fig. 5.3). Consequently, the next step is to transform from the rotor system to the laboratory frame (LAB) over the Euler angles $\omega_r t$, θ_m, 0.

$$\text{PAS} \xrightarrow{\alpha,\beta,\gamma} \text{RAS} \xrightarrow{\omega_r t,\theta_m,0} \text{LAB} \tag{5.3}$$

$$R_{2,0} = \sum_{m'} D^2_{m',0}(\omega_r t,\theta_m,0) \sum_{m''} D^2_{m'',m'}(\alpha,\beta,\gamma)\, \rho^{PAS}_{2,m''}$$

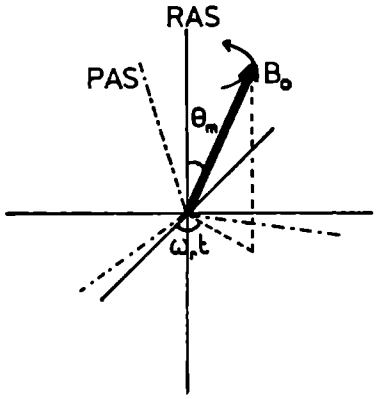

Fig. 5.3 Principal axes system of the shielding tensor (PAS) and the external field B_0 as viewed from a coordinate system defined in the rotor (RAS).

Evaluating eq. (5.3) (appendix I) and substitution in eq. (5.2) then gives us the Hamiltonian during t_1:

$$H_{CS} = -\gamma\hbar B_0 I_z [\sigma_1 + \tfrac{2}{3}(A_1\cos(2\omega_r t+2\gamma) + B_1\sin(2\omega_r t+2\gamma)) + \tfrac{2}{3}\sqrt{2}(C_1\cos(\omega_r t+\gamma) + D_1(\sin(\omega_r t+\gamma))] \tag{5.4}$$

with $A_1 = \frac{1}{8}\delta\,(\,\eta(3+\cos2\beta)\cos2\alpha + 3(1-\cos2\beta)\,)$

$B_1 = -\frac{1}{2}\delta\eta\cos\beta\sin2\alpha$

$C_1 = \frac{1}{4}\delta\sin2\beta\,(\eta\cos2\alpha - 3)$

$D_1 = -\frac{1}{2}\delta\eta\sin\beta\sin2\alpha$

from which the resonance frequency of each spin, as given by Herzfeld and Berger [HE80], follows directly. In chapter 1 we already mentioned that the intensities of spinning sidebands in a 1D spectrum can be calculated from these modulated resonance frequencies of the individual spins.

When any molecular motion or in general any spin exchange has occurred during τ_m, the orientation of the chemical shielding tensor may be different in t_1 and t_2. So we have to evaluate the Hamiltonian during the detection period after exchange has taken place. Now our starting point to calculate $R_{2,0}$ in eq. (5.2) is the principal axis system of the CSA tensor after exchange has occurred. From this coordinate system we transform to the CSA principal axis system before exchange, followed by a transformation to the rotor coordinate system, and finally to the laboratory frame.

$$\mathrm{PAS}_{t_2} \xrightarrow{\lambda,\mu,\nu} \mathrm{PAS}_{t_1} \xrightarrow{\alpha,\beta,\gamma} \mathrm{RAS} \xrightarrow{\omega_r t,\theta_m,0} \mathrm{LAB} \tag{5.5}$$

$$R_{2,0} = \sum_{m'} D^2_{m',0}(\omega_r t,\theta_m,0) \sum_{m''} D^2_{m'',m'}(\alpha,\beta,\gamma) \sum_{m'''} D^2_{m''',m''}(\lambda,\mu,\nu)\,\rho^{\mathrm{PAS}}_{2,m'''}$$

Some algebra will eventually yield a Hamiltonian with the same general appearance as eq. (5.4):

$$H_{CS} = -\gamma h B_0 I_z[\sigma_2 + \tfrac{2}{3}(A_2\cos(2\omega_r t+2\gamma) + B_2\sin(2\omega_r t+2\gamma)) + \tfrac{2}{3}\sqrt{2}(C_2\cos(\omega_r t+\gamma) + D_2\sin(\omega_r t+\gamma))] \tag{5.6}$$

$$\begin{aligned} A_2 = \tfrac{1}{8}\delta\,[&\tfrac{1}{4}(3+\cos2\beta)\,\{(((1-\cos2\mu)\,(3-\eta\cos2\lambda) + 4\eta\cos2\lambda)\cos(2\alpha+2\nu) \\ &\qquad -4\eta\cos\mu\sin2\lambda\sin(2\alpha+2\nu)\} \\ &+ \sin2\beta\,\{\sin2\mu\,(3-\eta\cos2\lambda)\cos(\alpha+\nu) + 2\eta\sin\mu\sin2\lambda\sin(\alpha+\nu)\} \\ &+ \tfrac{3}{4}(1-\cos2\beta)\,(4 - (1-\cos2\mu)\,(3-\eta\cos2\lambda))] \end{aligned}$$

$$B_2 = \frac{1}{4}\delta\,[\cos\beta\,\{-2\eta\,\cos\mu\,\sin 2\lambda\,\cos(2\alpha+2\nu) - \tfrac{1}{2}((1-\cos 2\mu)\,(3-\eta\cos 2\lambda) + 4\eta\cos 2\lambda)\,\sin(2\alpha+2\nu)\} + \sin\beta\,\{2\eta\,\sin\mu\,\sin 2\lambda\,\cos(\alpha+\nu) - \sin 2\mu\,(3-\eta\cos 2\lambda)\,\sin(\alpha+\nu)\}]$$

$$C_2 = \frac{1}{8}\delta\,[\sin 2\beta\,\{\tfrac{1}{2}((1-\cos 2\mu)\,(3-\eta\cos 2\lambda) + 4\eta\cos 2\lambda)\,\cos(2\alpha+2\nu) - 2\eta\,\cos\mu\,\sin 2\lambda\,\sin(2\alpha+2\nu)\} - 2\cos 2\beta\,\{\sin 2\mu\,(3-\eta\cos 2\lambda)\,\cos(\alpha+\nu) + 2\eta\,\sin\mu\,\sin 2\lambda\,\sin(\alpha+\nu)\} - \tfrac{3}{2}\sin 2\beta\,(4 - (1-\cos 2\mu)\,(3-\eta\cos 2\lambda))]$$

$$D_2 = \frac{1}{4}\delta\,[\sin\beta\,\{-2\eta\,\cos\mu\,\sin 2\lambda\,\cos(2\alpha+2\nu) - \tfrac{1}{2}((1-\cos 2\mu)\,(3-\eta\cos 2\lambda) + 4\eta\cos 2\lambda)\,\sin(2\alpha+2\nu)\} - \cos\beta\,\{2\eta\,\sin\mu\,\sin 2\lambda\,\cos(\alpha+\nu) + \sin 2\mu\,(3-\eta\cos 2\lambda)\,\sin(\alpha+\nu)\}]$$

Having defined our system we now turn to the calculation of the sideband intensities. As was explained in paragraph 5.2 the signal detected during t_2 is modulated in amplitude by the cosine (or sine) of the angle θ_1 a certain spin packet has passed through during t_1. Neglecting relaxation effects, the FID of one spin is given by

$$g(t_1,t_2) = \cos(\theta_1(\alpha,\beta,\gamma,t_1))\,\exp(i\theta_2(\alpha,\beta,\gamma,\lambda,\mu,\nu,t_2)) \qquad (5.7)$$

The angles θ_1 and θ_2 the spins have passed through in the rotating frame are no longer simply the product of the resonance frequency ω and the evolved time t. Since the resonance frequency of each spin is now time dependent (frequency modulation) we have to evaluate the integral of ω over t

$$\theta_1 = \int_0^{t_1} \omega_1(\alpha,\beta,\gamma,t)\,dt \quad \text{and} \quad \theta_2 = \int_{t_1+\tau_m}^{t_1+\tau_m+t_2} \omega_2(\alpha,\beta,\gamma,\lambda,\mu,\nu,t)\,dt \qquad (5.8)$$

ω_1 and ω_2 are determined by eq. (5.4) and (5.6) and represent the resonance frequency in respectively evolution and detection period. In case of pure amplitude modulation, the FID can be split in a term with negative and a term with positive modulation frequency, generally referred to as the echo and the anti-echo [BA82 and references therein]. The spectra resulting from these

terms are, except for line shape effects, normally each others mirror image. In the case of slow spinning, as we shall see in the following, this will no longer be true. For the time being we concentrate on the anti-echo component. The anti-echo for the whole sample is

$$g_{ae}(t_1,t_2) = \int_0^{2\pi}\int_0^{\pi}\int_0^{2\pi} \exp\left(i\int_0^{t_1}\omega_1(t)dt\right) \exp\left(i\int_{t_1+\tau_m}^{t_1+\tau_m+t_2}\omega_2(t)dt\right) d\alpha \sin\beta d\beta\, d\gamma \quad (5.9)$$

where the integration over α, β, γ represent a powder average over all orientations on a sphere. Evaluation of eq. (5.8) in Bessel functions using the property

$$\exp(iA\sin\varphi) = \sum_{k=-\infty}^{\infty} \exp(ik\varphi)\, J_k(A) \quad (5.10)$$

gives the following contribution of one spin to the anti-echo

$$\frac{1}{2} \sum_{N_a}\sum_{N_b}\sum_{N_a'}\sum_{N_b'} F_1(N_a)\, F_1^*(N_a')\, F_2(N_b)\, F_2^*(N_b') \quad (5.11)$$
$$\cdot\exp i\{-\gamma B_0\sigma_1 t_1 + \omega_r(N_b-N_b'+N_a)t_1 - \gamma B_0\sigma_2 t_2 + \omega_r N_b t_2 + \gamma(N_a+N_b-N_a'-N_b')\}$$

$$F_1(N) = \sum_j\sum_k\sum_m J_j(\bar{A}_1)\, J_k(\bar{B}_1)\, J_m(\bar{D}_1)\, J_{N-2j-2k-m}(\bar{C}_1)\, \exp -i\tfrac{\pi}{2}(k+m)$$

$$F_2(N) = \sum_p\sum_q\sum_s J_p(\bar{A}_2)\, J_q(\bar{B}_2)\, J_s(\bar{C}_2)\, J_{N-2p-2q-s}(\bar{C}_2)\, \exp -i\tfrac{\pi}{2}(q+s)$$
$$\exp iN\omega_r\tau_m$$

where $\bar{A}_1 = \frac{\gamma B_0}{3\omega_r} A_1$ (c/f $\bar{A}_2, \bar{B}_1, \bar{B}_2$) and $\bar{C}_1 = \frac{\gamma B_0}{3\omega_r} 2\sqrt{2}\, C_1$ (c/f $\bar{C}_2, \bar{D}_1, \bar{D}_2$)

A two-dimensional Fourier transform of this anti-echo signal thus consists of a whole pattern of diagonal as well as off-diagonal spinning sidebands. Eq. (5.11) and eq. (5.9) now give us for the intensity of the sideband at position $-\gamma B_0\sigma_1 + N_1\omega_r$, $-\gamma B_0\sigma_2 + N_2\omega_r$

$$I(N_1,N_2) = \frac{1}{8\pi}\int_0^{2\pi}\int_0^{\pi}\sum_{N_b'} F_1(N_1-N_2+N_b')\, F_1^*(N_1)\, F_2(N_2)\, F_2^*(N_b')\, \sin\beta d\beta d\alpha \quad (5.12)$$

note that the integral over γ has already been carried out and gave the contribution $2\pi\,\delta(N_1-N_a')$. Using the relationship

$$J_n(A) = \frac{1}{2\pi}\int_0^{2\pi} \exp(iA\sin\theta - in\theta)\, d\theta \tag{5.13}$$

and $$\sum_{N=-\infty}^{\infty} \exp(-iNx) = 2\pi\,\delta(x) \tag{5.14}$$

we eventually get the intensity of sideband N_1,N_2

$$I(N_1,N_2)= \int_0^{2\pi}\int_0^{\pi}\int_0^{2\pi} f_1(\theta)\, f_2^*(\theta+\omega_r\tau_m)\, \exp i((N_2-N_1)\theta+N_2\omega_r\tau_m)d\theta \int_0^{2\pi} f_1^*(-\theta')\exp\{-iN_1\theta'\}d\theta' \int_0^{2\pi} f_2(\varphi)\exp\{-iN_2\varphi\}d\varphi\ \sin\beta d\beta d\alpha \tag{5.15}$$

with $f_1(\theta)=\frac{1}{2\pi}\exp i(\bar{A}_1\sin2\theta-\bar{B}_1\cos2\theta+\bar{C}_1\sin\theta-\bar{D}_1\cos\theta)$

and $f_2(\varphi)=\frac{1}{2\pi}\exp i(\bar{A}_2\sin2\varphi-\bar{B}_2\cos2\varphi+\bar{C}_2\cos\varphi-\bar{D}_2\sin\varphi)$

This expression shows that there will be signal intensity at all cross-points of the 2D spinning sideband spectrum. Even if there is no exchange, in which case $f_2(\theta)=f_1(\theta)$, there will be diagonal ($N_1=N_2$) as well as off-diagonal ($N_1\neq N_2$) peaks present. However, when we take the mixing time as an integer number of spinner rotations, $\omega_r\tau_m$ becomes an integer multiple of 2π and vanishes from eq. (5.15), and when there is no exchange, the off-diagonal peaks vanish along with it. Then

$$I(N_1,N_2)=\int_0^{2\pi}\int_0^{\pi}\int_0^{2\pi} f_1(\theta)\, f_2^*(\theta)\exp\{i(N_2-N_1)\theta\}d\theta \int_0^{2\pi} f_1^*(-\theta')\exp\{-iN_1\theta'\}d\theta' \int_0^{2\pi} f_2(\varphi)\exp\{-iN_2\varphi\}d\varphi\ \sin\beta d\beta d\alpha \tag{5.16}$$

with $f_1(\theta)=f_2(\theta)$ and $\int_0^{2\pi} |f_1(\theta)|^2\exp\{i(N_2-N_1)\theta\}d\theta = \frac{1}{2\pi}\,\delta(N_2-N_1)$

gives $$I(N,N) = \frac{1}{8\pi}\int_0^{2\pi}\int_0^{\pi}\left|\int_0^{2\pi} f_1(\varphi)\exp\{-iN\varphi\}d\varphi\right|^2 \sin\beta d\beta d\alpha \tag{5.17}$$

This equation is equivalent to that given by Herzfeld and Berger [HE80] for the intensities of the spinning sidebands in a 1D spectrum. So when there is no exchange and the mixing time is chosen as an integer number of rotor periods, the conventional 1D spinning sideband pattern will appear at the anti-echo component of the resulting 2D spectrum.

A similar evaluation of the echo component of an experiment with a rotor synchronized mixing period gives the sideband intensity

$$I(N_1,N_2)= \int_0^{2\pi}\int_0^{\pi}\int_0^{2\pi} f_1^*(-\theta)\, f_2^*(-\theta)\, \exp\{i(N_1-N_2)\theta\}d\theta \int_0^{2\pi} f_2(\varphi)\, \exp\{-iN_2\varphi\}d\varphi \int_0^{2\pi} f_1(\theta')\, \exp\{iN_1\theta'\}d\theta' \sin\beta d\beta d\alpha \qquad (5.18)$$

which shows that there will be off-diagonal peaks even if there is no exchange. So in this experiment the echo and the anti-echo component of the spectrum are not each others mirror image. For the detection of exchange it is thus desirable to acquire the anti-echo only, which can easily be achieved by appropriate phase cycling (table 5.1).

These mathematical results can be understood by the following physical picture. At the beginning of the evolution period, the magnetization vectors of every spin packet lie along the same axis (determined by the ^{13}C rf field) of the rotating frame. During t_1, each individual component follows a specific path in the xy-plane, with a time-dependent precession frequency (see fig. 5.4) determined by eq. (5.4). These magnetization paths are periodic with period $2\pi/\omega_r$ (drawings of these paths are given by Olejniczak et al.[OL84]). At the end of the evolution period, the components are brought to the z-axis with an amplitude which depends on the whole specific precession history of each individual component during t_1. Now when the mixing time τ_m is synchronized with the rotor, the spinner orientation is exactly the same at the end of the evolution period as at the beginning of the detection period. When in addition there has been no exchange during τ_m, each spin packet starts at t_2=0 with exactly the same precession frequency it had at the end of the evolution period and the precession history seems uninterrupted. As a result only diagonal peaks will appear in the anti-echo spectrum. Even in the case that the total (macroscopic) magnetization of the sample has vanished because the individual components have dephased at the

end of the evolution, there is still some order and because the labeling takes place for each individual spin packet, this label will then be recovered for the anti-echo magnetization emerging directly after the last pulse. For the echo component, however, pulsed echo formation and rotational echo formation (by MAS) interfere, i.e. if they don't coincide they destruct each other even if the mixing period is an integral number of rotor periods. Thus we will always get a rotational echo pattern, and thus spinning sidebands, in both dimensions of the spectrum.

Table 5.1 Phase cycling for the 2D exchange experiment as shown in fig. 5.1, to select the anti-echo and suppress axial peaks. This can be further extended with a cyclops sequence.

CP-phase	first $\pi/2$	second $\pi/2$	receiver
y	x	x	x
y	-y	y	-x
y	-x	x	-x
y	y	y	x

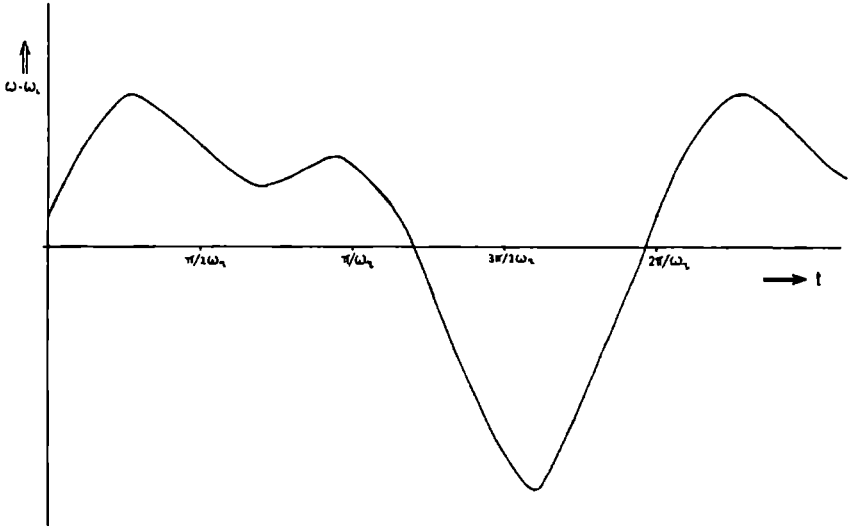

Fig. 5.4 Variation of the resonance frequency of a spin packet during sample rotation about the magic angle.

5.4.2 Experimental realization

In the preceding section it was concluded that the mixing period has to be synchronized with the rotor in order to be able to detect an exchange process by the presence of cross peaks. That this synchronization can not simply be reached by making the mixing time in the pulse programmer an integer multiple of rotor periods may become clear by the following example. Assume we like to work with a mixing time of 1 second. If the spinner frequency has drifted by only 0.1 Hz during that time, the position of the rotor at the end of the mixing time will be turned 36° with respect to its starting position. This, of course, will give rise to the appearance of cross-peaks. To achieve exact synchronization, an optical sensor was used to generate short trigger pulses synchronous with the spinner rotation. These trigger signals were fed into a specially designed apparatus, the "Synchro-spin". Every period of the spinner such a trigger signal resets to zero a counter of the Synchro-spin (operating at 10 Mhz). At the end of the evolution period, a gate of the pulse programmer stops this counter and the Synchro-spin responds by holding the pulse programmer (point H in fig. 5.1), and storing the value the counter has reached. A separate counter counts N trigger pulses (for N spinner revolutions). When the Nth trigger pulse has arrived, the 10 Mhz counter starts counting back to zero. When zero is reached, the Synchro-spin releases the pulse programmer (point C in fig. 5.1) which then continues with the final $\pi/2$ pulse. The effect is a mixing time of $N2\pi/\omega_r$ seconds with a accuracy better than 1° in the orientation of the spinner at the beginning and end of the mixing period, independent of N. Fluctuations in spinner frequency will now only alter the mixing time by a negligible amount.

To demonstrate the effect of a synchronous mixing time experimentally, we took spectra of hexamethylbenzene (HMB). The experiments were carried out on a Bruker CXP 300, with a carbon frequency of 75.4 MHz. The spinners were of the Andrew-Beams type, as they are implemented in standard Bruker CP-MAS probes. The aromatic carbons of HMB have a large chemical shielding anisotropy. At room temperature, no exchange takes place on the timescale of this experiment (msec - sec region). In fig. 5.5a, the anti-echo component of the spectrum of the aromatic carbon of HMB is shown as results from a 2D exchange experiment with an asynchronous mixing time. A complete 2D spinning sideband pattern is found. If the Synchro-spin controls the mixing time, however, excellent synchronization is achieved and all off-diagonal peaks

disappear, as can be seen in fig. 5.5b. The measured intensities agree well with our computer simulations based on eq. (5.17). Manual adjustment of the mixing time, without Synchro-spin control, always gave rise to the appearance of off-diagonal peaks, even at mixing times as short as 10 msec.

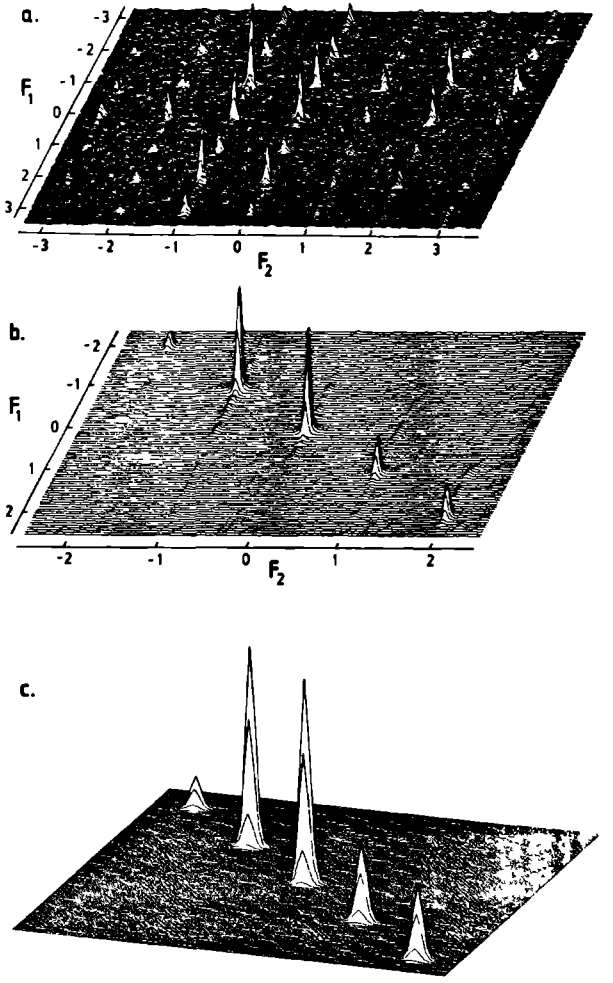

Fig. 5.5 Absolute mode spectra of the aromatic carbon atoms of hexamethylbenzene. Sine-bell filters were used in both dimensions. Numbers indicate the position of the spinning sidebands. a) Asynchronous mixing time of 10 ms with ν_R = 2220 Hz. b) Synchronous mixing time of 30 rotor periods with ν_R = 2980 Hz (τ_m = 10.1 ms). c) Computer simulation of the spectrum shown in b).

Another testcase for this experiment forms dimethylsulfone (DMS), which exhibits a two-site jump about its twofold symmetry axis. This process has been characterized by a powder pattern analysis [SO83]. DMS has one ^{13}C NMR line with a moderate anisotropy ($\sigma_{11} = \sigma_{22} = 63$ ppm, $\sigma_{33} = 7$ ppm relative to TMS). The molecule jumps about its C2 axis (fig. 5.6c), so that the two methyl groups change place. The principal axis systems of the CSA tensors of these methyl groups can be related by a rotation over 108° about the σ_{22} axis (perpendicular to the C-S-C plane). At room temperature the exchange rate is 314 s^{-1} [SO83], which means an average jump time of ≈ 3 msec. Figs. 5.6a and 5.6b give the results of the 2D exchange experiment, with synchronous mixing times of 0 and 6.4 msec, respectively. As expected, fig. 5.5a shows only diagonal peaks. In fig. 5.5b the effect of the molecular motion is clearly seen in the appearance of cross peaks in the spectrum.

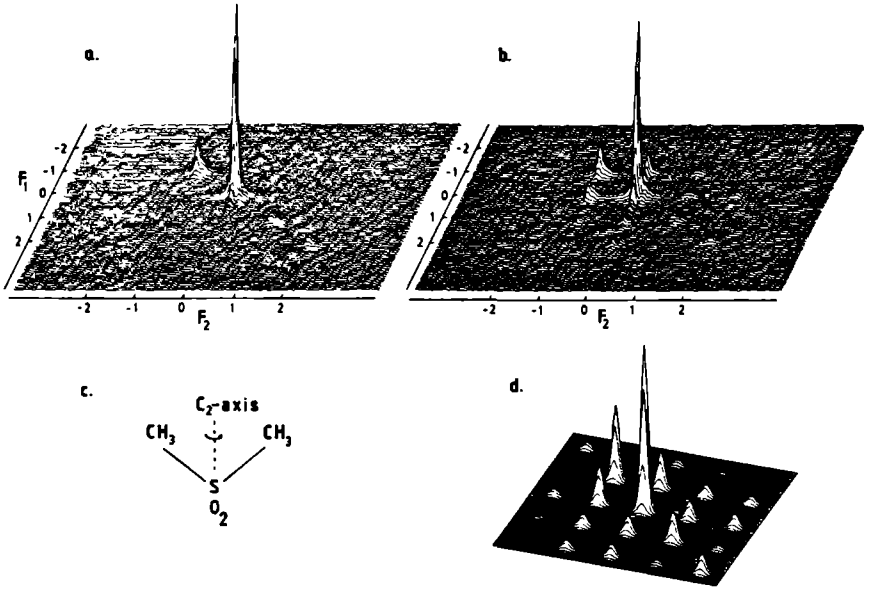

Fig. 5.6 Absolute mode spectra and molecular structure of dimethylsulfone. The experimental spectra (a,b) were obtained at a spinner speed of 1250 Hz. Sine-bell filters were used in both dimensions. Numbers indicate the positions of the sidebands. a) Mixing time of 0 ms. The arrow indicates a small artefact. (128 x 96 FIDs). b) Synchronous mixing time of 8 rotor periods (τ_m = 6.4 ms) (128 x 1100 FIDs). c) Structure of DMS, indicating the 180° rotation about the C_2 axis. d) Computer simulation of (b).

In order to simulate such a spectrum we have to take the change in orientation of the CSA tensor into account, and calculate the resulting sideband intensities using eq. (5.16). Furthermore, we have to know how many methyl groups have changed their position during τ_m, i.e. we have to know the conditional probability $W(\sigma_1|\sigma_2,\tau_m)$ that the orientation of the CSA tensor is σ_2 at the beginning of the detection period, when we know it had orientation σ_1 at the end of the evolution period. When we assume the jumping to be a stationary Markov process, this conditional probability is given by the differential equations [AB61]

$$\frac{dW(\sigma_i|\sigma_j,t)}{dt} = \sum_{k=1}^{n} W(\sigma_i|\sigma_k,t)\ \Pi(\sigma_k,\sigma_j) \tag{5.19}$$

where Π is the n-dimensional exchange matrix [AB61]. For the simple case of jumps between n equivalent sites with the probability of a jump between any two sites Ω, the elements of this exchange matrix are all Ω, except for the diagonal terms which are $-(n-1)\Omega$. The solution of the differential equations then gives

$$\begin{aligned} W(\sigma_i|\sigma_i,\tau_m) &= \frac{1}{n}\,[1 + (n-1)\exp(-n\Omega\tau_m)] \\ W(\sigma_i|\sigma_j,\tau_m) &= \frac{1}{n}\,[1 - \exp(-n\Omega\tau_m)] \quad i\neq j \end{aligned} \tag{5.20}$$

For DMS, n=2 and the jump frequency Ω= 314 Hz. With a mixing time of 6.4 msec this would mean that 50% of the methyl groups are in a different position in the detection period with respect to their position in the evolution period. Fig. 5.6d shows the simulation for DMS with 50% exchange. The result agrees very reasonable with the experimental spectrum, except for the central peak. The differences in peak heights occur due to extra broadening of the sidebands, resulting from (long time) fluctuations in the spinning frequency. This affects sidebands ($N\omega_r$!) stronger when they are further away from the central peak. This central peak is not affected by the fluctuations. Long-time instability of the rotor speed is one of the weak points of the Andrew-Beams type rotor. A further disadvantage is that it will not allow rotation at speeds below ≈ 1200 Hz.

In conclusion we can say that the results on DMS show that the technique works. It appears that this version of the 2D exchange experiment is an excellent method to study exchange processes (including molecular motions) in systems with a large chemical shielding anisotropy. In the next section this

technique will be used to detect and characterize super-slow motions in poly-(oxymethylene). In general, a study of such motions might be hampered, however, by the presence of ^{13}C-^{13}C spin diffusion. Further investigations are needed to establish at which τ_m spin diffusion starts to be effective. Edzes and Bernards [ED84] showed the presence of spin diffusion in a static sample of polyethylene using a mixing time of 10 seconds. In adamantane such effects were already present after 2 s [BR83]. The effect of MAS on spin diffusion is not entirely clear. Of course, spinning at very high speeds would certainly eliminate ^{13}C-^{13}C spin diffusion [VA79]. For adamantane, spin diffusion is indeed reduced drastically by MAS [BR83]. In p-dimethoxybenzene, cross-peaks due to spin diffusion in the presence of MAS showed up with a mixing time of 90 s [SZ82].

A prerequisite for the experiment is a spinner design, with an accurate angle positioning, that spins constantly over longer periods of time. Furthermore it is desirable to have temperature control, in order to study the temperature dependence of the exchange process. This might e.g. give a clue whether one is dealing with molecular motions or spin diffusion. Modern double-bearing spinners, do meet these conditions.

5.5 Slow molecular motions in crystalline poly-(oxymethylene)

It needs no further explanation that molecular reorientations of macromolecules exert great influence on relevant physical properties of polymers. Among the different techniques to study molecular motions, NMR has become a very valuable one. In NMR information about molecular motions is usually obtained by measurements of relaxation times T_1, T_2, $T_{1\rho}$, etc. These relaxation times each have a specific range of sensitivity for molecular mobility. Spin-lattice relaxation, characterized by T_1, is sensitive for motions with frequencies at about the Zeeman frequency, whereas relaxation in the rotating frame, $T_{1\rho}$, is dominated by molecular motions in the kHz regime (the magnitude of the B_1 field). Slower motions can be studied via the NMR line shape. Characteristic line shapes can be obtained for systems exhibiting reorientations with correlation times corresponding to the total (static) width of the powder line shape. Still slower motions ($\tau_c \geq 1$ sec) can not be studied by this type of measurements. Spiess [SP85] used the Jeener-Broeckaert three-pulse technique to investigate such ultra-slow molecular reorientations in deuterated samples. As we have seen in the preceding

paragraph, the slow spinning 2D exchange experiment offers an excellent opportunity to explore these motions via natural abundance ^{13}C NMR.

At this moment most information about these slow molecular motions is obtained from mechanical and dielectrical relaxation measurements. Such experiments are, however, in general not very suitable to give an accurate description of the type of motion on a molecular level. The α-relaxation in poly-(oxymethylene) (POM) for instance has been studied extensively, and is generally attributed to motions within the crystalline regions. Various models have been proposed, but no unique answer has emerged.

5.5.1 Elucidation of super-slow motions in poly-(oxymethylene)

Poly-(oxymethylene) is a highly crystalline polymer of formaldehyde. The unit cell consists of chains in a helical conformation with nine monomer units in 5 turns of the helix [HU45]. This model has been refined by Uchida and Tadokoro [UC67] to 29 units in 16 turns, such small refinements, however, bear no significance for the present study. Within one crystal all helices are parallel and have the same helix form (right or left handed) [UC67,WU73].

Preliminary 2D exchange experiments on bulk crystallized POM (commercially available Hostaform-C from Hoechst) showed that there are indeed slow molecular motions, with a correlation time $\tau_c \approx 1$ sec at 50 °C, present in the crystalline part of the polymer [KE85]. These results were obtained with Andrew-Beams type rotors at a spinning speed of 1500 Hz. At this speed the sidebands are very small, allowing no exact analysis of the pattern. Therefore the experiments were carried out once more in a double-bearing MAS probe with temperature control. A cylindrical piece of Hostaform-C was machined to fit exactly in the double-bearing rotor. Thus stable spinning could be achieved over a large interval of spinning frequencies and various temperatures.

It is known that only the crystalline part of POM gives rise to a full NMR powder pattern at room temperature. In the amorphous part the chemical shielding anisotropy is partly averaged by molecular motions so that it gives a relatively narrow line [VE79]. As a result we will with slow magic angle spinning only see spinning sidebands from the crystalline part of the polymer. In addition, the short ^{13}C T_1 of the amorphous part (amorphous $T_1 \approx 90$ msec; crystalline $T_1 \approx 18$ sec at room temperature) ensures that when the mixing time $\tau_m \geq 1$ sec, amorphous spins only contribute to axial peaks, which are removed by proper phase cycling (see table 5.1).

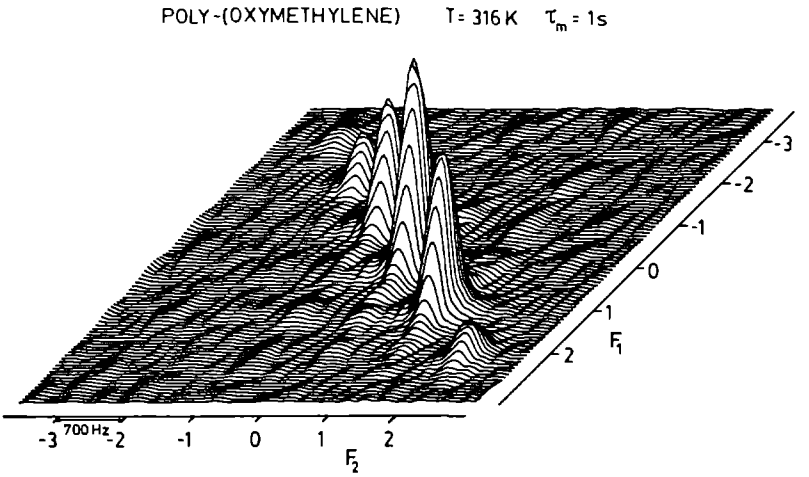

Fig. 5.7 ^{13}C 2D exchange spectrum of poly-(oxymethylene) at 316 Kelvin with a rotor synchronous (ν_R = 700 Hz) mixing time of 1 s. 240 scans were accumulated for 64 t_1 values (13 h experiment time). Sine-bell filters were applied in both dimensions prior to Fourier transformation.

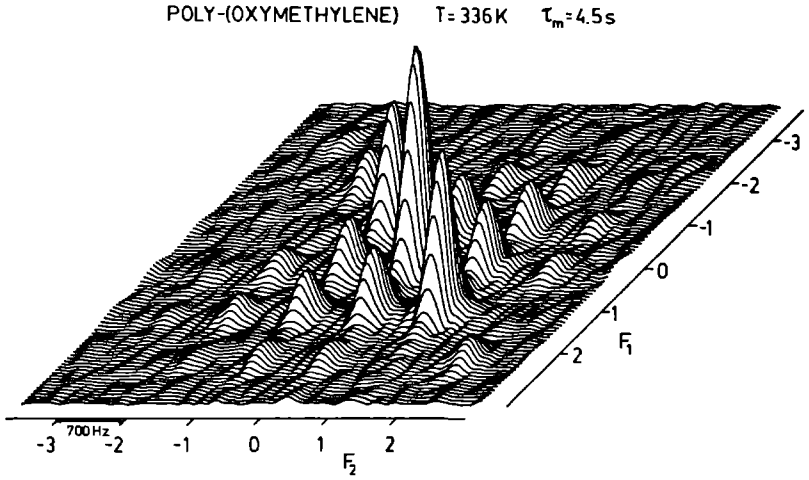

Fig. 5.8 ^{13}C 2D exchange spectrum of POM at 336 Kelvin with a mixing time of 3150 rotor periods at a spinning speed of 700 Hz (τ_m = 4.5 s). 320 FIDs were accumulated for 64 t_1 values (experiment time 37 h). Sine-bell filters were used in both dimensions.

Fig. 5.7 shows the result of the 2D exchange experiment, with a mixing time of 1 s, applied to POM at a temperature T = 316 K, and a spinning speed of 700 Hz. Besides the spinning sideband pattern of POM on the diagonal, some extremely weak cross-peaks show up indicating exchange between orientationally different sites. At a temperature of 336 K, the off-diagonal peaks are already very intense for τ_m = 1 s. Increasing the mixing time (fig. 5.8) or the temperature results in a further increase of the off-diagonal intensity. This temperature dependence shows that we are dealing with molecular motions and not with spin diffusion.

Analysis of these 2D spinning sideband patterns can yield the relative orientation of the CSA tensor of a group of spins in the detection period with respect to their orientation in the evolution period. In order to obtain information about the type of motion causing the off-diagonal peaks, it is essential that we know the orientation of the CSA tensor within the molecule and its principal values. The principal values were recovered from a static 1D powder pattern giving σ_{XX} = 67 ppm, σ_{YY} = 86 ppm and σ_{ZZ} = 111 ppm. The orientation of the shielding tensor within the monomer unit was determined by correlating the chemical shielding anisotropy to the heteronuclear dipolar ^{13}C-^{1}H interaction, whose orientation is known. From this 2D dipolar correlation spectrum, as was described in chapter 4, it appears that the orientation of the CSA tensor is determined by the local tetrahedral symmetry of the CH_2O_2 unit i.e. the Z axis is oriented perpendicular to the O-C-O plane, and makes an angle of 55° with the helix axis. The Y axis lies within the O-C-O plane and bisects the O-C-O angle. The X axis is of course perpendicular to the Y and Z axis.

From the experimental spectra it is seen that the off-diagonal intensity is of considerable magnitude. This suggests that the motion involved can not be restricted to the loops of the polymer chains at the surface of the crystal lamellae or to crystal defects. As the majority of polymer chains are involved in the motion a rotation of the chains, combined with a translation, seems the most plausible mechanism. When the helical polymer chains (9 monomer units in 5 turns) make a 200° jump, their starting and end position will be identical, and thus there is no elevation of the energy. So the energy required for this motion to occur, is the energy required to overcome the barrier to chain rotation. In a bulk-crystallized polymer, which is thought to consist of spherulites with crystalline lamellae connected to each other with amorphous material [TA62] (fig. 5.9), the rotation of polymer chains in the crystals might be brought about by torsional forces exerted on

the chains in the crystalline phase by chains in the highly mobile amorphous phase. Another explanation is that lattice defects move through the crystal, leaving behind a polymer chain that is rotated over 200°.

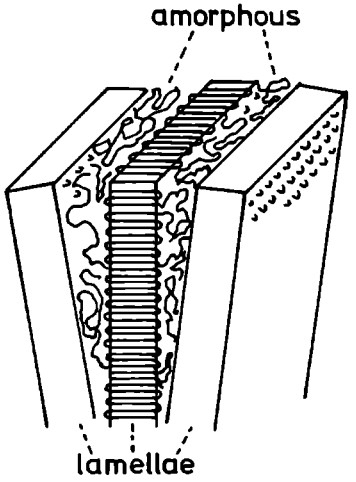

Fig. 5.9 Spherulites of bulk-crystallized POM consist of crystalline lamellae in which the helical chains are folded. Drawn are the radial lamellae that are connected to each other with amorphous material.

In order to simulate the effect of such a rotational motion we have to find the Euler angles λ,μ,ν, in the coefficients A_2 to D_2 of eq. (5.16), that relate the orientation of the CSA tensor in the detection period to that in the evolution period. This can be accomplished by dividing the process into three consecutive steps; We start in the principal axis system of the shielding tensor, which is determined by the local tetrahedral symmetry of the CH_2O_2 unit, and transform to an axis system with one axis along the helix axis. Then the rotation of 200° (or 400°, 600° etc. when the polymer chain has experienced more than one displacement) about the helix axis is brought into account, followed by a transformation back to the shielding principal axis system. The product of the these three transformation matrices gives the final transformation matrix (determined by the Euler angles λ,μ,ν).

A striking point in the simulations is that, if one calculates a 2D spinning pattern for all spins that have rotated over +200° from their original position, this does not necessarily give a symmetric pattern around the diagonal. The pattern for a -200° rotation, however, is the mirror image of the +200° spectrum and as both steps are equally likely to happen, the final simulated spectrum will always be symmetric with respect to the diagonal. With the orientation of the chemical shift tensor as obtained in chapter 4 the resulting simulation are symmetric for every reorientation of

the polymer chain. Furthermore reorientations of the left-handed chains result in the same spectra as those of the right-handed chains.

Another important point in the simulation is formed by the statistics involved in this type of motion. This is less straightforward than in the case of jumps between n equivalent sites. Neglecting effects of chain ends, the differential equation that determines the probability W_n, that a chain is displaced n steps from its starting position, is given by

$$\frac{dW_n(t)}{dt} = \Omega W_{n-1}(t) - 2\Omega W_n(t) + \Omega W_{n+1}(t) \qquad (5.21)$$

where Ω is the average jump frequency. This is the differential equation describing a one-dimensional random walk in continuous time, which can be solved with the aid of Bessel functions, as can be found in textbooks on statistics [FE66, BA70].

$$W_n(t) = I_n(\Omega t)\, e^{-\Omega t} = \sum_{k=0}^{\infty} \frac{(\frac{1}{2}\Omega t)^{n+2k}}{k!\,(n+k)!}\, e^{-\Omega t} \qquad (5.22)$$

Hence, 2D spinning sideband intensity patterns were calculated for rotations over 0°, ±200°, ±400° etc. and combined according to eq. (5.22) for a given Ω (which has to be determined in the simulations). These simulations were then compared to the peak intensities in the experimental spectra. As all spinning sidebands have the same line shape, these intensities were simply obtained as peak heights. In the calculated and experimental spectra the central peak was scaled to 100 units, in which case the noise was 2-3 units. It appears that we are able to simulate the experimental spectra very well with this model. The simulations are shown in table 5.2. In every spectrum, calculated and experimental intensities do not differ more than 3 units, which is well within experimental error. In some cases 1 line differs by 4 or 5 units, but because this occurs for only 1 line out of 36 this not is considered significant. The worst fit is obtained for the spectrum measured at T = 336 K and a mixing time of 1 sec, here the 2 diagonal lines next to the central peak show a rather large difference of 5 and 7 units, but still the overall agreement of the calculated and experimental spectrum seems satisfactory. For the spectrum obtained at 360 K and τ_m = 1 sec it was no longer possible to take the central peak to scale the spectrum. At this temperature the T_1 of the amorphous part of the polymer has become so long that it gives a contribution to central peak of the 2D spectrum (fig. 5.10).

As this amorphous signal only affects the intensity of the central line, another peak was taken for reference. After simulation, the calculated as well as the experimental spectrum were rescaled by the same amount so that the intensity of the central peak of the calculated spectrum was again 100 units. In that case the intensity of the central peak in the experimental spectrum has become 120 units, showing the influence of the amorphous signal.

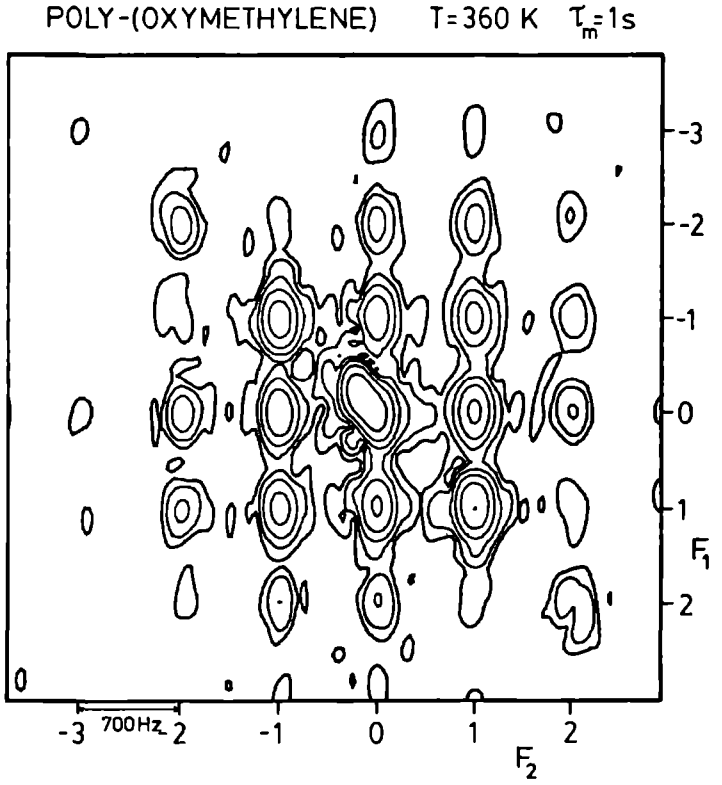

Fig. 5.10 Contour plot of the 2D exchange spectrum of POM obtained at a temperature of 360 Kelvin and a mixing time of 1 s (700 rotor periods). The numbers indicate the position of the sidebands. In this case signal of the amorphous part of the polymer overlaps with the central line (0,0).

To summarize, the α-relaxation seems to be governed by chain rotation. It is not clear, however, if the chains rotate as rigid rods. For longer chains it is also possible that a region with a more tightly wound helix arises, which then runs through the polymer chain, as has been proposed for

the α_c-relaxation in polyethylene. Whether such a twist is energetically favorable over rigid rod rotation depends on the intermolecular potential barrier. It is not obvious what the effect of such a twisted region on the spectrum would be.

In fig. 5.11 log(Ω) is plotted against the reciprocal temperature. The error intervals in this plot were obtained by varying Ω until simulations diverted to much from the experimental spectra, and are thus somewhat arbitrary. This plot obviously shows an Arrhenius type of behaviour for the rotational motion. The activation energy is found to be 20 ± 5 kcal/mole, in agreement with values found from mechanical measurements [ST86, MC67], although also higher values have been reported [MC67].

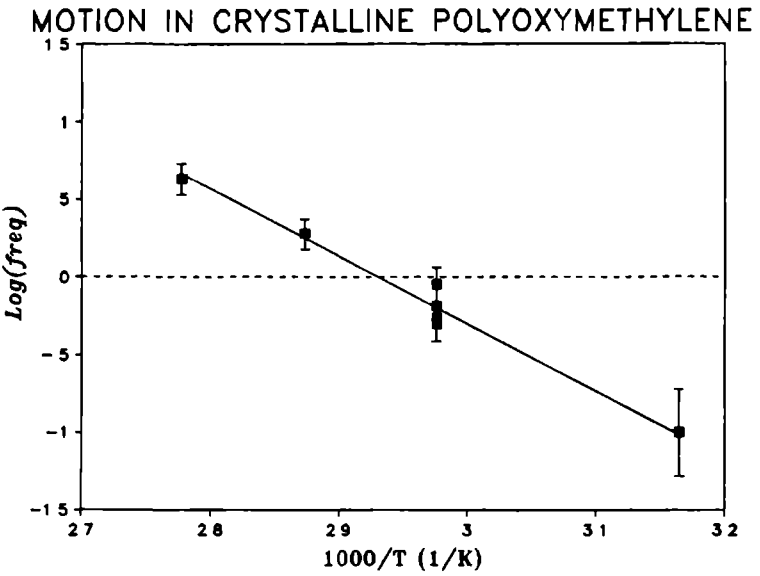

Fig. 5.11 Arrhenius plot of the motion detected in poly-(oxymethylene).

5.5.2 Conclusions

From these observation we can conclude that the α-relaxation in poly-(oxymethylene) involves chain rotations in the crystalline phase. To our knowledge this is the first time that this type of motion is demonstrated by a direct measurement on a molecular level. This demonstrates the great potential of the 2D exchange experiment to study very slow molecular motions,

especially when performed under slow MAS conditions to enhance sensitivity and resolution. Experimental times varied from 10 (τ_m = 1 s) to 40 (τ_m = 4.5 s) hours, making these experiments ideal for overnight or weekend runs. An advantage is that no extra sample preparation is required because natural abundance ^{13}C CP-MAS is employed. Computer simulations take approximately 250 s on a mainframe computer, which is rather time consuming. Therefore it is advantageous if there exist already some ideas about the type of motion. Such models can then be tested with these calculations, as it is very unlikely to find the right solution just by trial and error.

The fact that the mixing time can be rather long gives the 2D exchange experiments some exciting perspectives for the future. One might, for instance, use the mixing time to raise the temperature of a sample with a phase transition above the transition temperature and allow the temperature to drop below the transition temperature in the recycle delay. In that way it should be possible to study the conformational change a nucleus undergoes due to the phase transition. Another interesting experiment might be to manipulate the sample mechanically during the mixing time so that the molecular effects of such a mechanical treatment can be studied. It is obvious that one has to work with static samples to manipulate the sample mechanically.

Table 5.2 Calculated and experimental sideband intensities for the 2D exchange experiment.

EXPERIMENT						CALCULATION					
T = 336 K, τ_m = 1 s						Ω = 0.90 Hz					
5	-	-	3	3	-	5	-	1	3	2	1
-	20	-	6	7	3	-	19	1	7	8	3
2	-	64	15	15	5	1	1	59	16	13	6
2	8	18	100	21	5	3	7	16	100	20	6
2	8	15	20	82	-	2	8	13	20	75	-
-	3	6	6	-	13	1	3	6	6	-	15

$T = 336\ K,\ \tau_m = 2\ s$

4	-	-	3	3	-
-	18	-	8	10	3
-	-	60	19	17	7
3	8	21	100	26	7
3	10	17	24	78	-
-	3	7	6	-	13

$\Omega = 0.65\ Hz$

4	-	1	4	3	1
-	18	1	9	10	3
1	1	59	20	16	7
4	9	20	100	25	8
3	10	16	25	74	1
1	3	7	8	1	14

$T = 336\ K,\ \tau_m = 3\ s$

4	-	-	3	3	-
-	18	-	9	11	4
-	-	58	21	20	6
5	10	23	100	28	7
3	11	21	27	77	-
-	-	8	7	-	11

$\Omega = 0.55\ Hz$

4	-	1	4	3	1
-	17	2	10	10	3
1	2	58	22	18	8
4	10	22	100	28	8
3	10	18	28	73	2
1	3	8	8	2	13

$T = 336\ K,\ \tau_m = 4.5\ s$

4	-	-	3	3	-
-	16	-	9	11	6
-	-	58	24	21	7
4	11	26	100	33	8
4	10	21	31	75	-
-	3	8	8	-	11

$\Omega = 0.50\ Hz$

4	-	1	4	3	1
-	16	3	11	11	4
1	3	57	25	20	8
4	11	25	100	32	9
3	11	20	32	72	3
1	4	8	9	3	13

$T = 348\ K,\ \tau_m = 1\ s$

3	-	-	3	3	-
-	17	-	9	10	4
-	-	60	25	19	7
4	10	25	100	30	7
2	10	20	31	75	-
-	3	8	9	-	12

$\Omega = 1.9\ Hz$

4	-	1	4	3	1
-	16	2	11	11	4
1	2	58	24	19	8
4	11	24	100	30	9
3	11	19	30	73	2
1	4	8	9	2	13

T = 360 K, τ_m = 1 s						Ω = 4.3 Hz					
3	-	-	5	4	-	3	-	-	5	3	1
-	13	3	11	12	5	-	14	5	14	13	4
-	3	52	30	23	7	-	5	54	31	24	9
3	14	32	120	40	9	5	14	31	100	40	10
2	10	23	38	70	4	3	13	24	40	69	5
-	3	8	8	4	7	1	4	9	10	5	12

References

AB61 A. Abragam, "Principles of Nuclear Magnetism", Oxford University Press, London, 1961.

BA70 M.N. Barber and B.W. Ninham, "Random and Restricted Walks", Gordon and Breach Science Publishers, New York, 1970.

BA82 A. Bax, "Two-Dimensional Nuclear Magnetic Resonance in Liquids", D. Reidel Publishing Co., Dordrecht, 1982.

BR83 C.E. Bronniman, N.M. Szeverenyi and G.E. Maciel, J. Chem. Phys. 79, 3694, 1983.

DY75 C.R. Dybowsky and R.W. Vaughan, Macromolecules 8, 50, 1975.

ED84 H.T. Edzes and J.P.C. Bernards, J. Am. Chem. Soc. 106, 1515, 1984.

FE66 W. Feller, "An introduction to Probability Theory and Its Applications", vol. II, J. Wiley and Sons, Inc., New York, 1966.

HA76 U. Haeberlen, "High Resolution NMR in Solids", Advances in Magnetic Resonance, supplement 1, J.S. Waugh Ed., Academic Press, New York, 1976.

HA85 G.S. Harbison, D.P. Raleigh, J. Herzfeld and R.G. Griffin, J. Magn. Res. 64, 284, 1985.

HE80 J. Herzfeld and A.E. Berger, J. Chem. Phys. 73, 6021, 1980.

HE84 P.M. Henrichs and M. Linder, J. Magn. Res. 58, 458, 1984.

HU45 M.L. Huggins, J. Chem. Phys. 13, 37, 1945.

JE67 J. Jeener and P. Broekaert, Phys. Rev. 157, 232, 1967.

JE79 J. Jeener, B.H. Meier, P. Bachmann and R.R Ernst, J. Chem. Phys. 71, 4546, 1979.

JO84 A.F. de Jong, A.P.M. Kentgens and W.S. Veeman, Chem. Phys. Lett. 109, 337, 1984.

KE85 A.P.M. Kentgens, A.F. de Jong, E. de Boer and W.S. Veeman, Macromolecules 18, 1045, 1985.

KE87 A.P.M. Kentgens, W.S. Veeman and J. van Bree, to appear in Macromolecules.

MA79 M.M. Maricq and J.S. Waugh, J. Chem. Phys. 70, 3300, 1979.

MC67 N.G. McCrum, B.E. Read and G. Williams, "Anelastic and Dielectric Effects in Polymeric Solids", J. Wiley and sons, Inc. London, 1967.

OL84 E.T. Olejniczak, S. Vega and R.G. Griffin, J. Chem. Phys. 81, 4804, 1984.

SC72 J. Schaefer, Macromolecules 5, 427, 1972.

SC86 C. Schmidt, S. Wefing, B. Blümich and H.W. Spiess, Chem. Phys. Lett. 130, 84, 1986.

SH72 J. Schaefer, S.H. Chin and S.I. Weissman, Macromolecules 5, 798, 1972.

SO83 M.S. Solumn, K.W. Zilm, J. Michl and D.M. Grant, J. Phys. Chem. 87, 2940, 1983.

SP85 H.W. Spiess, Advances in Polymer Science, 66, 37, 1985.

ST86 H.W. Starkweather, Macromolecules 19, 2538, 1986.

SU82 D. Suter and R.R. Ernst, Phys. Rev. B, 25, 6038, 1982.

SZ82 N.M. Szeverenyi, M.J. Sullivan and G.E. Maciel, J. Magn. Res. 47, 462, 1982.

SZ83 N.M. Szeverenyi, A. Bax and G.E. Maciel, J. Am. Chem. Soc. 105, 2579, 1983.

TA62 M. Takayanagi, M. Yoshino and S. Minami, J. Polym. Sci. 61, S7, 1962.

TA86 K. Takegoshi and C.A. McDowell, J. Chem. Phys. 84, 2084, 1986.

UC67 T. Uchida and H. Tadokoro, J. Polym. Sci. A2 5, 63, 1967.

VA79 D.L. VanderHart and A.N. Garroway, J. Chem. Phys. 71, 2773, 1979.

VE79 W.S. Veeman, E.M. Menger, W. Ritchey and E. de Boer, Macromolecules 12, 924, 1982.

WU73 B. Wunderlich, "Macromolecular Physics", vol. I, Academic Press, New York, 1973.

CHAPTER 6

TWO-DIMENSIONAL NUTATION NMR OF HALF-INTEGER NUCLEI

6.1 Introduction

The majority of elements in the periodic table have nuclei with half-integer quadrupole spins. So it is not surprising that there is an increased interest in high resolution NMR spectra of quadrupole nuclei in solids. Especially the recent studies of zeolites, clays and ceramics have focused the attention on getting structural information from NMR spectra of quadrupolar spins.

In comparison to nuclear spins with spin quantum number I=1/2, the NMR spectra of quadrupolar spins contain two new features: 1) several transitions are possible because I>1/2 and 2) the transition frequencies are not only determined by the interaction between the magnetic moment of the nucleus and the static external field but also by the interaction between the nuclear electric quadrupole moment and the electric field gradient at the site of the particular nucleus. The chemical information an NMR spectrum of a quadrupolar spin offers is therefore not limited to the chemical shift data but in addition such a spectrum can provide the parameters that describe the quadrupolar interaction. These parameters depend on the local symmetry around the nucleus in consideration and thus give direct structural information.

Traditionally, quadrupole interaction parameters can be determined by NQR, nuclear quadrupole resonance. There, usually, no or a small magnetic field is present and the nuclear spin levels are split mainly by the quadrupole interaction. The frequencies of the transitions between these levels provide the quadrupole parameters. The disadvantages of NQR are its low sensitivity when the quadrupole interaction is rather small (0 - 10 MHz) and the wide frequency range one has to search for possible resonances. Both of these disadvantages can be overcome in principle, at least for small quadrupole interactions, in an NMR experiment.

The description of the NMR spectra of quadrupolar spins very much depends on the spin quantum number I and the relative magnitude of the Zeeman and the quadrupole interaction. Here we limit our discussion to half-integer spins (I=3/2, 5/2, 7/2, 9/2) and assume the quadrupole interaction to be small with respect to the Zeeman interaction. The (anisotropic) contribution

of the quadrupole term to the NMR transition frequencies can then be calculated by perturbation theory.

In high magnetic fields all Zeeman transitions m,m' shift in first order because of the quadrupole interaction except the 1/2,-1/2 transition which experiences a (much smaller) second-order shift. As a result of this, typical spectra of polycrystalline samples containing quadrupolar spins give characteristic powder patterns for the 1/2,-1/2 transition whereas all other transitions are usually broadened beyond detection [NA66, BA69]. As the Magic Angle has no "magic" properties for the second-order quadrupolar interaction, MAS will not average this interaction, but yields powder patterns for the 1/2,-1/2 transition which are approximately four times narrower than for static samples [KU81, BE82, SA82].

Although, in principle, it is possible to extract information about the electric field gradient from the spectra of static or spinning polycrystalline samples, in practice the powder patterns are often blurred by a spread in chemical shift and/or by the presence of more than one quadrupole interaction. To overcome these problems Samoson and Lippmaa [SA83, SM83] introduced a simple two-dimensional experiment which allows one to separate the quadrupole interaction from the chemical shift interaction. This technique is based on a nutation experiment [YA81] where the evolution of the spin system in the presence of a radiofrequency field B_1 is studied in the rotating frame. This evolution yields a low field ($B_1 \sim 0.001\ B_0$) NMR spectrum, the nutation spectrum, with the sensitivity of the high-field spectrometer. In this respect it can directly be compared to the zero-field NMR technique developed by Pines and coworkers [ZA85] where the sample is pneumatically shifted in and out the magnet. The advantage of the nutation experiment is that, in contrast to the zero-field technique, there is no limitation on the T_1 spin-lattice relaxation time. A nutation spectrum however is more difficult to analyze than a zero-field spectrum.

In this chapter we discuss the calculation of these nutation spectra using the density matrix formalism, and present a number of simulated spectra for all half-integer quadrupole spins (I=3/2 to I=9/2) which can be used in a qualitative way to determine the quadrupole interaction from experimental spectra. Moreover, some experimental aspects of the method will be discussed [KE87]. It will be shown how ^{27}Al nutation NMR can be used to separate the signals from ^{27}Al with a large quadrupole interaction from signals of ^{27}Al with a small quadrupole interaction in zeolites [GE85]. Finally, we show that by comparing an experimental spectrum to the set of simulated spectra one can

determine the quadrupole parameters. This will be demonstrated for ^{27}Al in spodumene and for ^{45}Sc in $Sc_2(SO_4)_3$.

6.2 Calculation of nutation spectra

The pulse scheme of the experiment is outlined in fig. 6.1. During the evolution period t_1 an rf field is present and the system evolves under the secular Hamiltonian H_1 in the rotating frame, assuming that the sample is static (i.e. no MAS):

$$H_1/\hbar = (H_{off} + H_{rf} + H_Q)/\hbar = (\omega_0-\omega)I_z - \omega_{rf}I_x + \omega_Q^*(3I_z^2-I(I+1)) \qquad (6.1)$$

with $\omega_Q^* = \omega_Q(3\cos^2\theta - 1 + \eta \sin^2\theta \cos 2\varphi)$ where $\omega_Q = \frac{e^2qQ/\hbar}{8I(2I-1)}$ and $\omega_{rf}=\gamma B_1$.

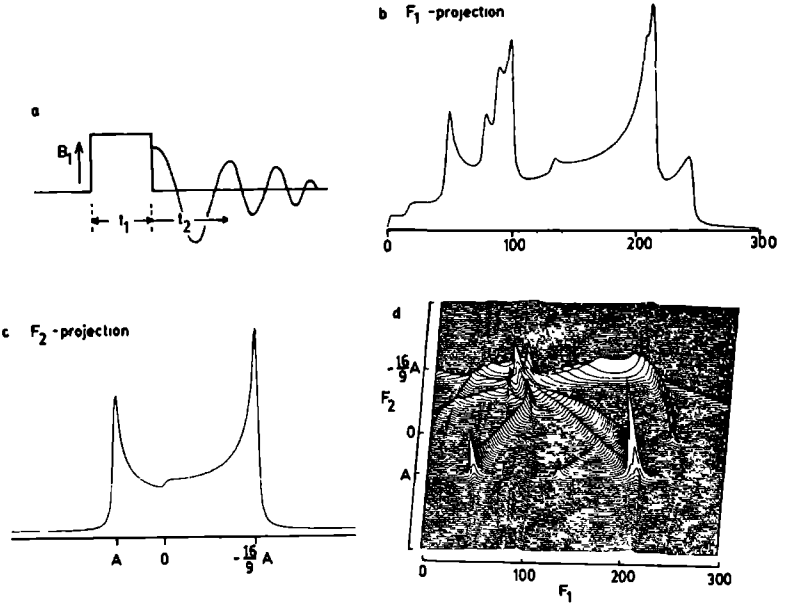

Fig. 6.1 (a) Pulse scheme of the experiment; a free induction decay is acquired during t_2 as a function of the pulse length t_1. Subsequent Fourier transformation of the signals obtained yields a typical 2D powder pattern as shown in (d). This spectrum was calculated for I=5/2 with a ratio ω_Q/ω_{rf} = 0.45 and η=0. The F_2 projection of this pattern (c) gives the second order quadrupole powder pattern, and the F_1 projection (b) is a characteristic nutation spectrum for the ratio ω_Q/ω_{rf}.

θ and φ are the polar angles orienting the magnetic field B_0 in the principal axes system of the field gradient. η represents the asymmetry parameter. Here dipolar interactions and the non-secular part of the quadrupole Hamiltonian have been neglected. During t_2 there is no rf field present and the FID of the 1/2,-1/2 transition is acquired (assuming that all other transitions are too broad to be detected). The system is now governed by the Hamiltonian H_2:

$$H_2 = H_Z + H_{CS} + H_Q \tag{6.2}$$

Where H_z and H_{CS} are the Zeeman and the chemical shift interaction and H_Q is the quadrupole interaction which only contributes in second-order to the line shape of the central 1/2,-1/2 transition [AB61]. With the knowledge of these Hamiltonians we can calculate the signal $S(t_1,t_2)$ using the density matrix formalism. At time t_1=0 we start with the equilibrium density matrix $\sigma(0) = \sigma_{eq}$ in the high temperature approximation. As one can see the dominating Zeeman interaction H_z is not present in H_1. So if we irradiate close enough to resonance (H_{off} small) then H_Q and H_{rf} are the most important terms of H_1. This means that the eigenfunctions of H_1 depend on the ratio of ω_Q^* and ω_{rf}. From the Liouville - von Neumann equation we get at time t_1

$$\sigma(t_1) = \exp\{-iH_1t_1/\hbar\}\cdot\sigma(0)\cdot\exp\{iH_1t_1/\hbar\} \tag{6.3}$$

Starting in a basis of eigenfunctions of I_z, we get after diagonalization of H_1, using the orthogonal transformations T:

$$\sigma(t_1) = \bar{\bar{T}}\cdot\exp\{-i\bar{\bar{E}}t_1/\hbar\}\cdot\bar{\bar{T}}^+\cdot\sigma(0)\cdot\bar{\bar{T}}\cdot\exp\{i\bar{\bar{E}}t_1/\hbar\}\cdot\bar{\bar{T}}^+ \tag{6.4}$$

As there is no explicit mixing period $\sigma(t_1,0) = \sigma(t_1)$. E represents the diagonalized matrix of H_1 with the eigenvalues

$$E_j = \sum_p \sum_q T_{pj}\, H_{1pq}\, T_{qj} \tag{6.5}$$

and eigenfunctions

$$|j\rangle = \sum_i T_{ij}|I,m_i\rangle \tag{6.6}$$

We assume that we only detect the coherence between the 1/2 and the -1/2 states during t_2, so only the element $\sigma(t_1)_{1/2,-1/2}$ has to be evaluated. The signal of the central transition then can be calculated as a function of t_1 and t_2:

$$S(t_1,t_2) = Tr\{\sigma(t_1,t_2)\cdot I_x+iI_y\} \sim \sigma(t_1)_{1/2,-1/2}\exp\{-i\omega_2 t_2\}$$

$$= \sum_{i,j} (R_{-1/2,1/2})_{i,j}\exp\{i\omega_{ij}t_1\}\exp\{-i\omega_2 t_2\} \qquad (6.7)$$

where ω_2 represents the Larmor precession of the spins during t_2 and $\omega_{ij}=(E_i-E_j)/\hbar$ is the transition frequency in the rotating frame between the states $|i\rangle$ and $|j\rangle$. The coefficients $(R_{-1/2,1/2})_{ij}$

$$(R_{-1/2,1/2})_{i,j} = T_{1/2,i}T_{-1/2,j}\sum_k T_{k,i}T_{k,j}\sigma(0)_{k,k} \qquad (6.8)$$

represent the contributions of the coherence between $|i\rangle$ and $|j\rangle$ in the rotating frame during t_1 to the 1/2,-1/2 coherence detected during t_2.

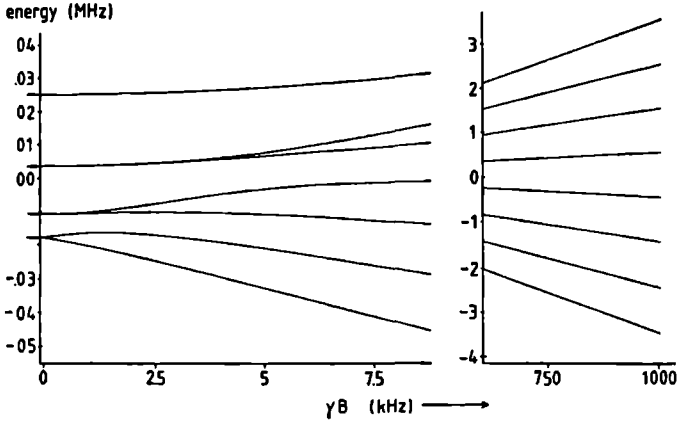

Fig. 6.2 Energy diagram of an isolated spin I=7/2 in the presence of a magnetic field B with quadrupole parameters e^2qQ/h = 1 MHz and η=0. On the left is the low-field situation $H_Z < H_Q$ and on the right is the situation $H_Z >> H_Q$, where H_Q appears to be negligible.

To summarize, we have during t_1 a system with eigenfunctions and eigenvalues which depend on the ratio of ω_Q^* and ω_{rf} (fig. 6.2). The coherences between all these levels, with frequency ω_{ij}, develop during t_1

and give a certain contribution to the 1/2,-1/2 coherence detected during t_2. Therefore, a two-dimensional Fourier transformation of the acquired signal will give a characteristic powder pattern (fig. 6.1d), whose projection on the F_2 axis (fig. 6.1c) yields the normal (1/2,-1/2) powder line shape due to the combined effect of chemical shift anisotropy and quadrupole interaction. Projection onto the F_1 axis (fig. 6.1b) gives the nutation spectrum which depends on the quadrupole parameters e^2qQ/h and η, the spin quantum number I and the rf field strength B_1, and is independent of the chemical shift. As we shall see later, the nutation spectra show more detail than MAS NMR spectra. When the system consists of only one quadrupolar nucleus at a certain site, it is sufficient to study the 1D nutation spectrum (i.e. the F_1 projection). If there are several different sites, however, it is advantageous to study the whole 2D powder pattern.

In the extreme cases $|H_Q| << |H_{rf}|$ and $|H_Q| >> |H_{rf}|$ the nutation spectrum consists of a single line. In the first situation H_Q may be neglected with respect to H_{rf} and the nutation frequency is simply ω_{rf}. In the second situation the rf Zeeman interaction may be considered to be a small perturbation to H_Q and in first order the eigenstates of H_1 are the eigenstates of H_Q which are characterized by the same magnetic quantum number m that characterizes the eigenstates of H_2. Therefore the projection of the eigenstates of H_1 onto the eigenstates of H_2 is trivial: the only nutation frequency observed in our 2D experiment is the transition frequency between the m = ±1/2 states of H_Q split by the action of H_{rf}. From the eigenvalue equation for these two states of a spin I

$$\begin{vmatrix} \langle 1/2|\hbar\omega_{rf}I_x|1/2\rangle - E & \langle 1/2|\hbar\omega_{rf}I_x|-1/2\rangle \\ \langle -1/2|\hbar\omega_{rf}I_x|1/2\rangle & \langle -1/2|\hbar\omega_{rf}I_x|-1/2\rangle - E \end{vmatrix}$$

$$= E^2 - 1/4(I+1/2)^2\omega_{rf} = 0 \qquad (6.9)$$

we derive an energy splitting of $(I+1/2)\hbar\omega_{rf}$ and thus a nutation frequency of $(I+1/2)\omega_{rf}$ [AB61].

In intermediate cases, $|H_Q| \sim |H_{rf}|$, the spectra are complicated and several peaks can occur because many transition frequencies ω_{ij} in the rotating frame exist. This becomes clear when we diagonalize H_1. For a spin 3/2 this can be done analytically (when H_{off} is negligible). The

diagonalization matrix T, which has been determined by Wokaun and Ernst [WO77], allows us to determine the eigenvalues of H_1:

$$
\begin{aligned}
E_1 &= \omega_{rf}/2 + \sqrt{(9\omega_Q^{*2} - 3\omega_Q^*\omega_{rf} + \omega_{rf}^2)} \\
E_2 &= -\omega_{rf}/2 + \sqrt{(9\omega_Q^{*2} + 3\omega_Q^*\omega_{rf} + \omega_{rf}^2)} \\
E_3 &= \omega_{rf}/2 - \sqrt{(9\omega_Q^{*2} - 3\omega_Q^*\omega_{rf} + \omega_{rf}^2)} \\
E_4 &= -\omega_{rf}/2 - \sqrt{(9\omega_Q^{*2} + 3\omega_Q^*\omega_{rf} + \omega_{rf}^2)}
\end{aligned}
\qquad (6.10)
$$

Note that we use a different ordering of the eigenstates than Wokaun and Ernst and that our ω_Q^* is $\omega_Q/3$ in their paper [WO77]. The eigenvalues are plotted in fig. 6.3a as a function of ω_Q^*/ω_{rf}. We easily recognize the extreme situations, for $\omega_Q^* = 0$ we find four equidistant eigenvalues with a splitting of ω_{rf}. When $\omega_Q^* >> \omega_{rf}$ two levels are split by $2\omega_{rf}$, whereas the other two levels are degenerate. Evaluation of the coefficients $(R_{-1/2,1/2})_{ij}$ gives us the amplitude coefficient of the FID of the central 1/2,-1/2 transition detected during t_2:

$$S(t_1,0) \sim A_{12}\sin\{\omega_{12}t_1\}+A_{23}\sin\{\omega_{23}t_1\}+A_{34}\sin\{\omega_{34}t_1\}+A_{14}\sin\{\omega_{14}t_1\} \qquad (6.11)$$

with $A_{12} = 3\sin2\theta_-\sin2\theta_+ + (1-\cos2\theta_-)(1-\cos2\theta_+)$

$A_{23} = 3\sin2\theta_-\sin2\theta_+ + (1+\cos2\theta_-)(1+\cos2\theta_+)$

$A_{34} = 3\sin2\theta_-\sin2\theta_+ - (1+\cos2\theta_-)(1-\cos2\theta_+)$

$A_{14} = -3\sin2\theta_-\sin2\theta_+ + (1-\cos2\theta_-)(1+\cos2\theta_+)$

where $\tan2\theta_- = \dfrac{\sqrt{(3)}\ \omega_{rf}/2}{3\omega_Q^* - \omega_{rf}/2}$ and $\tan2\theta_+ = \dfrac{\sqrt{(3)}\ \omega_{rf}/2}{3\omega_Q^* + \omega_{rf}/2}$

The transitions 13 and 24 do not appear in this expression. To visualize the importance of the four terms in eq. 6.11, the transition frequencies ω_{ij} and their amplitude factors A_{ij} are plotted in fig. 6.3b and c as a function of ω_Q^*/ω_{rf}. We see that A_{14} is very small over the whole range and the 14

transition thus hardly contributes to the nutation spectrum. When ω_Q^* is small with respect to ω_{rf} there are contributions of the 12, 23 and 34 transitions, which all have a transition frequency in the vicinity of ω_{rf}. When ω_Q^* gets bigger (in the positive direction), ω_{12} decreases to zero but its amplitude factor A_{12} also decreases. ω_{23} increases very rapidly with increasing ω_Q^* but A_{23} decreases to zero. For large ω_Q^* only A_{34} (with $\omega_{34} = 2\omega_{rf}$) is of significant magnitude. For negative ω_Q^* the situation is the same but the labels differ (fig. 6.3). To get the nutation spectrum for a polycrystalline sample, this analysis has to be repeated for every value of ω_Q^*. Fig. 6.3d shows the angular distribution of ω_Q^*/ω_{rf} values for a given ω_Q ($\omega_Q = e^2qQ/\hbar 8I(2I-1)$) and η.

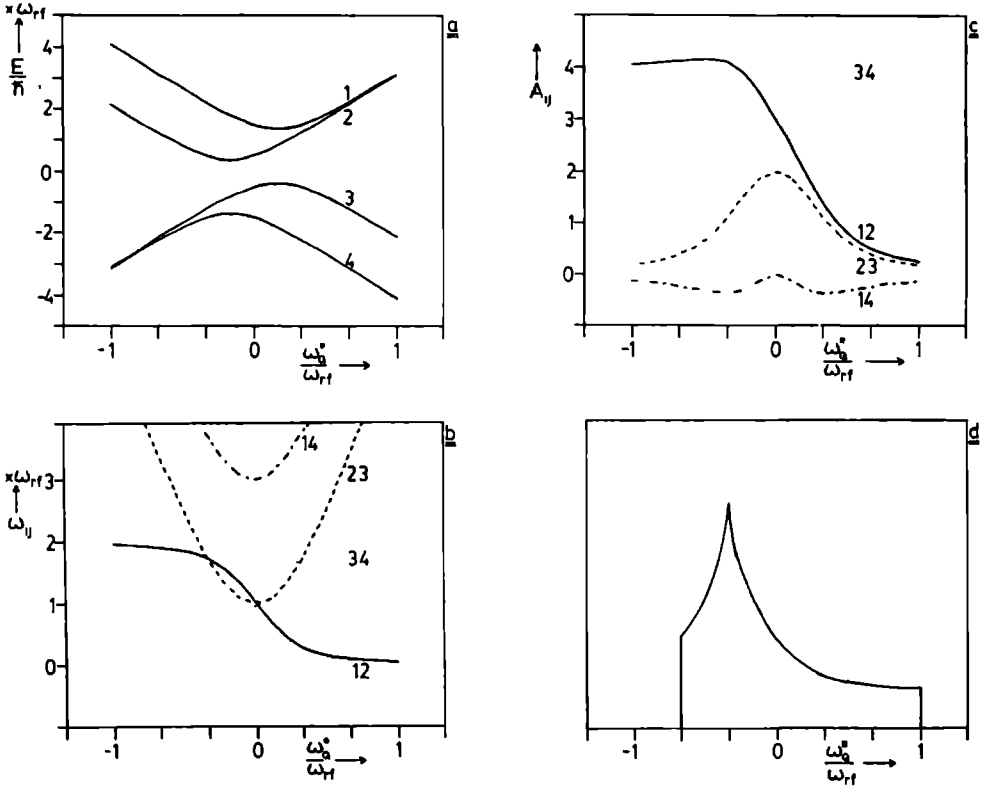

Fig. 6.3 Energy diagram (a) and transition frequencies (b) of an isolated spin I=3/2 during the evolution time t_1 as a function of the ratio ω_Q^*/ω_{rf}. With the amplitude coefficients A_{ij} (c) and the angular distribution of ω_Q^*/ω_{rf} values (d) for a given ω_Q/ω_{rf} (=0.5) and η (=1/3) one can calculate the nutation spectrum.

The diagonalization matrix T has only been determined for a spin 3/2, thus for a general approach for all possible spins (I=3/2, 5/2, 7/2, 9/2) the diagonalization of H_1 has to be carried out numerically. This diagonalization has to be carried out for every value of Θ and φ on a sphere. Fig. 6.4 shows a series of calculated nutation spectra for different ratio ω_Q/ω_{rf}, for spins I=5/2. In all spectra the asymmetry parameter η and the resonance offset are assumed to be 0. The spectra appear to be very characteristic powder patterns so for these intermediate cases with ω_{rf} known, one can determine ω_Q ($\omega_Q = e^2qQ/\hbar 8I(2I-1)$) at least in a qualitative way. Because ω_Q depends on the nuclear quadrupole moment Q and the spin quantum number I, and with ω_{rf} limited for experimental reasons, it will depend on the nucleus in question, what range of electric field gradients eq can be determined without getting in one of the extreme situations with only one nutation frequency left.

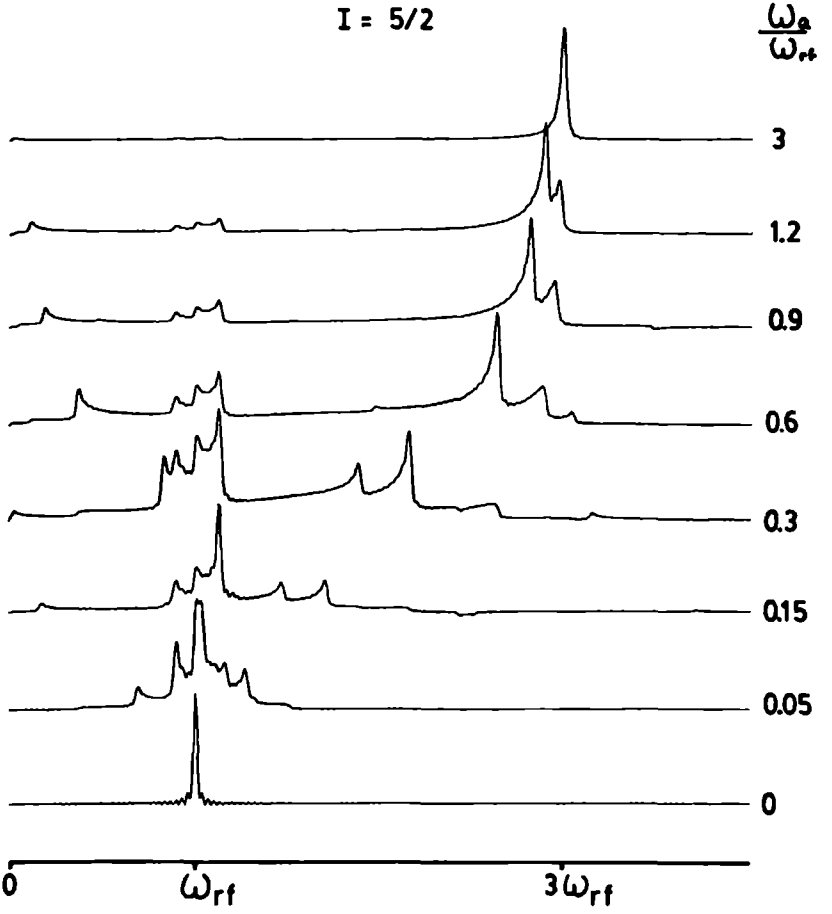

Fig. 6.4 Calculated nutation spectra as a function of ω_Q/ω_{rf} (η=0).

Fig. 6.5 shows the effect of the change of the asymmetry parameter η for a spin I=5/2 with ω_Q/ω_{rf}=0.6. The overall appearance of the powder pattern remains the same but the intensity of some of the lines changes drastically. So it is also possible to get a good estimate of η from the nutation spectra. It must be noted, however, that the changes of the powder pattern with changing η are more pronounced when η is small, this means that the accuracy of determining η is smaller for large η values. Calculated nutation spectra for all spins (I=3/2 to I=9/2) with asymmetry parameter variation can be found in appendix II. The spectra were calculated in the time domain, multiplied by an exponential decay function and then Fourier transformed to the frequency domain. Generally 10000 crystallite orientations were sampled, taking approximately 10 min computer time on a mainframe computer.

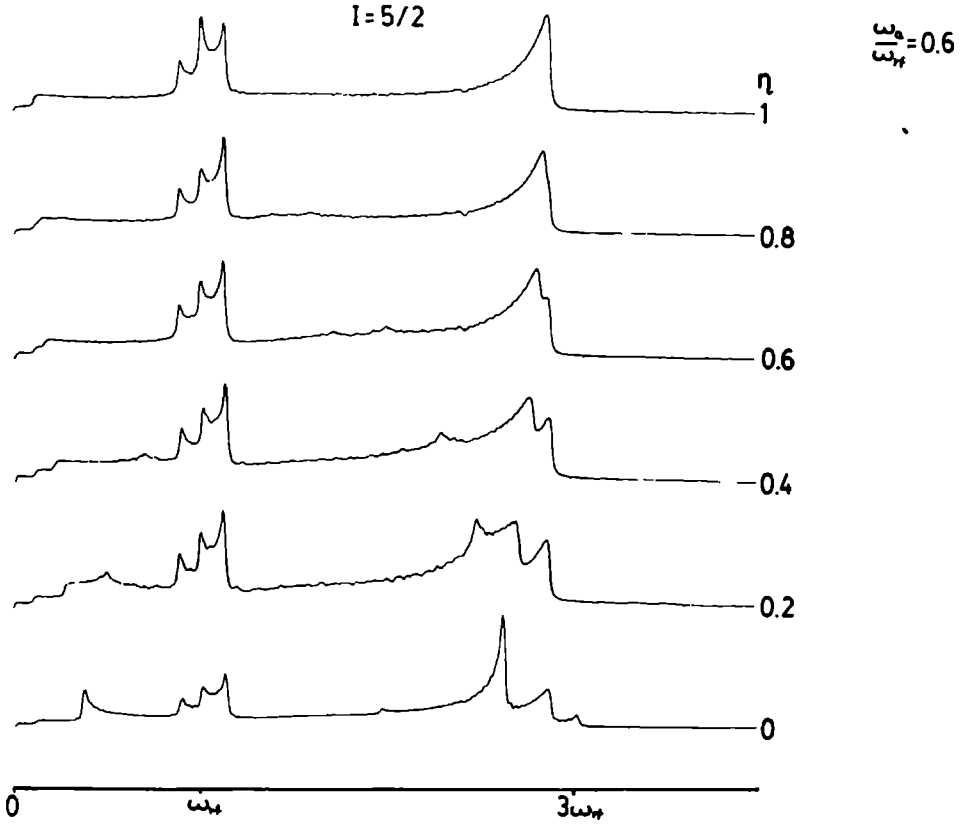

Fig. 6.5 Nutation spectra for a spin I=5/2 as a function of the asymmetry parameter η (ω_Q/ω_{rf} = 0.6). For small η values the spectra undergo characteristic changes when η changes. Determination of large η values will be less accurate.

So far it has been assumed that the sample is static, i.e. no magic angle spinning applied. As magic angle spinning narrows the (second-order) powder pattern of the central transition by a factor 4, it would be desirable in view of the resolution along F_2. However, numerical calculation of the simulated nutation spectra under MAS conditions becomes very (computer)time consuming, because the change of the orientation of the sample during t_1 and thus of H_1 cannot be neglected. Experimentally it has been observed that the nutation spectra change with MAS, except for the cases $\omega_Q \sim 0$ and $\omega_Q >> \omega_{rf}$.

6.3 Experimental aspects of nutation NMR

To get neat experimental nutation spectra which can be compared to the calculated spectra it is important to keep several experimental conditions in mind:

6.3.1 Resonance offset

When the system is irradiated on-resonance ($\omega=\omega_0$) then the matrix of H_1 in equation (6.2) becomes symmetrical with respect to both diagonals of the matrix. As a result of this

$$(R_{-1/2,1/2})_{i,j} = -(R_{-1/2,1/2})_{j,i} \qquad i\neq j$$
$$\text{and} \quad (R_{-1/2,1/2})_{i,j} = 0 \qquad i=j \tag{6.12}$$

Substitution in equation (6.7) shows that the signal then becomes

$$S(t_1,t_2) = \sum_{i<j} (R_{-1/2,1/2})_{i,j} \sin\{\omega_{ij}t_1\}\exp\{-i\omega_2 t_2\} \tag{6.13}$$

The amplitude of the signal detected during t_2 is sine modulated which allows us to obtain pure absorption spectra [BA82]. The presence of an off-resonance term in H_1 lowers the symmetry of its matrix and the modulation now becomes a phase-modulation, which cannot be changed to amplitude-modulation by phase-cycling. Thus there will be dispersive contributions to the line shapes which can easily distort powder patterns.

Another effect of off-resonance irradiation is the appearance of a dispersive line at $\omega_1=0$. This is due to the magnetization component along the B_{eff} field in the rotating frame which does not evolve during t_1.

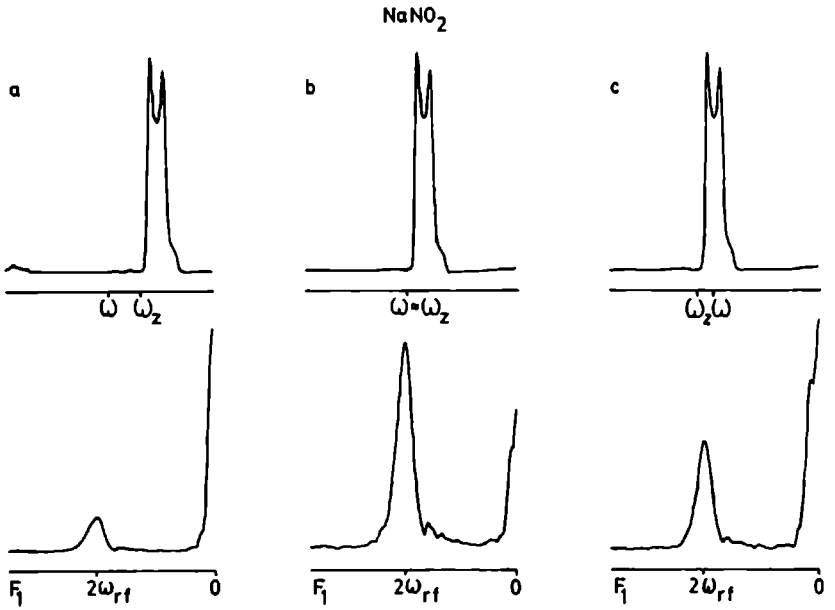

Fig. 6.6 MAS spectra of $NaNO_2$ together with their nutation spectra as a function of the excitation frequency ω. a) Off-resonance irradiation; In the nutation spectrum we see a large line at $\omega_1=0$. b) Irradiation close to the Larmor frequency (outside the powder pattern) gives the best nutation spectrum. c) With the carrier frequency equal to the average 1/2,-1/2 transition frequency (in the middle of the powder pattern) the line at $\omega_1=0$ increases again.

Both effects of off-resonance irradiation can even be observed for spins with I=1/2 for which the signal in such a case can be written as:

$$S(t_1,t_2) \sim [A\,(1 - \cos(\omega_{eff}t_1) + iB\,\sin(\omega_{eff}t_1)]\exp\{-i\omega_2 t_2\} \qquad (6.14)$$

where $A = \omega_{rf}\Delta\omega/2(\omega_{rf}^2+\Delta\omega^2)$ and $B = \omega_{rf}/2\sqrt{(\omega_{rf}^2+\Delta\omega^2)}$. When $\Delta\omega = \omega-\omega_0 \neq 0$ then $A \neq 0$ and thus a constant and a $\cos(\omega_{eff}t_1)$ term is introduced causing respectively the $\omega_1=0$ signal and the phase-modulation. To avoid complications it is clearly recommendable to irradiate on-resonance, i.e. with the excitation frequency ω equal to the Larmor frequency γB_0. That on-resonance in this case does not mean equal to the 1/2,-1/2 transition frequency is shown by the following magic angle spinning experiment. Here the Larmor

frequency lies outside of the quadrupole line shape [KU81, BE82, SA82] and fig. 6.6 shows the nutation spectra of NaNO2 (e^2qQ/h=1.1 MHz, η=0.1) as a function of the excitation frequency. In this case we are in the extreme situation $\omega_Q >> \omega_{rf}$ and MAS does not influence the nutation spectrum. It is clear that the line at ω_1=0 increases relative to the line at $2\omega_{rf}$. The line at ω_1=0 is minimal when we irradiate outside the powder pattern near the Larmor frequency. An easy method to reduce the line at ω_1=0 is to subtract the last (longest t_1 value) experiment in the 2D experiment from all the previous experiments. When enough t_1 experiments are performed, the quadrupolar modulation has damped out, and the only signal emerging after a long rf pulse is that of the magnetization causing the zero frequency signal in the F_1 direction. Because the magnetization component along B_{eff} has the same magnitude in every experiment (assuming no relaxation), subtraction of the last experiment reduces its influence on the spectrum.

6.3.2 Phasing of the spectra

As was discussed in chapter 2 it is important to obtain pure absorption spectra when one wants to obtain 2D powder patterns which can be analyzed in a straightforward way. Because we want no dispersion signals to appear in the spectrum it is not possible to perform an absolute value calculation. Therefore, the spectra have to be phased manually. As we have seen in the preceding paragraph, off-resonance irradiation introduces phase-modulation and thus dispersive line shapes are introduced in the spectra. This makes it very difficult to phase the spectra properly. This is so difficult because when phasing a 2D spectrum one has to set the phase correction on one slice (row or column) of the spectrum and it is not possible to inspect the effect of such a phase correction on the total spectrum. It would be desirable to have a program that shows the phase corrections of the whole spectrum directly on the display. As modern NMR spectrometers are equipped with minicomputers using array processors it should be possible to do so because nutation spectra are generally of small size.

When one is only interested in the 1D nutation spectrum (the F_1-projection) of a sample, there is a way to avoid phasing the whole 2D spectrum. In this case we can take the first point of every FID emerging directly after the pulse of length t_1. If we arrange these points as a function of t_1 we have the amplitude modulation of the detected t_2 signal as

a 1D interferogram. A straightforward 1D Fourier transform of this interferogram will give us the nutation spectrum which can be phased easily.

6.3.3 Linebroadening

An important cause for linebroadening in the F_1-dimension is the inhomogeneity of the rf magnetic field. The effect of rf inhomogeneity cannot simply be described with a Lorentzian broadening $\exp(-t_1/\tau_1)$ because a spread in ω_{rf} will also cause a spread in the ratio ω_Q/ω_{rf}, and will thus change the whole nutation spectrum. Furthermore the line shapes due to rf inhomogeneity will not be Lorentzian but asymmetric [HO83 fig.3]. Only in the extreme case $\omega_{rf} >> \omega_Q$ we get a line at nutation frequency ω_{rf} with a line width directly determined by the rf inhomogeneity. In the other extreme case $\omega_{rf} << \omega_Q$ there will be a line at $(I+1/2)\omega_{rf}$, so the line width will be $(I+1/2)\gamma$ times the rf inhomogeneity. It is therefore important to use a probe with an accurately formed rf coil to reduce rf inhomogeneity as much as possible and care should be taken that the whole sample is in the coil.

6.3.4 Recycle delay

Another important experimental aspect in the nutation experiment is that one has to ensure that the recycle delay or relaxation delay is long enough for the system to return to equilibrium before the next pulse arrives. If the recycle delay is short with respect to T_1 then the build up of magnetization along the z axis is incomplete. This will distort the pure sine amplitude-modulation of the FID (equation (6.13)). Fourier transformation of a distorted $\sin\omega_1 t$ wave will give a line at frequency ω_1 plus a number of harmonics at $2\omega_1$, $3\omega_1$, ... The number and amplitude of these harmonics depend on the distortion of the sine wave, and they can easily be mistaken for components with a large quadrupole frequency. Fig. 6.7 shows this effect for the ^{7}Li nutation spectrum of LiCl. Here Li has a very small quadrupole interaction, but due to the short repetition rate we do not only see a line at $\omega_1=\omega_{rf}$ but also at $\omega_1=2\omega_{rf}$, $3\omega_{rf}$ and $4\omega_{rf}$. In fact this experiment is proposed as a method to determine ω_{rf} in solution, for nuclei with long T_1 and low natural abundance [WE85].

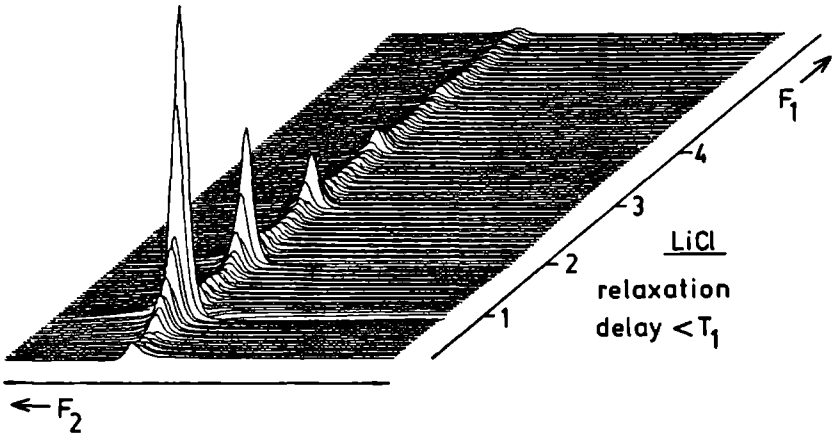

Fig. 6.7 2D nutation spectrum of ^{7}Li in LiCl where the recycle delay (0.25 s) is short with respect to T_1. Li has a small ω_Q in LiCl so only one line at ω_{rf} is expected. Because of the short recycle delay, however, there are several harmonics of this frequency present.

6.3.5 Experimental realization

$NaNO_2$ and spodumene spectra were recorded on a Bruker CXP-300 with respectively 64 and 128 t_1 increments of 2 μsec. A standard Bruker probe with an rf field of 36 kHz was employed. LiCl and $Sc_2(SO_4)_3$ spectra were recorded on a Bruker WM-500 (with 256 t_1 increments of 2 and 1.5 μsec respectively). Here a specially constructed probe equipped with a 6 x 12 mm solenoid B_0, operating with an rf field strength up to 70 kHz, was used. Zeolite ZSM-5 spectra were taken on the Bruker CXP-300 with an rf field of ~ 60 kHz (64 t_1 increments of 2 μsec).

6.4 Application of Nutation NMR

6.4.1 Spodumene

To demonstrate the effectiveness of the nutation experiment, fig. 6.8a displays the NMR spectrum of ^{27}Al in powdered spodumene recorded on a Bruker CXP 300 at 78.2 MHz. The spectrum consists of one featureless line 5 kHz wide. It is clear that no accurate quadrupole interaction parameters can be

extracted from this spectrum. In addition, MAS does not solve the problem, again we see a rather featureless line 1.5 kHz wide. Samoson and Lippmaa [SM82] have shown that this MAS spectrum can be reproduced theoretically (using a large linebroadening) with the known quadrupole parameters (e^2qQ/h=2.95 MHz, η=0.94 [PE53]), but it will be clear that it is almost impossible to do so without any preknowledge of the quadrupole parameters. The result of the 2D nutation experiment however, appears to be a well-structured pattern (fig. 6.8b). From the F_1-projection of this pattern (fig 6.8c) we can estimate the magnitude of the quadrupole parameters e^2qQ and η using our set of calculated spectra. It appears that $\omega_Q/\omega_{rf} \sim 1$ with an rf field strength of 36 kHz, this means that $e^2qQ/h \sim 3 \pm 0.5$ MHz, furthermore it is seen that η must be between 0.8 and 1. More accurate predictions can only emerge when a larger rf field is employed. At ω_Q/ω_{rf} = 0.3, for instance, intensity is more dispersed over the whole frequency range.

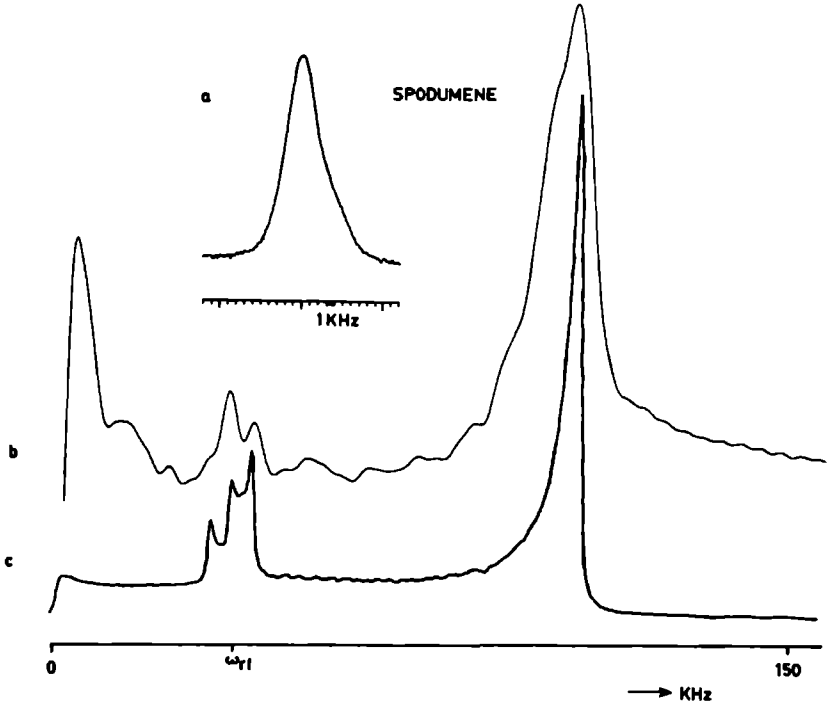

Fig. 6.8 a) ^{27}Al spectrum of the central transition of spodumene recorded at 78.2 MHz. b) F_1 projection of spodumene recorded on a Bruker CXP-300 (128 t_1 increments of 2 μs and ω_{rf} = 36 kHz). Simulated spectrum for e^2qQ/h=2.95 MHz and η=0.94 [PE53] and a Lorentzian linebroadening of 2.5 kHz.

6.4.2 $Sc_2(SO_4)_3$

Another example is the ^{45}Sc (I=7/2) nutation spectrum of $Sc_2(SO_4)_3$ (fig. 6.11). The spectrum of the central transition measured at 121.5 MHz is 2.6 kHz wide and shows no structure, MAS narrows the spectrum to 600 Hz. The MAS spectrum recorded at 43.8 MHz does show some structure from which it becomes clear that there must be sites with different quadrupole parameters but the same chemical shift. The 2D nutation spectrum is well structured (fig. 6.11). Comparing its projection to our set of calculated spectra reveals that the major constituent has a $e^2qQ/h \sim 2$ MHz with a low asymmetry parameter ($\eta \sim 0.2$). P.P. Man recently also showed an intermediate case for Mn in $KMnO_4$ [MA86].

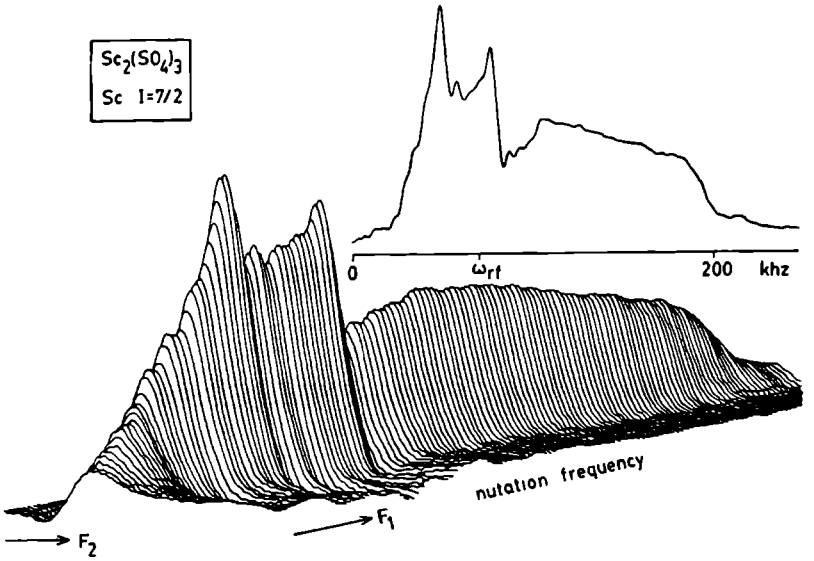

Fig. 6.9 2D nutation spectrum of ^{45}Sc in $Sc_2(SO_4)_3$ recorded on a Bruker WM-500, together with its F_1 projection (256 t_1 increments of 1.5 μs with a 70 kHz rf field).

6.4.3 Zeolite ZSM-5

We also applied the nutation experiment to the study of ZSM-5 zeolite catalysts. It has been reported before that in this zeolite the state of hydration affects the local symmetry around the Al nucleus at the Brønstedt sites in the pores of the material [KE83]. For hydrated ZSM-5 the local

symmetry around Al is high and consequently the quadrupole interaction small and the MAS line shape of the 1/2,-1/2 transition relatively narrow. On dehydration this line width broadens, as proposed due to a distortion of the AlO_4^- tetrahedra. This distortion depends on the counter ion, present in the pores to achieve electric neutrality. For H^+ the line width seems to double at 78.2 MHz (but the results of this investigation will show that the situation is more complicated). With Na^+ as a counter ion, the Al line becomes too broad to be detectable when the sample is dehydrated [KE83].

Fig. 6.10 shows the ^{27}Al nutation spectra for H-ZSM-5; for the chemical composition of this sample see table 6.1. We believe that comparison with the simulated spectra in fig. 6.4 shows that the experimental nutation spectra consist of contributions of at least two spin species with different quadrupole interactions. With increasing hydration spectral components at ω_{rf} ~ 60 kHz increase, showing that on hydration more and more Al nuclear spins find themselves in a relatively symmetric AlO_4^- tetrahedron. This is completely in agreement with earlier MAS experiments [KE83], however, it is surprising that the increase of spins with a small quadrupole interaction is not accompanied by a decrease of the line at $3\omega_{rf}$ (~ 180 kHz) due to spins with a quadrupole interaction large compared to ω_{rf}. In fact this line or group of lines hardly changes on hydration. This proofs that in the dehydrated zeolite a reservoir of Al nuclear spins exist which have such a large quadrupole interaction that their 1/2,-1/2 transition is not observed in our (non-spinning) 2D experiment. As mentioned above, when the AlO_4^- tetrahedron is charge compensated by Na^+, it has been experimentally demonstrated that in the dehydrated state the Al resonance is too broad to be observable. Table 6.1 shows that in our sample of ZSM-5 25% of all Al sites are neutralized by Na^+ but this percentage is not enough to explain the nutation spectra as a function of hydration. Further, more quantitative, work is needed to explain the observed phenomena especially because we noted that different ZSM-5 samples give different results. For the moment, a preliminary conclusion is that in contrast to earlier conclusions also the NMR line of Al sites with H^+ as a counter ion broadens so much on dehydration that they become undetectable. This would be in line with results on H-Boralite [SC85], a system with the same structure as H-ZSM-5 except that the place of Al in the lattice is taken by B in Boralite. The MAS NMR line width of ^{11}B in hydrated H-Boralite is ~ 80 Hz, in the dehydrated sample ~ 3 kHz. By taking into account the difference in quadrupole moment Q, Sternheimer antishielding factor, spin I and Larmor precession frequency γB_0 between ^{11}B and ^{27}Al one

can calculate that for the same electrical field gradient that causes the quadrupole interaction resulting in a 3 kHz line width for ^{11}B in dehydrated H-Boralite, should give a 80 x larger ^{27}Al line width in dehydrated H-ZSM-5. For a static sample this line width is even 4 x greater. This certainly results in an unobservable ^{27}Al resonance.

Table 6.1 Chemical composition per unit cell of the H-ZSM-5 sample used in the hydration/dehydration study discussed in paragraph 6.4.3

Si/Al ratio	H	Na/K	AlO_2	SiO_2
11	6	2	8	88

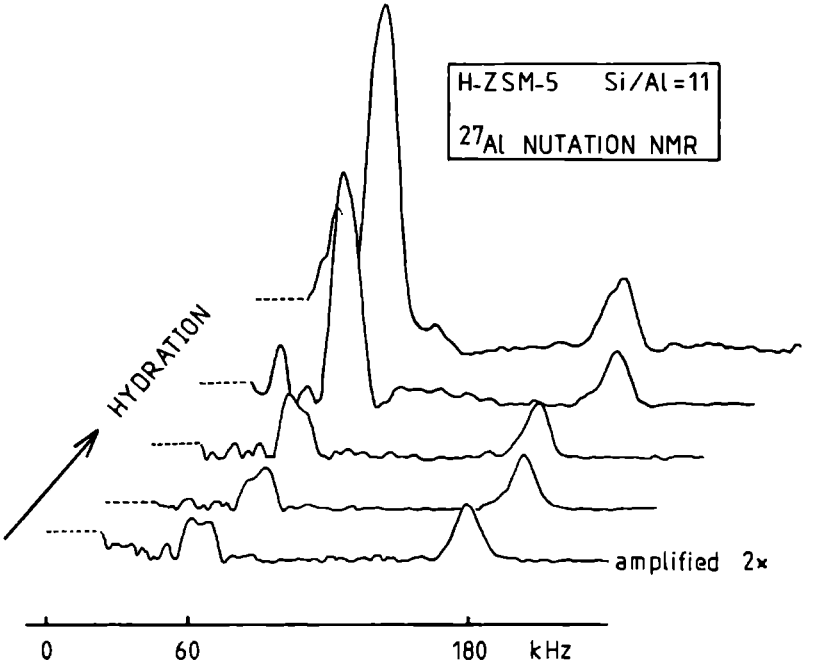

Fig. 6.10 ^{27}Al nutation spectra for H-ZSM-5 as a function of rehydration. The lowest spectrum is of the dehydrated material, the next spectra are found after 1/2 h, 2 h, 8 h and 156 h of exposing the material to water vapour.

6.5 Conclusions

The 2D nutation method appears to be very useful for the determination of quadrupole interaction parameters of half integer quadrupole nuclei, especially when these parameters cannot be determined from MAS experiments. The method combines the sensitivity of high-field measurements with the information one gets from experiments at low (zero) field. The spectra can easily be simulated with a straightforward density matrix calculation. In order to get high sensitivity and maximum resolution in the F_2-dimension, which is advantageous if nuclei with different chemical shift are present, one preferably performs the experiment in the highest available magnetic field. Because there is no obvious need for MAS the method will also be very suited for high temperature studies (e.g. of zeolites).

References

AB61 A. Abragam, "Principles of Nuclear Magnetism", Oxford University Press, Oxford, 1961.

BA69 J.F. Baugher, P.C. Taylor, T. Oya and P.J. Bray, J. Chem. Phys. 50, 4914, 1969.

BA82 A. Bax, "Two Dimensional Nuclear Magnetic Resonance in Liquids", D.Reidel Publishing Company, Dordrecht, 1982.

BE82 H.-J. Behrens and B. Schnabel, Physica 114B, 185, 1982.

SC85 K.F.M.G.J. Scholle and W.S. Veeman, Zeolites 5, 118, 1985.

GE85 F.M.M. Geurts, A.P.M. Kentgens and W.S. Veeman, Chem. Phys. Lett. 120, 2, 1985.

HO83 D. Horne, R.D. Kendrick and C.S. Yannoni, J. Magn. Res. 52, 299, 1983.

KE83 A.P.M. Kentgens, K.F.M.G.J. Scholle and W.S. Veeman, J. Chem. Phys. 87, 4357, 1983.

KE87 A.P.M. Kentgens, J.J.M. Lemmens, F.M.M. Geurts and W.S. Veeman, J. Magn. Res. 71, 62, 1987.

KU81 E. Kundla, A. Samoson and E. Lippmaa, Chem. Phys. Lett. 83, 229, 1981.

MA85 P.P. Man, H. Theveneau and P. Papon, J. Magn. Res. 64, 271, 1985.

MA86 P.P. Man, J. Magn. Res. 67, 78, 1986.

NA66 K. Narita, J-I. Umeda and H. Kusumoto, J. Chem. Phys. 44, 2719, 1966.

PE53 H.E. Petch, N.G. Granna and G.N. Volkoff, Can. J. Phys. 31, 837, 1953.

SA82 A. Samoson, E.Kundla and E. Lippmaa, J. Magn. Res. 49, 350, 1982.

SA83 A. Samoson and E. Lippmaa, Chem. Phys. Lett. 100, 205, 1983.

SM83 A. Samoson and E. Lippmaa, Phys. Rev. B 28, 6567, 1983.

TR85 A. Troniker, P.P. Man, H. Theveneau and P. Papon, Solid State Comm. 55, 929, 1985.

WE85 J.R. Wesener and H. Günther, J. Magn. Res. 62, 158, 1985.

WO77 A. Wokaun and R.R. Ernst, J. Chem. Phys. 67, 1752, 1977.

YA81 C.S. Yannoni and R.D. Kendrick, J. Chem. Phys. 74, 747, 1981.

ZA85 D.B. Zax, A. Bielecki, K.W. Zilm, A. Pines and D.P. Weitekamp, J. Chem. Phys. 83, 4877, 1985.

APPENDIX I

TRANSFORMATION OF IRREDUCIBLE TENSORS

We are used to present tensor interactions in their Cartesian form. As was explained in paragraph 1.2.6 it is possible to decompose a Cartesian tensor into its irreducible components. A detailed treatment of irreducible spherical tensors can be found in the books of Rose [RO57], Edmonds [ED57] and Brink and Satchler [BR79]. The advantage of irreducible tensors is that they transform among themselves under rotations. The tensor interactions encountered in NMR are symmetric. This means that the Cartesian tensors can be decomposed in a scalar (tensor of rank zero), which is invariant under rotations, and a second rank tensor, which transforms by definition as

$$T'_{2,q} = \sum_{p=-2}^{2} D^2_{p,q}(\alpha,\beta,\gamma)\ T_{2,p} \qquad (I.1)$$

α,β,γ are the Euler angles of the rotation taking the old, unprimed, axes into the new, primed, axes. Thus (I.1) expresses a component $T'_{2,q}$ with respect to the new axes in terms of the components $T_{2,p}$ with respect to the old axes. $D^2_{p,q}$ represents the Wigner rotation matrix which is given in table I.1. This rotation matrix was obtained using the definitions of Brink and Satchler [BR79] which means that a positive rotation is defined by the right hand screw sense in the direction of the positive rotation axis.

As was shown in chapter 1 it is possible to express a spin Hamiltonian as a product of an irreducible tensor $R_{1,-m}$, which contains the geometrical dependence of the spin interactions, and an irreducible tensor $T_{1,m}$ containing the spin variables of the interaction. The internal Hamiltonians can thus be written as

$$H_X = C^X \sum_{l=0}^{2} \sum_{m=-1}^{1} (-1)^m R^X_{1,-m} T^X_{1,m} \qquad (I.2)$$

It was further shown in chapter 1 that it is possible to give a general relation between the components of the irreducible tensors and the principal values of the Cartesian tensor in the principal axis system of the spin interaction.

$$\rho_{0,0} = \frac{1}{3}\,\mathrm{Tr}(R) = \frac{1}{3}(R_{XX}+R_{YY}+R_{ZZ}) = R_{iso}$$

$$\rho_{2,0} = \sqrt{(3/2)}\ (R_{ZZ}-R_{iso}) = \sqrt{(3/2)}\ \delta \qquad \text{(I.3)}$$

$$\rho_{2,\pm2} = \frac{1}{2}\ (R_{XX}-R_{YY}) = \frac{1}{2}\ \delta\eta$$

where R_{XX}, R_{YY} and R_{ZZ} represent the components of the Cartesian tensor in the principal axes system. The irreducible tensors are expressed as $\rho_{1,m}$ in that coordinate frame. To find the appropriate expressions of a truncated spin Hamiltonian in the rotating frame we only have to evaluate the component $R_{2,0}$. This is because only the components $T_{0,0}$ and $T_{2,0}$ (table 1.1) of the spin Hamiltonians survive truncation, which means that the general appearance of a truncated Hamiltonian is

$$H_X \sim R^X_{0,0}T^X_{0,0} + R^X_{2,0}T^X_{2,0} \qquad \text{(I.4)}$$

Consequently, the angular dependence of any first order spin interaction is found by transforming $R_{2,0}$ from the principal axes system to the laboratory frame. Note that, because of the invariance of the angular part of a spin interactions to rotations about the magnetic field, it does not matter if we transform to the rotating frame or the laboratory frame. In fact, the rotating frame only exists in spin space. When θ and φ are the polar angles orienting the external magnetic field in the principal axes system, the transformation to the laboratory frame is given by

$$R_{2,0} = \sum_m D^2_{m,0}(\varphi,\theta,0)\ \rho_{1,m} \qquad \text{(I.5)}$$

$$= D^2_{0,0}(\varphi,\theta,0)\ \sqrt{(3/2)}\ \delta + \{D^2_{2,0}(\varphi,\theta,0) + D^2_{-2,0}(\varphi,\theta,0)\}\ \eta\delta/2$$

$$= \sqrt{(3/8)}\ \delta(\ 3\cos^2\theta - 1 + \eta\sin^2\theta\cos2\varphi\ )$$

Note that we would have had to multiply three 3x3 matrices to obtain this result using Cartesian tensors.

When the sample is spinning about the magic angle, the principal axes system of a certain spin constantly changes its position with respect to the magnetic field. This process is described most easily by defining an axis system in the rotor. The correct Hamiltonian is then found by transforming from the principal axes system to this rotor axis system followed by a transformation to the laboratory frame. This transformation is given in equation (1.38) of chapter 1. Using table I.1 this can easily be converted to the expression of equation (1.39). Generally transformation of spin Hamiltonians using irreducible tensors reduces the amount of calculation.

REFERENCES

BR79 D.M. Brink and G.R. Satchler, "Angular Momentum", Oxford University Press, Oxford, 1979.

ED57 A.R. Edmonds, "Angular Momentum in Quantum Mechanics", Princeton University Press, Princeton, New Jersey, 1957.

RO57 M.E. Rose, "Elementary Theory of Angular Momentum", J. Wiley and Sons, New York, 1957.

Table I.1: $D^2_{m',m}(\alpha,\beta,\gamma)$ according to the definitions of Brink, and Satchler [BR79].

m' \ m	2	1	0	-1	-2	
2	$\cos^4(\frac{\beta}{2}).e^{-2i(\alpha+\gamma)}$	$-\frac{1}{2}\sin\beta(1+\cos\beta).e^{-i(2\alpha+\gamma)}$	$\sqrt{\frac{3}{8}}\sin^2\beta\ e^{-2i\alpha}$	$-\frac{1}{2}\sin\beta(1-\cos\beta)e^{-i(2\alpha-\gamma)}$	$\sin^4(\frac{\beta}{2})e^{-2i(\alpha-\gamma)}$	2
1	$\frac{1}{2}\sin\beta(1+\cos\beta).e^{-i(\alpha+2\gamma)}$	$\frac{1}{2}(2\cos\beta-1)(1+\cos\beta)e^{-i(\alpha+\gamma)}$	$-\sqrt{\frac{3}{8}}\sin2\beta\ e^{-i\alpha}$	$\frac{1}{2}(2\cos\beta+1)(1-\cos\beta)e^{-i(\alpha-\gamma)}$	$-\frac{1}{2}\sin\beta(1-\cos\beta)e^{-i(\alpha-2\gamma)}$	-1
0	$\sqrt{\frac{3}{8}}\sin^2\beta.e^{-2i\gamma}$	$\sqrt{\frac{3}{8}}\sin2\beta\ e^{-i\gamma}$	$\frac{1}{2}(3\cos^2\beta-1)$	$-\sqrt{\frac{3}{8}}\sin2\beta\ e^{i\gamma}$	$\sqrt{\frac{3}{8}}\sin^2\beta\ e^{2i\gamma}$	0
-1	$\frac{1}{2}\sin\beta(1-\cos\beta)e^{+i(\alpha-2\gamma)}$	$\frac{1}{2}(2\cos\beta+1)(1-\cos\beta)e^{+i(\alpha-\gamma)}$	$\sqrt{\frac{3}{8}}\sin2\beta\ e^{i\alpha}$	$\frac{1}{2}(2\cos\beta-1)(1+\cos\beta)e^{+i(\alpha+\gamma)}$	$-\frac{1}{2}\sin\beta(1+\cos\beta)e^{+i(\alpha+2\gamma)}$	-1
-2	$\sin^4(\frac{\beta}{2}).e^{+2i(\alpha-\gamma)}$	$\frac{1}{2}\sin\beta(1-\cos\beta)e^{+i(2\alpha-\beta)}$	$\sqrt{\frac{3}{8}}\sin^2\beta.e^{2i\alpha}$	$\frac{1}{2}\sin\beta(1+\cos\beta)e^{+i(2\alpha+\gamma)}$	$\cos^4(\frac{\beta}{2})e^{+2i(\alpha+\gamma)}$	-2

APPENDIX II

LIBRARY OF NUTATION SPECTRA

This appendix contains a complete series of nutation spectra for half-integer quadrupolar nuclei I=3/2, 5/2, 7/2 and 9/2 resulting from density matrix calculations discussed in chapter 6. These spectra can be used in a qualitative way to determine the quadrupole interactions from experimental spectra. For each spin the first figure represents a series of nutation spectra as a function of ω_Q/ω_{rf} for η=0. $\omega_Q = e^2qQ/\hbar\ 8I(2I-1)$ and ω_{rf} ($=\gamma B_1$) represents the strength of the radiofrequency B_1 field. In the subsequent figures η is varied for each ratio ω_Q/ω_{rf}.

Table II.1 This table gives the value of e^2qQ/h (in MHz) for a given ratio of ω_Q/ω_{rf}, for $\omega_{rf}/2\pi$ = 50 kHz.

ω_Q/ω_{rf}	I=3/2	I=5/2	I=7/2	I=9/2
0.05	0.06	0.20	0.42	0.72
0.15	0.18	0.60	1.26	2.16
0.30	0.36	1.20	2.52	4.32
0.60	0.72	2.40	5.04	8.64
0.90	1.08	3.60	7.56	12.96
1.20	1.44	4.80	10.08	17.28
3.00	3.60	12.00	25.20	43.20

Table II.2 This table gives the vertical scaling factor, with respect to the ω_Q=0 spectra, of every (η=0) spectrum.

ω_Q/ω_{rf}	I=3/2	I=5/2	I=7/2	I=9/2
0.05	4.7	7.4	6.7	12.1
0.15	15.2	8.2	16.0	25.2
0.30	14.9	25.0	22.0	19.8
0.60	10.2	25.1	39.6	72.0
0.90	7.3	19.4	32.6	61.1
1.20	5.7	15.7	26.2	52.3
3.00	3.0	6.9	12.7	25.7

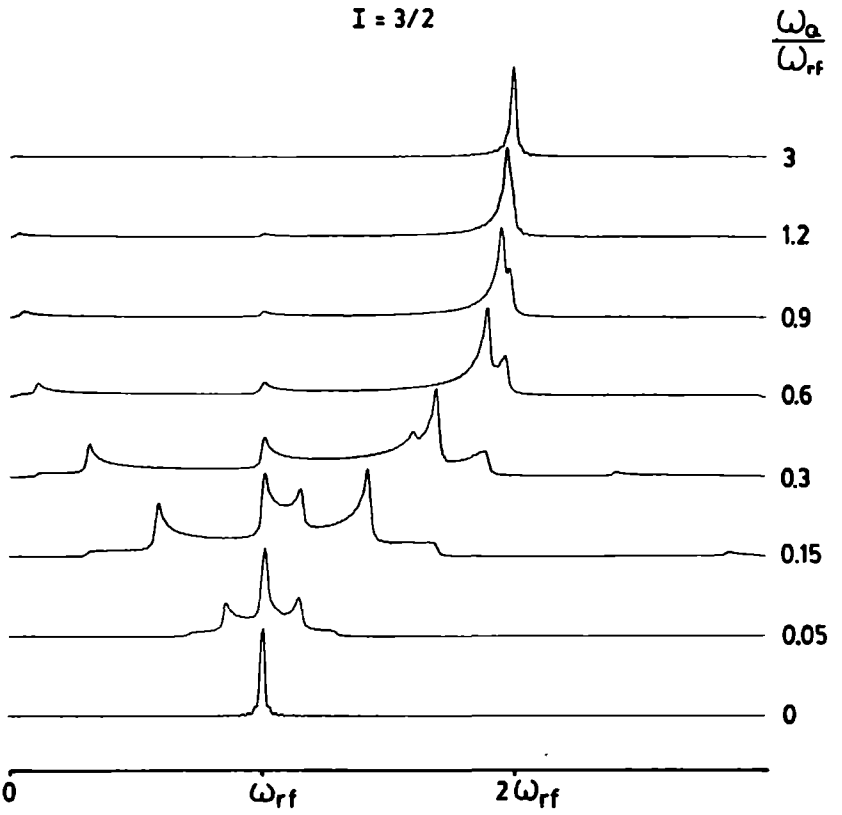
I = 3/2
ωa/ωrf
3
1.2
0.9
0.6
0.3
0.15
0.05
0
0
ωrf
2ωrf

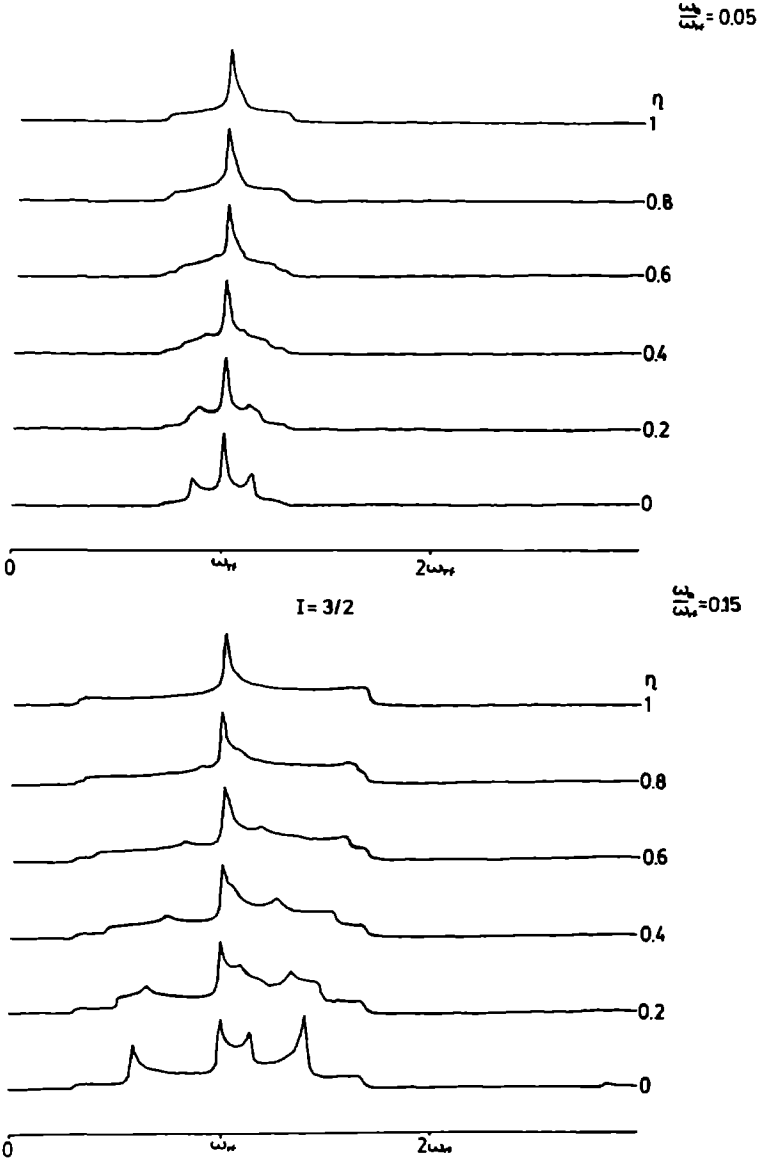
$\frac{\omega_Q}{\omega_0}$ = 0.05
η
1
0.8
0.6
0.4
0.2
0
0
ω_0
$2\omega_0$
I = 3/2
$\frac{\omega_Q}{\omega_0}$ = 0.15
η
1
0.8
0.6
0.4
0.2
0
0
ω_0
$2\omega_0$

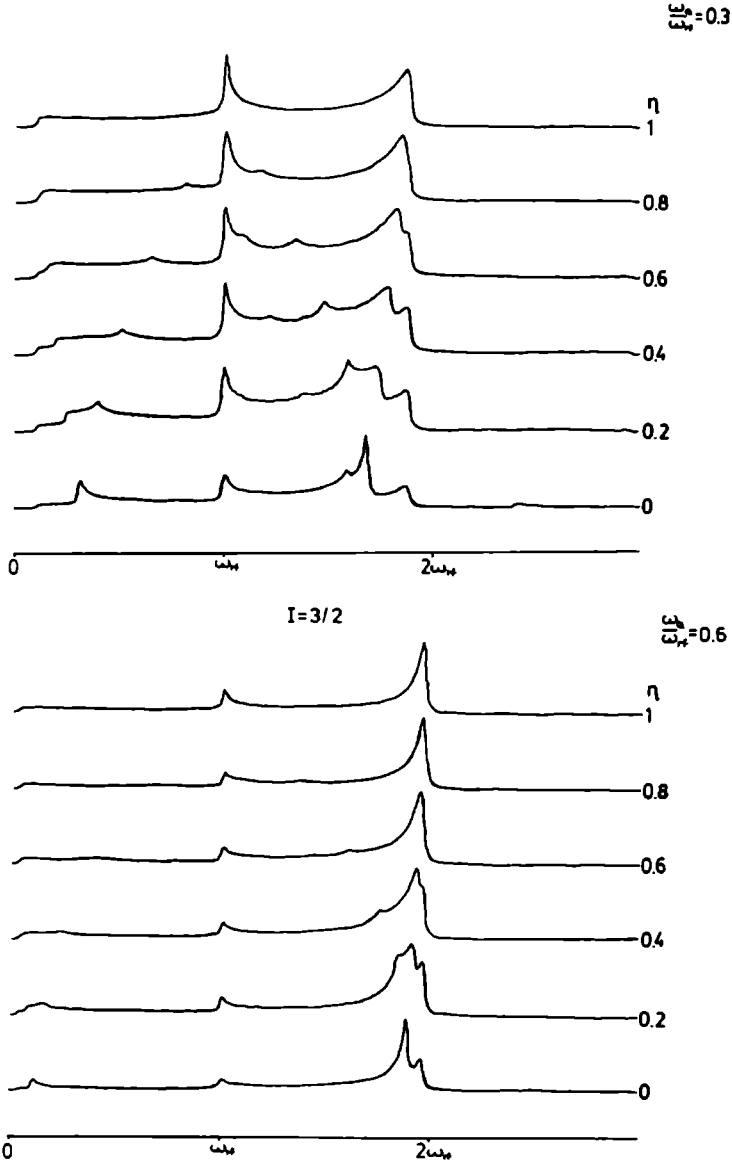
$\frac{\omega_Q}{\omega_0}$=0.3
η
1
0.8
0.6
0.4
0.2
0
0
ω_0
$2\omega_0$
I=3/2
$\frac{\omega_Q}{\omega_0}$=0.6
η
1
0.8
0.6
0.4
0.2
0
0
ω_0
$2\omega_0$

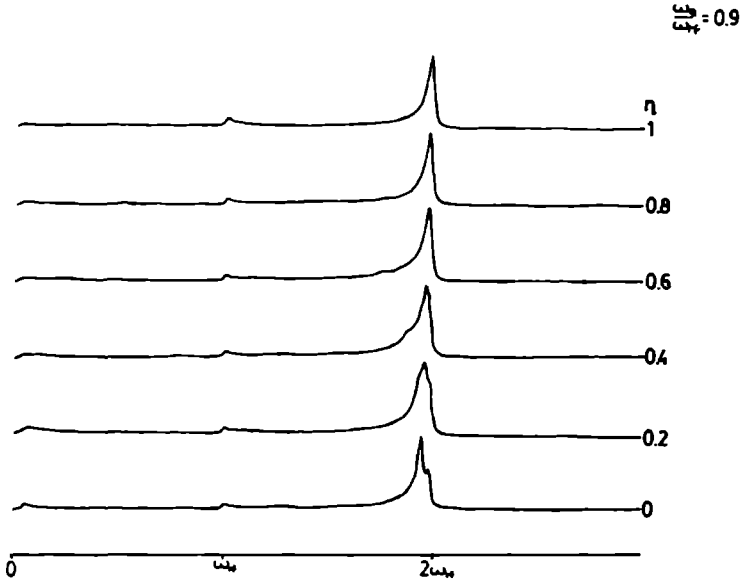
$\frac{\omega_Q}{\omega_{L_H}} = 0.9$
η
1
0.8
0.6
0.4
0.2
0
0
ω_{L_H}
$2\omega_{L_H}$

I=3/2

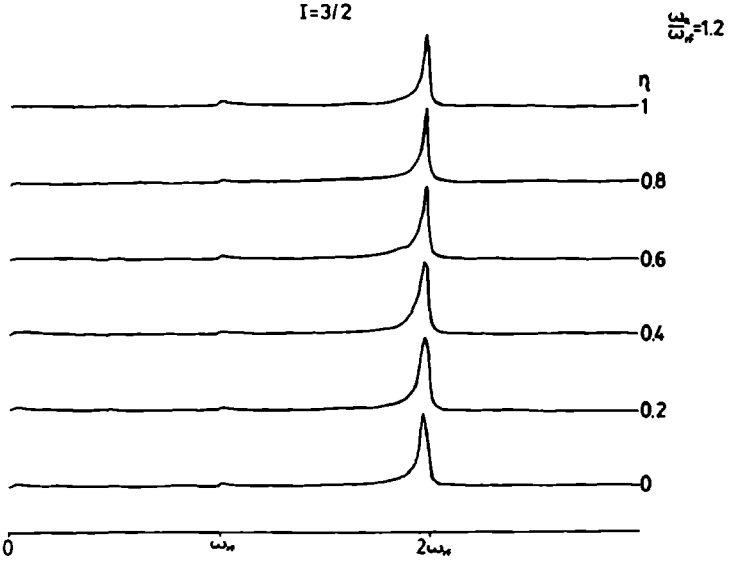
$\frac{\omega_Q}{\omega_{L_H}} = 1.2$
η
1
0.8
0.6
0.4
0.2
0
0
ω_{L_H}
$2\omega_{L_H}$

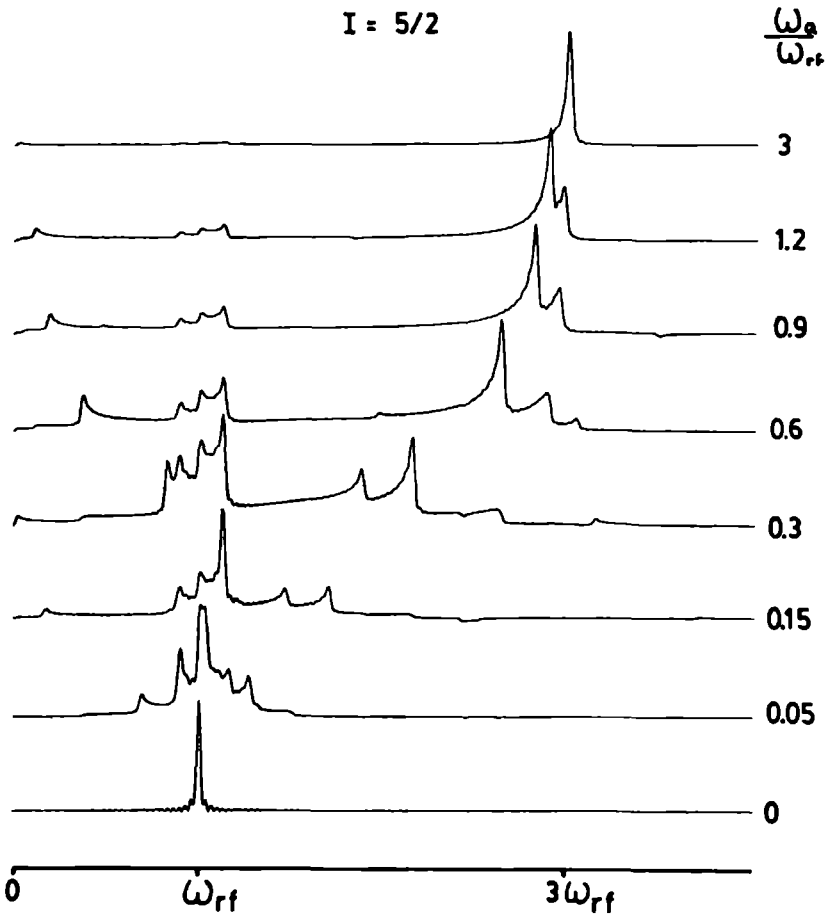
I = 5/2
$\frac{\omega_Q}{\omega_{rf}}$
3
1.2
0.9
0.6
0.3
0.15
0.05
0
0
ω_{rf}
$3\omega_{rf}$

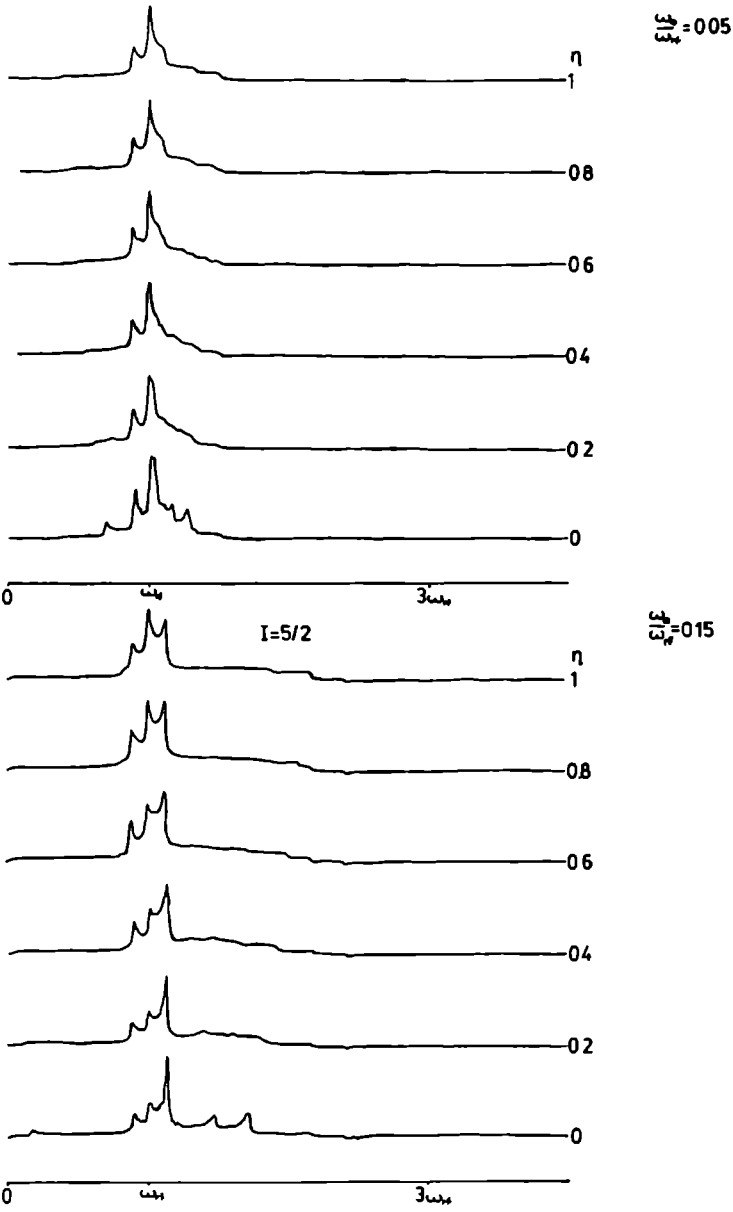
$\frac{3\omega_Q}{\omega_L}$=005
η
1
08
06
04
02
0
0
ω_L
$3\omega_L$
I=5/2
$\frac{3\omega_Q}{\omega_L}$=015
η
1
08
06
04
02
0
0
ω_L
$3\omega_L$

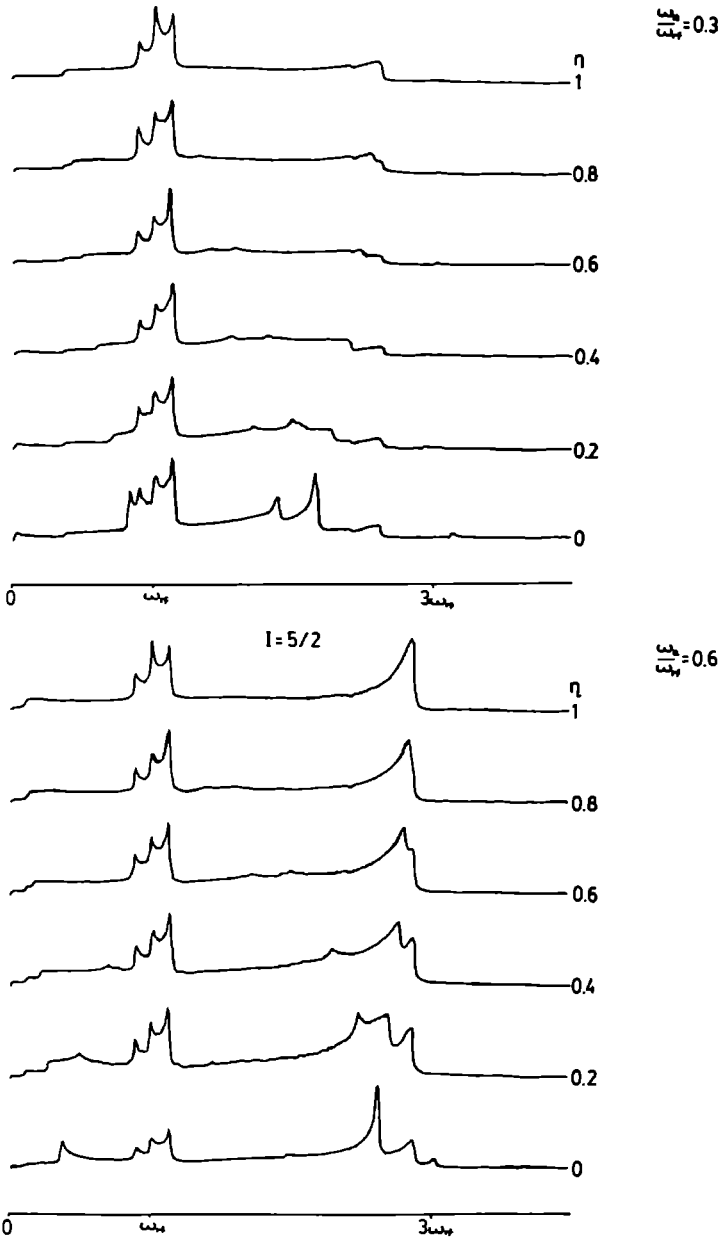
$\frac{3\hbar\chi}{\omega_0}$=0.3
η
1
0.8
0.6
0.4
0.2
0
0
ω_0
$3\omega_0$
I=5/2
$\frac{3\hbar\chi}{\omega_0}$=0.6
η
1
0.8
0.6
0.4
0.2
0
0
ω_0
$3\omega_0$

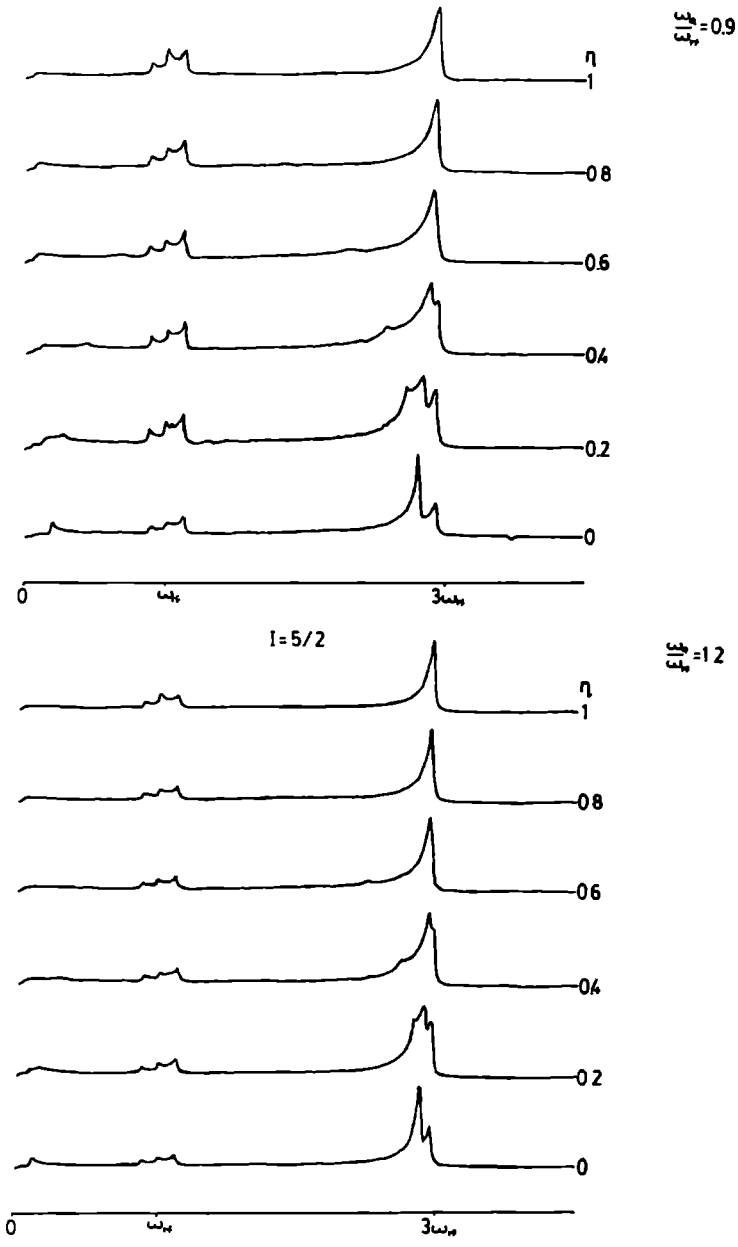
$\frac{3J}{\omega_0}$=0.9
η
1
0.8
0.6
0.4
0.2
0
0
ω_0
$3\omega_0$
I=5/2
$\frac{3J}{\omega_0}$=1.2
η
1
0.8
0.6
0.4
0.2
0
0
ω_0
$3\omega_0$

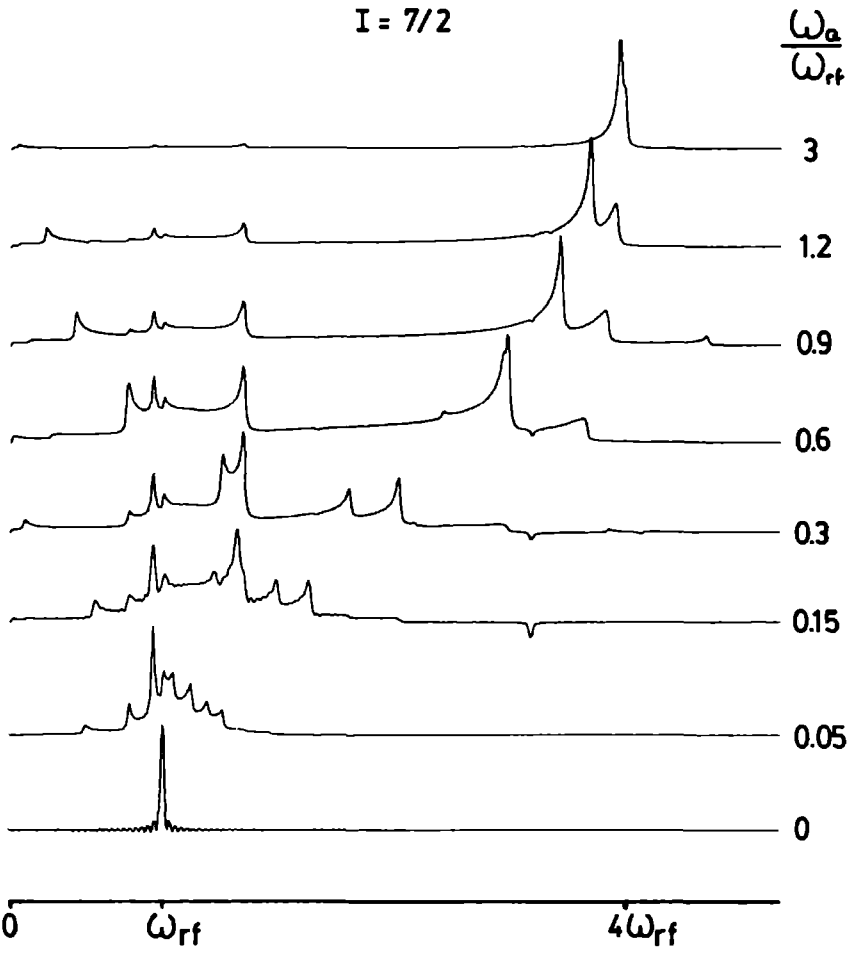
I = 7/2
ωa/ωrf
3
1.2
0.9
0.6
0.3
0.15
0.05
0
0
ωrf
4ωrf

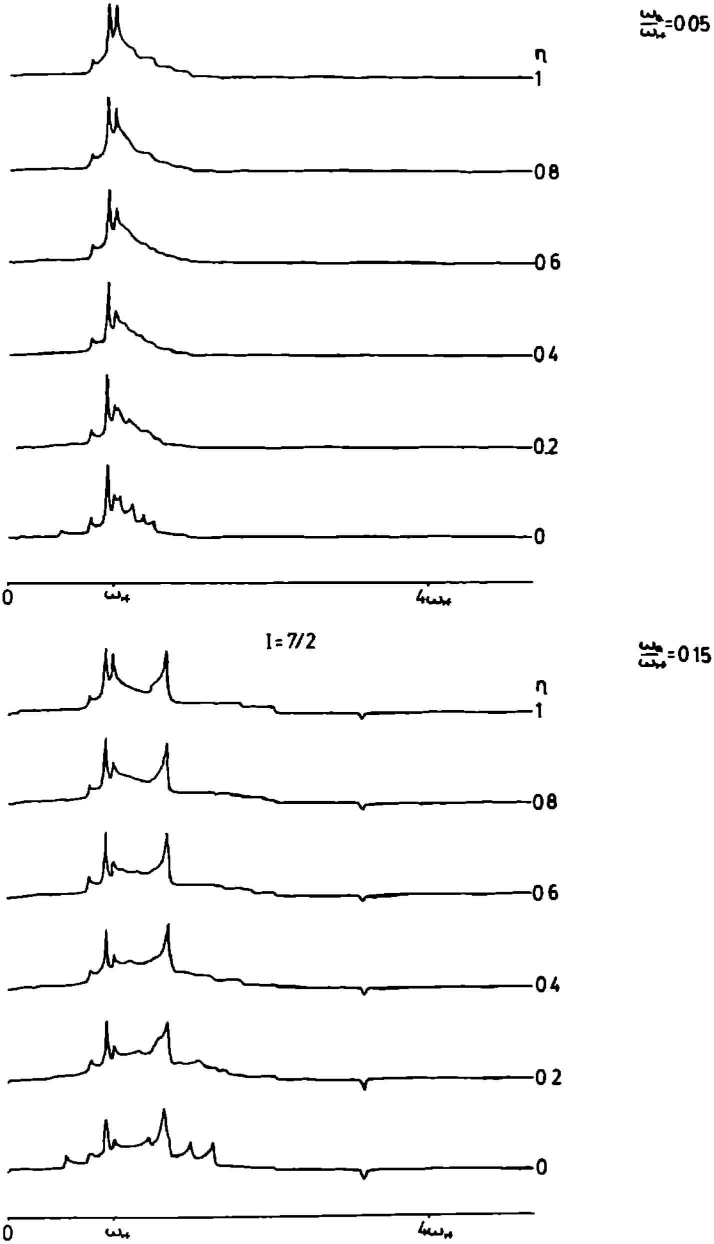

$\frac{\omega_a}{\omega_M}$=005
η
1
08
06
04
02
0
0
ω_M
$4\omega_M$
I=7/2
$\frac{\omega_a}{\omega_M}$=015
η
1
08
06
04
02
0
0
ω_M
$4\omega_M$

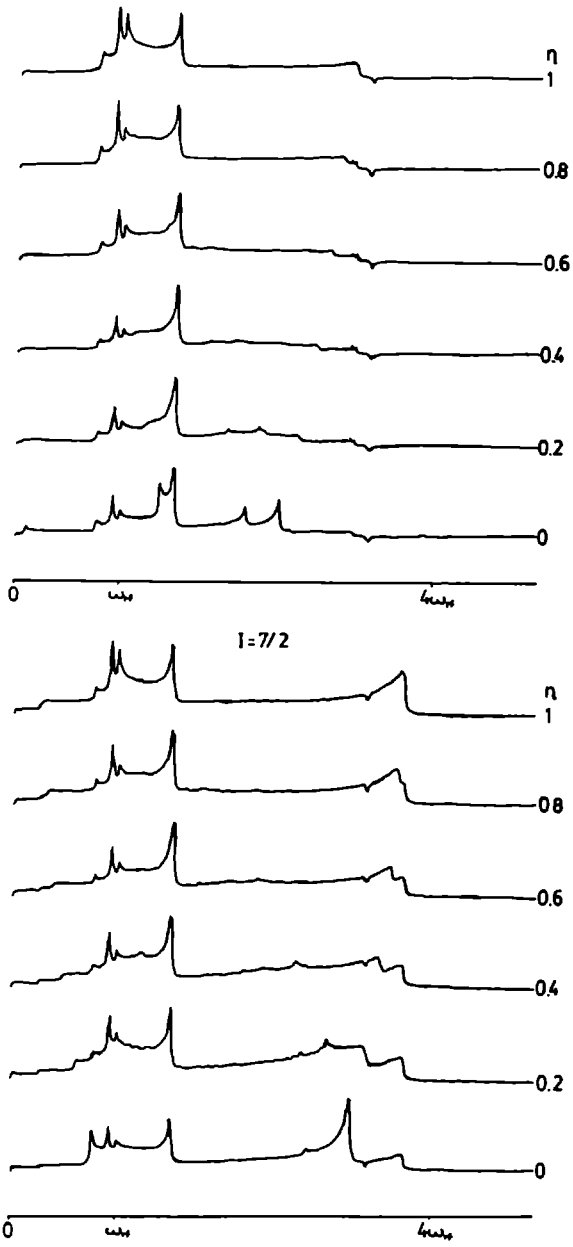
$\frac{\omega_{12}}{\omega_{34}}$=0.3
η
1
0.8
0.6
0.4
0.2
0
0
ω_{34}
$4\omega_{34}$
I=7/2
$\frac{\omega_{12}}{\omega_{34}}$=0.6
η
1
0.8
0.6
0.4
0.2
0
0
ω_{34}
$4\omega_{34}$

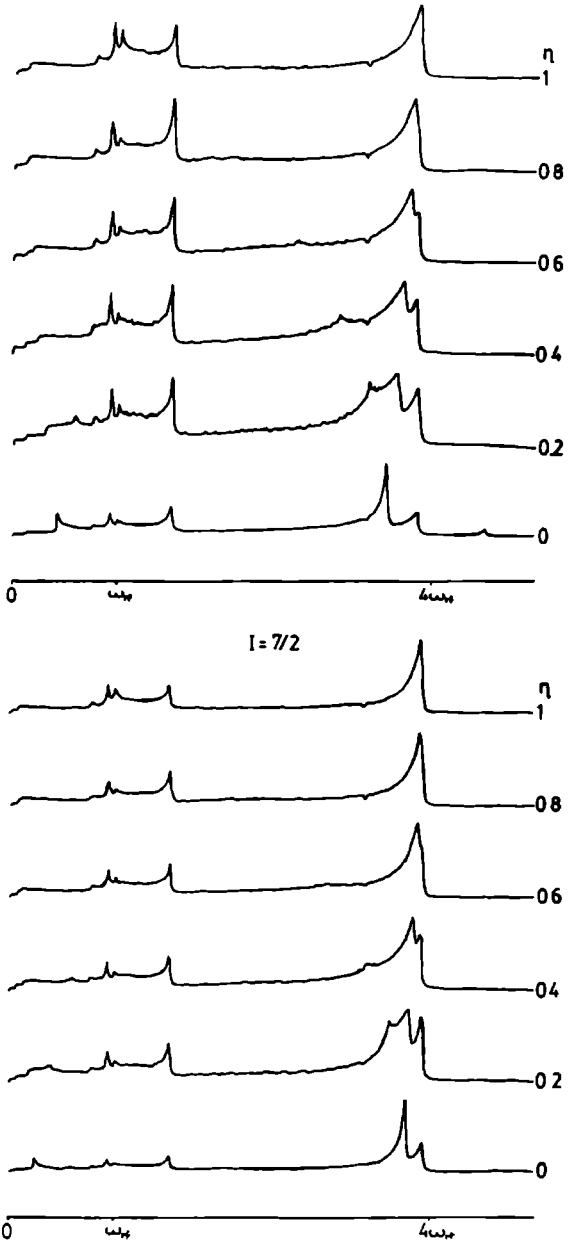
$\frac{\omega_{RF}}{\omega_{ex}}$=0.9
η
1
0.8
0.6
0.4
0.2
0
0
ω_{ex}
$4\omega_{ex}$
I = 7/2
$\frac{\omega_{RF}}{\omega_{ex}}$=1.2
η
1
0.8
0.6
0.4
0.2
0
0
ω_{ex}
$4\omega_{ex}$

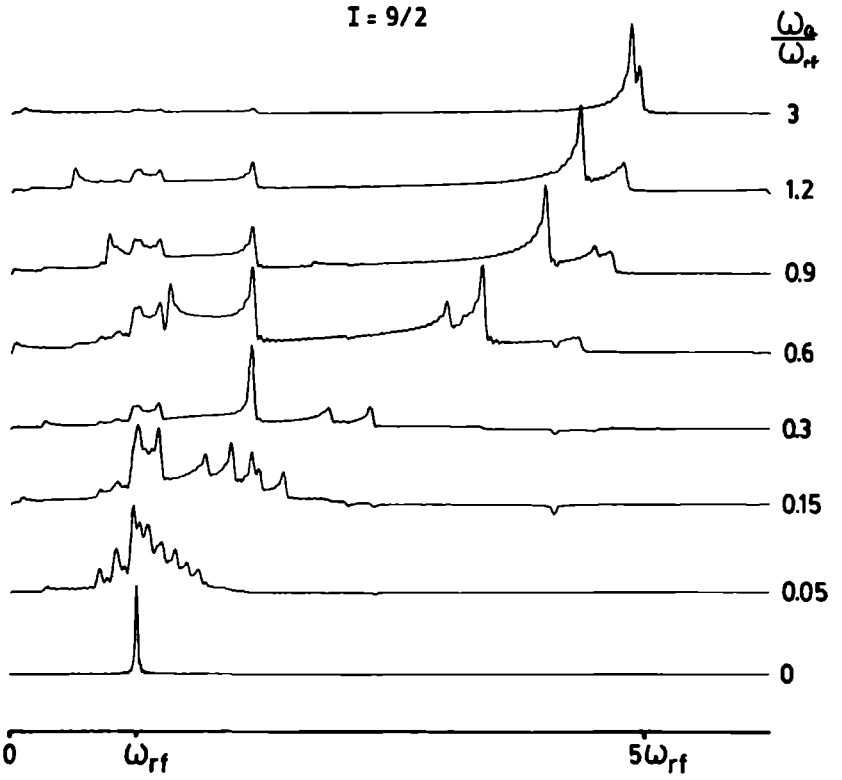
I = 9/2
$\frac{\omega_a}{\omega_{rf}}$
3
1.2
0.9
0.6
0.3
0.15
0.05
0
0
ω_{rf}
$5\omega_{rf}$

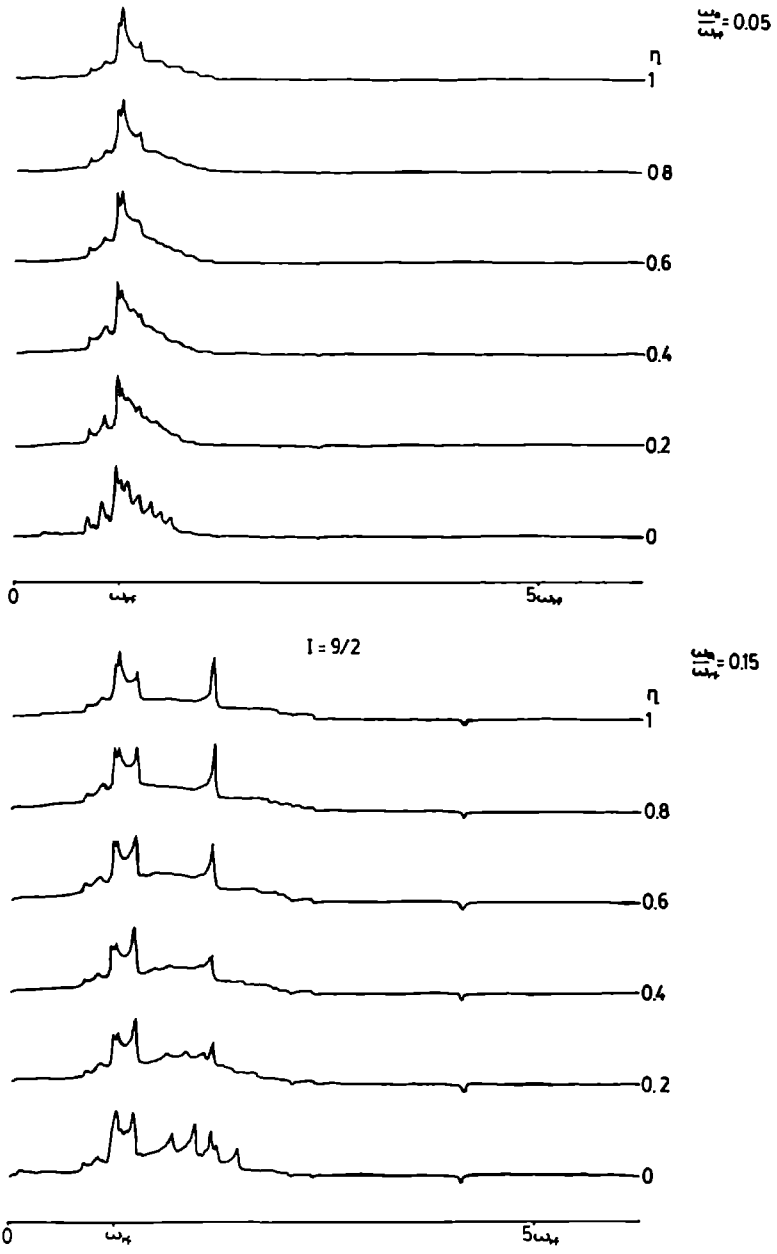
$\frac{\omega_Q}{\omega_H}$ = 0.05
η
1
0.8
0.6
0.4
0.2
0
0
ω_H
$5\omega_H$
I = 9/2
$\frac{\omega_Q}{\omega_H}$ = 0.15
η
1
0.8
0.6
0.4
0.2
0
0
ω_H
$5\omega_H$

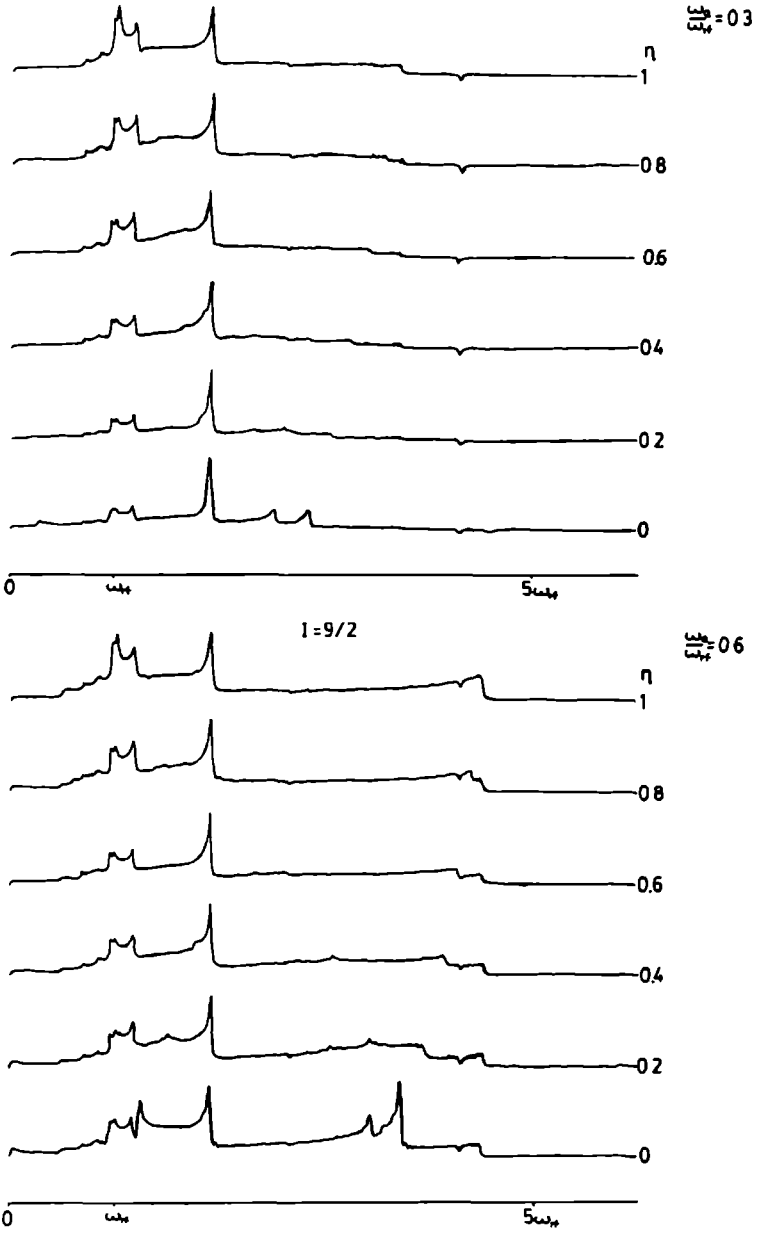
η
1
0.8
0.6
0.4
0.2
0
0
5
I=9/2
η
1
0.8
0.6
0.4
0.2
0
0
5

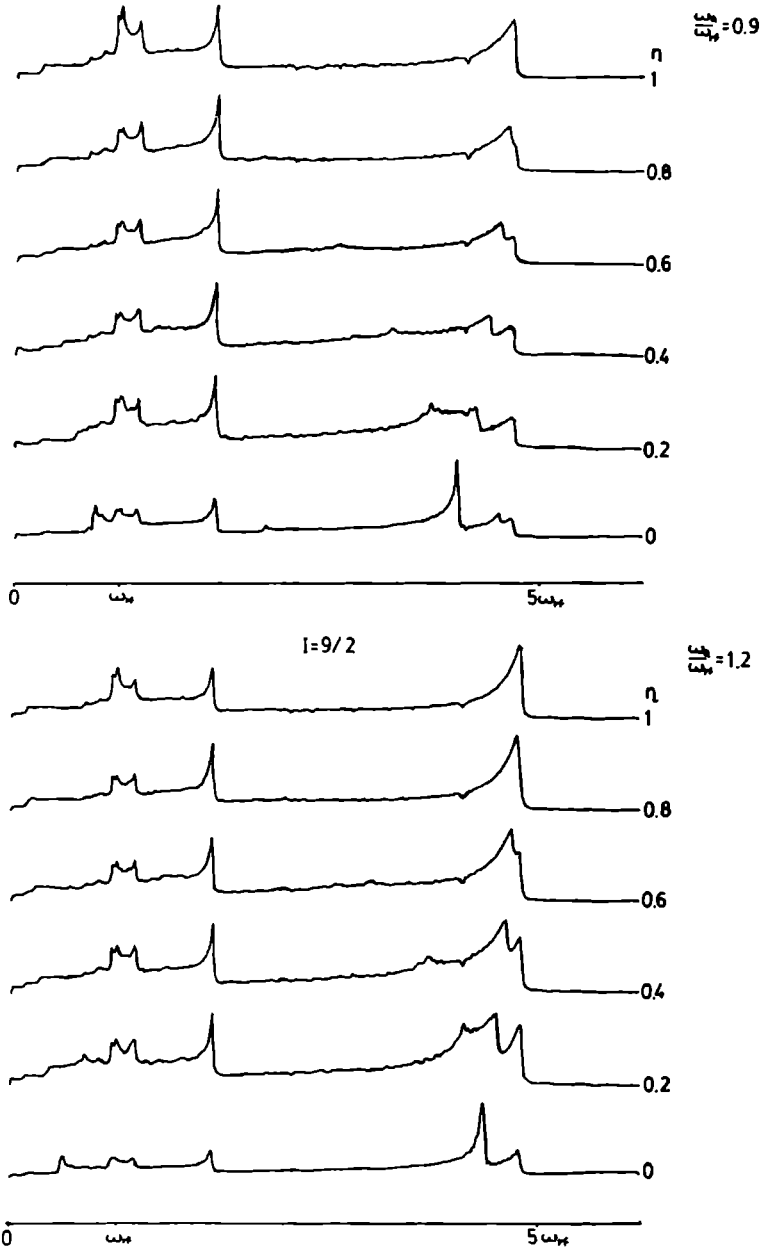
ω_{rf}=0.9
η
1
0.8
0.6
0.4
0.2
0
0
ω_{rf}
5ω_{rf}
I=9/2
ω_{rf}=1.2
η
1
0.8
0.6
0.4
0.2
0
0
ω_{rf}
5ω_{rf}

Nuclear Magnetic Resonance (NMR) has developed to one of the most important analysis tools in chemistry. This is because the spin interactions that the nuclear spins experience depend critically on the surroundings of the nucleus in a molecule. The technique has become so powerful that it is for instance possible to solve the 3-dimensional structure of large proteins in solution. The development of solid state NMR has been more painful. This is because the nuclei tumble around rapidly in solution and thus narrow (averaged) resonance lines are detected. In rigid solids, however, the resonance frequency of a spin depends on the orientation with respect to the magnetic field. As a result spectra of powdered solids are very broad and often featureless. However, several averaging techniques have been developed to obtain "liquid-like" spectra of solids. This thesis is dedicated to a new class of experiments in solids: two-dimensional NMR of solids.

Chapter 1 gives an overview of spin interactions that determine the resonance frequency of a nucleus. Furthermore it gives an overview of averaging techniques, like magic angle spinning and multiple pulse techniques, used to average anisotropic interactions in solids, in order to obtain "liquid-like" spectra.

In two-dimensional NMR the resonance signal is measured as a function of two time variables. The signal that is detected during a time domain t_2 is modulated in phase or amplitude by the spin interactions present during a previous period t_1. This is achieved by applying specific series of radiofrequency pulses to the sample. By manipulating the spin system in the right way it becomes possible to map out and correlate several spin interactions. Another possibility is to detect exchange between several states of a nucleus. The principle of 2D NMR is discussed in chapter 2.

In Chapter 3 we describe an experiment, using magic angle spinning and multiple pulse decoupling, that results in a spectrum that gives isotropic ^{13}C chemical shifts in one dimension and the corresponding heteronuclear J_{C-H} couplings in the other direction. This experiment is, except for the averaging techniques, analogous to such an experiment in a liquid. By applying this technique to natural rubber it appeared that not much averaging was needed to obtain a "liquid like" spectrum, which means that the macromolecules in the rubber must be very mobile.

At first, solid state NMR spectroscopists always aimed to perform experiments analogously to experiments in solution. It appears, however, that several experiments are possible that explicitly exploit the anisotropic behaviour of spin interactions in solids. As 2D NMR offers the possibility to map out different interactions it can be used to avoid spectral overlap. Such an experiment, that maps out the chemical shift anisotropy against the heteronuclear dipolar interaction, is described in chapter 4. This can be used to obtain geometrical, orientational and motional information. Poly-(oxymethylene) $(-CH_2-O-)_n$ is a polymer whose molecular chains form helices in the crystalline solid state. From the experiment described above it appears that the orientation of the ^{13}C chemical shift tensor is determined by the local tetrahedral symmetry of the CH_2O_2 unit. Consequently, this symmetry is not disturbed by the helix formation.

2D exchange experiments are used to detect some kind of exchange between different states of the spin system during a mixing time that separates the evolution and the detection periods. In chapter 5 2D exchange experiments are used to study super-slow molecular motions in solids. For instance, it was established that the very mobile rubber molecules do not travel through large distances in the sample within 40 milliseconds. The emphasis in chapter 5 lies on the description of a variant of the 2D exchange experiment developed by us to study super-slow molecular motions in polymers using magic angle spinning to increase sensitivity. As the chemical shift anisotropy is used in this experiment to detect the molecular motions, the spinning speed is chosen to be small so that the chemical shift anisotropy is not totally averaged, but so-called spinning sidebands appear. These experiments showed the presence of super-slow chain motions in poly-(oxymethylene). Using the results obtained in chapter 4 about the orientation of the chemical shift tensor, the motions could be characterized. It appears that the helices, in the crystalline part of the polymer, perform a screw like rotation over ±200°. At a temperature of 60 °C this motions, on the average, only occurs once a second for every chain. These kinds of motion are important because they are believed to influence the mechanical properties of polymers.

In chapter 6 the so-called 2D nutation experiment is described. It offers the possibility to study nuclei with a quadrupole moment. The quadrupole interaction is determined by the electrical interaction of the (asymmetric) nucleus and its surrounding charges and can thus yield valuable structural information. As the majority of nuclei in the periodic system possess a quadrupole moment this experiment should find many applications.

The interest on getting structural information from spectra of quadrupolar nuclei has been aroused because of the important role such atoms play in ceramics, clays and silicates (e.g. zeolites), which are important materials in material science because of their various applications. Zeolites are porous networks of SiO_4 and AlO_4 tetrahedra. A well-known zeolite is ZSM-5 which can be used as a catalyst to convert methanol into gasoline. The catalytic activity occurs at the aluminum nuclei. One application of nutation NMR in chapter 6 is a study of structural changes around the aluminum nuclei in ZSM-5 upon a change of the water content of the pores.

It can be concluded that 2D solid state NMR is a useful and important extension of the arsenal of analysis tools. For instance, the possibility to study molecular motions on a molecular level can lead to new viewpoints about the relation of these motions to mechanical properties of the polymer. Nutation NMR also offers some interesting possibilities, like the study of zeolites at high temperatures where they are catalytically active.

Atoomkernen zijn op te vatten als staafmagneetjes, dit noemt men de spin. Als gevolg hiervan zullen de spins een wisselwerking vertonen met een uitwendig magneetveld. Kernspin resonantie (Nuclear Magnetic Resonance NMR) maakt hier gebruik van; men brengt een stof in een hoog magneetveld, vervolgens verstoort men de in het magneetveld uitgerichte spins met een radiofrequente puls. Hierdoor gaan de spins met een specifieke frequentie trillen. Het is gebleken dat deze resonantie frequenties afhangen van de preciese omgeving van de atoomkernen. NMR heeft zich tot een belangrijke analyse techniek ontwikkeld in de chemie omdat men aan de hand van de resonantie frequenties van de spins informatie kan krijgen omtrent de structuur van een stof. Zo is het bijvoorbeeld mogelijk geworden om de 3-dimensionale structuur van eiwitten in oplossing op te lossen aan de hand van NMR experimenten.

In hoofdstuk 1 van dit proefschrift worden de, resonantie frequentie bepalende, interacties van de kernspins met hun omgeving beschreven. In vloeistoffen meet men door het snelle tuimelen van de moleculen een gemiddelde frequentie. In vaste stoffen hangen de resonantie frequenties af van de orientatie van een bepaald molecuul t.o.v. het uitwendige magneetveld. Dit heeft tot gevolg dat in poeders, waarin de moleculen alle mogelijke orientaties t.o.v. het magneetveld hebben, zeer brede frequentieverdelingen worden gemeten. Toch kan men vaak in vaste stoffen "vloeistof-achtige" spectra meten door uitmiddelings technieken toe te passen zoals magic angle spinning. Hierbij wordt het sample met zeer hoge snelheid om een as, die een hoek van 54.7° (de magische hoek) maakt met het magneetveld, geroteerd. De verschillende uitmiddelings technieken worden eveneens in hoofdstuk 1 besproken.

Bij twee-dimensionale (2D) NMR meet men een trillingssignaal in een tijddomein t_2 dat gemoduleerd wordt in fase en/of amplitude door de interacties die het spinsysteem gedurende een voorafgaande tijd t_1 beheersen. Dit wordt bereikt door het sample aan specifieke volgordes van radiofrequente pulsen te onderwerpen. Twee-dimensionale NMR kan men gebruiken om verschillende interacties tegen elkaar uit te zetten. Een andere mogelijkheid is het meten van uitwisseling (exchange) tussen verschillende toestanden van de spin gedurende een mixingtijd tussen t_1 en t_2. In hoofdstuk 2 wordt het principe van de twee-dimensionale NMR beschreven.

In hoofdstuk 3 wordt een 2D vaste stof NMR experiment beschreven dat de chemische verschuiving uitzet tegen de J-koppeling. De chemische verschuiving is een grootheid die bepaald wordt door de electronenwolken die een kern omringen, terwijl de J-koppeling informatie geeft over de chemische bindingen met buurkernen. Het sample wordt gedurende dit experiment aan bovengenoemde uitmiddelings procedures onderworpen zodat een spectrum wordt verkregen dat kan worden vergeleken met dat van vloeistoffen. Uit dit soort experimenten met rubber blijkt dat er nauwelijks uitgemiddeld hoeft te worden, wat betekent dat de macromoleculen in het rubber zeer beweeglijk zijn.

In veel 2D experimenten aan vaste stoffen wordt expliciet gebruikt gemaakt van het vaste stof karakter van de spin interacties, dus men meet dan niet alleen de gemiddelde frequenties. Zo kan het tegen elkaar uitzetten van interacties onder andere gebruikt worden voor het bepalen van relatieve orientaties van tensoren (=mathematische beschrijving van de interacties) t.o.v. elkaar om hieruit meer informatie te krijgen omtrent de lokale structuur in een materiaal ter plekke van een bepaalde kern. In hoofdstuk 4 wordt de dipolaire interactie, die de magnetische wisselwerking van een kern met zijn buren beschrijft, uitgezet tegen de chemische verschuiving. Polyoxymethylene $(-CH_2-O-)_n$ is een kunststof waarvan de molecuulketens in de kristallijne vaste stof helices vormen. Uit de zojuist beschreven metingen blijkt dat de orientatie van de ^{13}C chemische verschuivings tensor wordt bepaald door de lokale tetraedrische symmetry van de CH_2O_2 eenheid. Deze symmetry wordt dus niet verstoord door de helix vorming van de polymeerketens.

2D exchange experimenten worden gebruikt om bijvoorbeeld chemische exchange te meten. Dit is een proces waarbij een kernspin heen en weer pendelt tussen verschillende posities binnen een molecuul of tussen verschillende moleculen. In hoofdstuk 5 worden 2D exchange experimenten gebruikt om zeer langzame molecuulbewegingen op te sporen in de vaste stof. Dit leidt tot zeer interresante resultaten. Zo kon worden aangetoond dat de zeer beweeglijke rubber moleculen geen grote afstanden afleggen binnen het sample binnen een tijd van 40 milliseconden. De sterke nadruk in hoofdstuk 5 ligt op de beschrijving van een door ons ontwikkelde variant van het 2D exchange experiment om langzame bewegingen op te sporen in polymeren. Hierbij wordt magic angle spinning toegepast om de gevoeligheid te verhogen. De spin snelheid wordt echter zo klein gekozen dat de chemische verschuivings anisotropie, die hier gebruikt wordt om de beweging op te sporen, niet geheel wordt uitgemiddeld (er ontstaan dan zogenaamde spinning-zijbanden). Bij dit

soort experimenten aan polyoxymethyleen kwamen zeer langzame ketenbewegingen aan het licht. Om de beweging te kunnen beschrijven werd gebruikt gemaakt van de resultaten verkregen in hoofdstuk 4 omtrent de ligging van de chemische verschuivings tensor. Het blijkt dat de helixvormige macromoleculen schroefbewegingen uitvoeren in de kristallijne fase van het polymeer. Deze bewegingen treden bij een temperatuur van 60 °C gemiddeld slechts een keer per seconde op voor iedere keten. Dit is vooral van belang omdat dit soort ketenbewegingen waarschijnlijk de mechanische eigenschappen van polymeren beinvloeden.

In hoofdstuk 6 wordt het zogenaamde nutatie NMR experiment beschreven dat het mogelijk maakt om de quadrupool interactie te bestuderen. De quadrupool interactie beschrijft de electrische interactie van asymmetrische atoomkernen met de omringende ladingsverdeling, en geeft dus informatie omtrent de lokale structuur. Omdat het merendeel van de atoomkernen in het periodiek systeem een quadrupool moment heeft is dit experiment van groot belang. De belangstelling voor bepaalde quadrupoolkernen is vooral opgewekt omdat ze voorkomen in allerlei keramische materialen en zeolieten, die van groot belang zijn voor de chemische industrie. Zeolieten zijn materialen met daarin porie-netwerken. Een zeer bekend zeoliet is ZSM-5 dat als katalysator kan fungeren om methanol om te zetten in benzine. De katalytische werking treedt op bij aluminium kernen die in het materiaal ingebouwd zijn. In hoofdstuk 6 wordt o.a. de lokale structuur verandering rond aluminium kernen in ZSM-5 bestudeerd als functie van het water gehalte van de poriën.

Uit het voorgaande blijkt dat 2D NMR voor vaste stoffen een belangrijke en zinvolle uitbreiding van het arsenaal van analyse methodes biedt. Zo kan bijvoorbeeld de mogelijkheid om zeer langzame bewegingen in polymeren op moleculair niveau te bestuderen interessante resultaten opleveren wanneer bijvoorbeeld de invloed van mechanische bewerkingen op de stof wordt bestudeerd. Ook de nutatie NMR biedt belangrijke perspectieven, zo bestaat bijvoorbeeld de mogelijkheid om zeolieten bij hoge temperaturen, waarbij ze katalytisch werkzaam zijn, te onderzoeken.

Arno Kentgens werd op 15 augustus 1959 in Guttecoven geboren. Van 1971 tot 1977 bezocht hij het Bischoppelijk College St. Jozef te Sittard, waar het einddiploma Atheneum B werd behaald.

In september 1977 werd gestart met de studie scheikunde aan de Katholieke Universiteit Nijmegen. Het *kandidaatsexamen* S3 (*hoofdvakken* scheikunde en natuurkunde, bijvak wiskunde) werd behaald in september 1980. Hierna bestudeerde hij o.l.v. Dr. F.W. Pijpers en Prof.Dr. G. Vertogen, in het kader van de bijvakstages Analytische Chemie en Theoretische Fysica, het legeringsgedrag van twee metalen met behulp van patroonherkenning. De hoofdvakstage op de afdeling Molecuulspectroscopie (o.l.v. Prof.Dr.Ir. W.S. Veeman) betrof de bestudering van het zeoliet ZSM-5 met vaste stof NMR. Dit leidde tot het behalen van het doctoraal-examen scheikunde (cum laude) in april 1983.

Sinds 1 mei 1983 is hij als adjunct wetenschappelijk ambtenaar, gefinancieerd door de stichting SON, verbonden aan de Katholieke Universiteit Nijmegen. Hier werd op de afdeling Molecuulspectroscopie een promotie onderzoek uitgevoerd met als onderwerp twee-dimensionale NMR in vaste stoffen. Voor dit onderzoek werd hem een prijs toegekend in het kader van de DSM-prijzen voor Chemie en Technologie.

Ter invulling van de bij de promotie behorende onderwijstaak assisteerde hij bij het practikum fysische chemie voor tweedejaars studenten, en werd het werkcollege spectroscopische methoden voor studenten in de differentiatiefase verzorgd.

STELLINGEN

I

Het door Reuveni gegeven verband tussen de N-D bindingsafstand en de gemeten Deuterium quadrupool parameter e^2qQ/h gaat niet op voor 2 van de 4 besproken systemen.
-A. Reuveni, Can. J. Phys. 29, 79, 1984.

II

De door Man gegeven overgangsfrequenties in nutatiespectra kunnen niet worden verkregen uit de door hem gegeven Hamiltoniaan.
-P.P. Man, J. Magn. Res. 67, 78, 1986.

III

De afwijzende houding van veel fysici t.o.v. de toepassing van patroonherkenning op fysische problemen is niet gefundeerd.

IV

Met de opmerking "Surprisingly, the only treatments of half-integer spins in the literature seem to be some preliminary results by us for I = 3/2 and more recent ones by Fenzke et al. for I = 5/2." geven Pandey et al. aan niet op de hoogte te zijn van de bestaande literatuur op het gebied van de excitatie van quadrupool kernen.
-Lakshman Pandey, S. Towta and D.G. Hughes, J. Chem. Phys. 85, 6923, 1986.

V

Uit het feit dat in NMR boeken steeds een spectrum van ethylalcohol wordt getoond bij de bespreking van het begrip chemische verschuiving blijkt dat deze stof nog steeds zeer tot de verbeelding spreekt. De vertroebelende werking van alcohol blijkt echter uit de grote moeite die men vervolgens heeft met het consequent toepassen van de kurketrekker-regel bij het uitvoeren van rotaties.

VI

Nunome et al. en Shimida et al. interpreteren de toename van het product $T_1 \cdot T_2$ als functie van de temperatuur, voor radicalen in bestraald polyethyleen, ten onrechte als een toename van T_2.

-K. Nunome, H. Muto, K. Toriyama and M. Iwasaki, Chem. Phys. Lett. 39, 542, 1986.

-S. Shimida, Y. Hori and H. Kashiwabara, Radiat. Phys. Chem. 19, 33, 1982.

VII

De voorspelling van W.S. Veeman, dat de volgende Elfstedentocht pas in het jaar 3693 zou plaatsvinden, lijkt, gezien de recentelijke ontwikkeling rond de organisatie, eerder een wensdroom dan een wetenschappelijk gefundeerde voorspelling.

-W.S. Veeman, stelling 9 bij het proefschrift "Level anticrossing and cross-relaxation in phosphorescent organic crystals", november 1972.

VIII

Problematisch voor mensen die een afkeer hebben van politiek is dat zij geregeerd worden door politici.

IX

De voortgang van de automatisering zou zeer zijn gebaat met het verschijnen van duidelijke handleidingen bij zowel hard- als software.

Nijmegen, 4 juni 1987 A.P.M. Kentgens